TORQUE RIPPLE ATTENUATION FOR AN AXIAL PISTON SWASH PLATE TYPE HYDROSTATIC PUMP: NOISE CONSIDERATIONS

A Dissertation

presented to

the faculty of the Graduate School

University of Missouri – Columbia

In partial fulfillment of the requirements for the degree of

Doctor of Philosophy in Mechanical Engineering

By

VIRAL MEHTA

Dr. Noah Manring, Dissertation Supervisor

MAY 2006

The undersigned, appointed by the Dean of the Graduate School, have examined the dissertation entitled,

TORQUE RIPPLE ATTENUATION FOR AN AXIAL PISTON SWASH PLATE TYPE HYDROSTATIC PUMP: NOISE CONSIDERATIONS

Presented by VIRAL MEHTA

A candidate for the degree of Doctor of Philosophy

And hereby certify that in their opinion it is worthy of acceptance.

_____
Dr. Noah Manring

_____
Dr. Steven Borgelt (External Supervisor)

_____
Dr. Roger Fales

_____
Dr. Frank Feng

_____
Dr. Craig Kluever

ACKNOWLEDGEMENT

I would like to express my sincere gratitude to many people, without whom this dissertation would not have been completed. First and foremost, it is a great honor to express my deep gratitude to my advisor, Dr. Noah Manring, for his guidance, encouragement and warm support at every steps of my doctoral program at University of Missouri - Columbia. I give a special thanks to Dr. Brian Landsberger from University of Nevada, Las Vegas for defining this dissertation problem while working at Caterpillar Inc., and his insightful guidance. I would like to thank Dr. Steven Borgelt, Dr. Roger Fales, Dr. Craig Kluever and Dr. Frank Feng for being the reading committee as well.

Next, I am thankful to the engineers from Caterpillar Inc., especially Kevin Graf for his technical guidance and Frank Raab and Jerry Wear for providing me this opportunity and financial support to work on a Caterpillar project.

I am also very grateful to my friends who made this long and arduous Ph.D. process, an enjoyable and memorable time.

Most importantly, to my family in India, I owe a debt of gratitude for their unconditional love and support along the path of my academic pursuits. I would like to give special thanks to my brother and father for their confidence in my ability to do a Ph.D. I love you all.

TABLE OF CONTENTS

LIST OF FIGURES

LIST OF TABLES

NOMENCLATURE

A_b effective pressurized area on the cylinder block within a single piston chamber

A_o port area

A_p cross sectional area of a single piston

a offset dimension describing the position of the piston-slipper ball-joint relative to the swash plate pivot

C_d coefficient of discharge

d_n normal distance of the n^{th} piston away from the centerline of the pump shaft

e offset dimension of the swash plate pivot

$\boldsymbol{F}_{bal_n}$ force exerted on the slipper from the effective pressurized area on the face of n^{th} slipper

$\boldsymbol{F}_{B_n}$ force exerted on the cylinder block from the piston-bore spring

$\boldsymbol{F}_{c_n}$ clamping force from the pressure within each piston-bore

$\boldsymbol{F}_{hd}$ force exerted on a single slipper from the slipper hold-down mechanism

$\boldsymbol{F}_{l_n}^{\ y}, \boldsymbol{F}_{l_n}^{\ z}$ force exerted on the cylinder block at the inner edge of the n^{th} bushing from the n^{th} piston in the y and z-direction respectively

$\boldsymbol{F}_{o_n}^{\ y}, \boldsymbol{F}_{o_n}^{\ z}$ force exerted on the cylinder block at the outer edge of the n^{th} bushing from the n^{th} piston in the y and z-direction respectively

$\boldsymbol{F}_{p_n}$ force exerted on the cylinder block from the n^{th} piston

$\boldsymbol{F}_{pr_n}$ force exerted due to the pressure within the n^{th} piston-bore acting on the face of the piston

$\boldsymbol{F}_{s_n}$ force acting on the n^{th} piston due to the reaction of the n^{th} slipper at the piston/slipper ball-joint

$\boldsymbol{F}_{sh}$ force exerted on the cylinder block from the shaft

$\boldsymbol{F}_{sp_n}$ force exerted on the cylinder block from the cylinder block spring

$\boldsymbol{F}_{sw_n}$ force exerted on the n^{th} slipper from the swash plate

$\boldsymbol{F}_{v}$ force exerted on the cylinder block from valve plate

K Leakage coefficient

k spring-rate

L_1 distance of the n^{th} clamping force away from the shaft reaction

l_m distance from the piston-slipper ball-joint center to the piston mass-center

l_p length of the bushing

M_b cylinder block mass

$\boldsymbol{M}_{bal_n}$ moment exerted on the slipper from the effective pressurized area on the face of n^{th} slipper

$\boldsymbol{M}_{B_n}$ moment exerted on the cylinder block from the piston-bore spring

$\boldsymbol{M}_{c_n}$ moment exerted by clamping force from the pressure within each piston-bore

$\boldsymbol{M}_{hd}$ moment exerted on a single slipper from the slipper hold-down mechanism

$\boldsymbol{M}_{I_n}$ moment exerted on the cylinder block at the inner edge of the n^{th} bushing from the n^{th} piston

$\boldsymbol{M}_{o_n}$ moment exerted on the cylinder block at the outer edge of the n^{th} bushing from the n^{th} piston

M_p mass of a single piston

$\boldsymbol{M}_{p_n}$ moment exerted on the cylinder block from the n^{th} piston from the reaction between them

$\boldsymbol{M}_{pr_n}$ moment exerted due to the pressure within the n^{th} piston-bore acting on the face of the piston

M_s mass of a single slipper

$\boldsymbol{M}_{s_n}$ moment acting on the n^{th} piston due to the reaction of the n^{th} slipper at the piston/slipper ball-joint

$\boldsymbol{M}_{sh}$ moment exerted on the cylinder block from the shaft

$\boldsymbol{M}_{sp_n}$ moment exerted on the cylinder block from the cylinder block spring

$\boldsymbol{M}_{sw_n}$ moment exerted on the n^{th} slipper from the swash plate

$\boldsymbol{M}_{v}$ moment exerted on the cylinder block from valve plate

m linearized transition slope for the pressure-carry over angle

m_o distance from the swash-plate pivot to the outer edge of the n^{th} bushing

N total number of pistons

N_o odd number of pistons

N_e even number of pistons

n dummy variable for identifying the n^{th} piston

n' number of pistons pressurized by the discharge port

P_b boundary pressure outside the control volume

P_d pump discharge pressure

P_i pump intake pressure

P_n fluid pressure within the n^{th} piston chamber

Q discharge flow

Q_l leakage due to the clearance between the piston and bore

r piston pitch radius

T net instantaneous shaft torque

T_{o1} torque component generated due to pistons on high pressure side

T_{o2} torque component generated due to pistons on low pressure side

$\bar{T}$ average shaft torque produced the pump

$\bar{T}_s$ average starting shaft torque produced by the pump

T_n torque produced by the n^{th} piston

V_o piston chamber volume when $\alpha = 0$

V_d volumetric displacement

w distance from the piston-slipper ball-joint to the swash plate

α swash plate angle

β bulk modulus

δ index angle defining the separation of the first pistons of two rotating groups

ρ density of fluid

ς ratio $\frac{P_i}{P_d}$

ξ number defined in equation (5-19)

φ_n angular position of the n^{th} piston

φ_1 angular position of piston number one

ω angular velocity of the pump shaft

CHAPTER 1. INTRODUCTION

1.1 Introduction

A critical challenge in fluid power industry is excessive noise generated by axial piston pumps. Chapter 1 begins with the discussion on motivation to reduce the pump noise from current level. Thorough background information is given detailing the understanding of this problem and mechanisms involved with it. Some of the standard and in-test methods to alleviate the problem and work in progress by different research groups are presented subsequently. At the end of this chapter, a theory highlighting a different origin of the problem is proposed that challenges the generally accepted view about the noise problem in axial piston pumps and sets foundation for the analysis described in later chapters.

1.2 Motivation for the Research

Hydraulic power transmission has been in use for more than a century. It has many advantages over other modes of power transmission like electrical motors, such as fast response and high torque to inertia ratio. Also, hydraulic systems are very compact and offer higher efficiency across a wide range of operating conditions. However, it must be acknowledged that the fluid power technology has some weaknesses which do not beset other means of power transmission to the same extent. The prominent weakness is the loud noise generated by positive displacement pump. In hydraulic systems, power is

transmitted and controlled through liquid under pressure. Positive displacement pumps convert shaft rotation into hydraulic power. During this process pumps generate a loud noise which is undesirable and unacceptable to many applications. However, this noise is masked by the diesel engine noise on a mobile application but if used for a stationary application, could be annoying to the user [1].

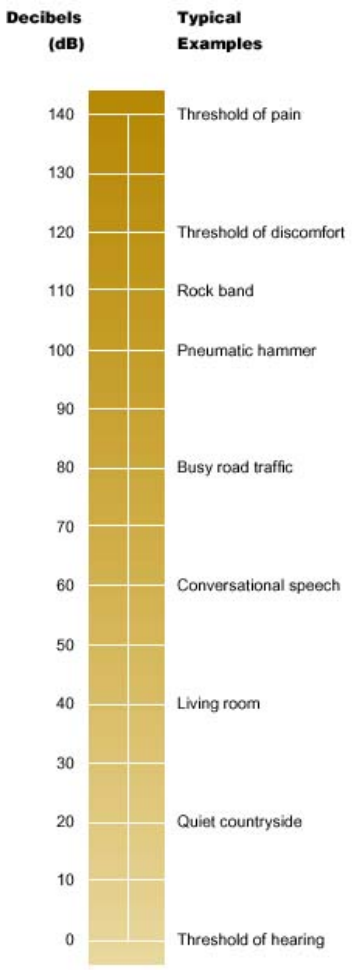

Figure 1-1 Decibel scale
(Source: Website of Department of Environment and Heritage, Government of Australia [2])

Sound is measured in decibels (dB). When measuring environmental noise, a weighting network is used which filters the frequency of the sound so that it corresponds to the response of the human ear. Noise measurements made using this filtering network are expressed as dBA. The decibel scale is logarithmic to manage the enormous range of sound pressures able to be detected by the human ear. This often leads to confusion. For instance, if two machines emit exactly the same noise level of 80 dBA, the total noise level is not 160 dBA, but 83 dBA. Also, a 10 dBA increase in sound level represents a doubling of loudness. Typical examples illustrating the decibel scale are shown in Figure 1-1 [2]. An axial piston pump produces noise level as high as 100 dBA; the equivalent noise level that is experienced when standing near a lawn mower or riding on a subway.

The effects of noise and vibration on the health of people and animal exposed to excessive levels have been extensively documented [2]. Investigations have found that prolonged exposure can adversely affect mental and physical health. Hence, it is very important to reduce the hydraulic system noise from its present levels.

1.3 Literature Review

1.3.1 Sources of Noise and Path

As stated earlier, in hydraulic systems, power is transmitted and controlled through liquid under pressure. Positive displacement pumps convert shaft rotation into hydraulic power. During this process pumps generate a loud and disturbing noise. Noise reduction has been a key issue to most hydraulic pump manufacturers and considerable

effort has been forth put to alleviate this problem. It is very important to understand what causes this noise in order to reduce it. Literature contains various theories [3-12] associated with the noise generation in axial piston pumps. The phenomenon of noise generation and transmission is very complex and has not been understood well as there are many sources for noise generation. The hydraulic system noise can be classified into three categories: fluid-borne noise (FBN), structure-borne noise (SBN) and air-borne noise (ABN). It is believed that the SBN and ABN are caused by the FBN to a large extent. The transfer function relationships between the FBN and the SBN and between the SBN and the ABN are extremely complex and are not well understood. However since the FBN is considered to be the biggest source of noise, it is expected that the reduction in the FBN levels would bring down the other noise levels. Fluid-borne noise itself is caused by a multiple factors like flow fluctuations, cavitation and valve instability, again the flow fluctuations being the main contributor [13]. Once the forcing function (flow ripple) generates pump noise, it gets transmitted and radiated by different components of the pump.

Malaney [14] describes the hydraulic noise and vibration path as shown in Figure 1-2. Figure 1-2 shows that there is some SBN due to vibration of housing and other internal components at their natural frequencies. Also there is the FBN (flow ripple), which is transferred to the fluid lines and other fixtures resulting in the SBN. Any FBN or SBN ultimately gets radiated as ABN.

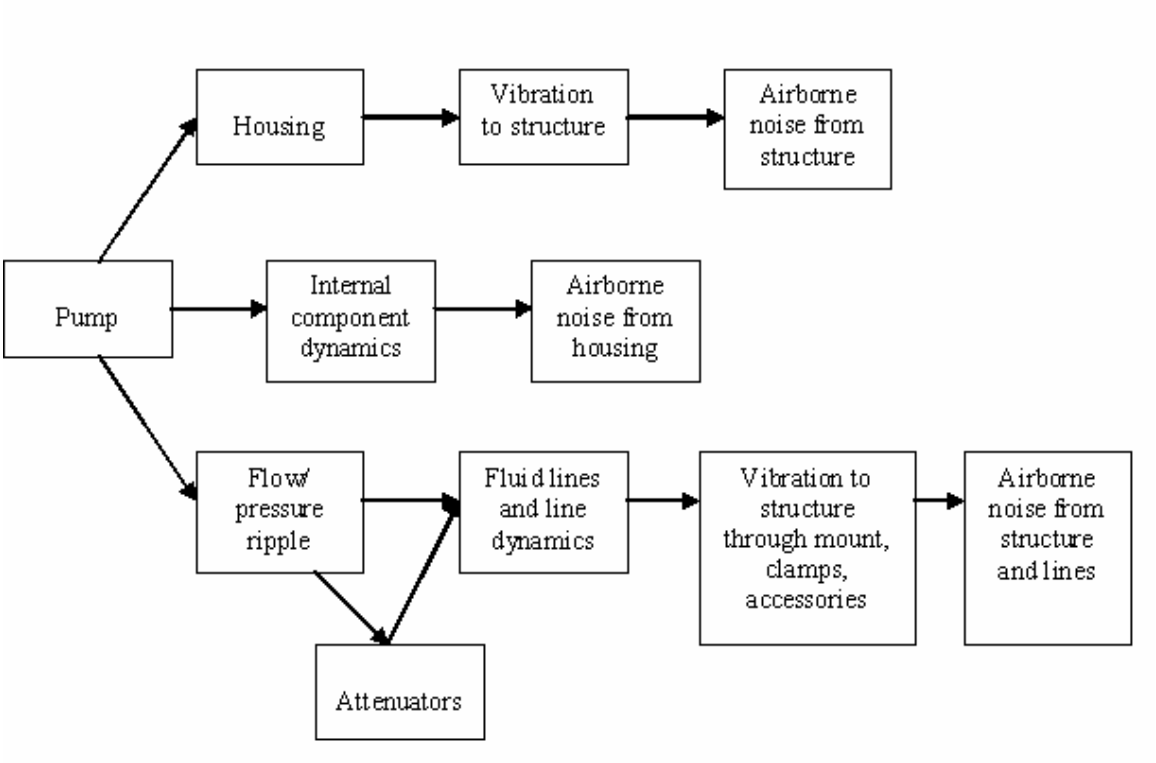

Figure 1-2 Hydraulic noise and vibration path
(Source: Malaney [14])

1.3.2 Flow Ripple as Main Source

It is also known that the flow variation is basically caused by (a) the periodic variation in geometric displacement and (b) the oil compression and expansion processes at transitions between high and low pressure. Also, the reason for geometric displacement variation is that the total flow is a summation of the flows from individual pumping elements. Based on this knowledge, the flow ripple is categorized as the kinematic flow ripple and dynamic flow ripple. The dynamic component is much worse both in amplitude and frequency than the kinematic flow component, i.e. contribution of dynamic

flow ripple is significantly higher towards the total flow ripple [7]. It is very intuitive to suggest that the smoother the flow, the lower the noise.

1.3.3 Standard Noise Reduction Methods

Some of the solution techniques for reducing noise have become industry standards while the others are still in the investigation stage. Following is a list of some of the traditional techniques or sort of guiding principles used by the pump industry to reduce the noise level of axial piston pumps; 1) Use multiple pumps in parallel, 2) Use a large oil volume at the discharge port, 3) Use hydraulic acoustic filter, 4) Use the lowest practical pump speed, 5) Do system tuning- selection of size, type, quality of pump etc., 6) Use flexible hose and supports.

1.3.4 Noise Reduction Methods for Axial Piston Pumps

Edge and Darling [3] suggests a few techniques to reduce noise in axial piston pumps. One of the most common techniques is to optimize the port plate geometry. Axial piston pumps now come with relief grooves at the leading edges of the inlet and outlet ports. They eliminate cylinder pressure undershoot at top dead center (TDC) and overshoot at bottom dead center (BDC) which help reduce the noise level. The use of the capped pistons to attenuate noise is an established industry practice. A couple of recommendations regarding the port geometry are that the slope of the groove should not be more than 30 degrees while groove length should be kept at minimum.

An extensive review of the progress that has been made over the last 25 years in the understanding of noise is presented by Harrison and Edge [4]. Following is a brief overview of techniques mentioned in the article and possible problems associated with each. 1) Use of an anti-noise devices is cost prohibitive, more ever it introduces many other technical problems. 2) It is generally recognized that the compression and decompression phenomenon and the resulting swash plate vibration can be controlled by varying valve plate timing, i.e., the initiation of communication between the kidney port and the fluid inlet or fluid outlet in the valve plate. However, varying valve plate timing during operation of an axial piston pump requires rotating the valve plate while it is under heavy axial loading from the cylinder barrel, which is not very practical. Also it reduces volumetric efficiency of the pump and introduces the cavitations problem. 3) Use of independent suction and delivery timing is also unaffordable by high cost. 4) The delay in communication between the port plate and the cylinder is achieved by a check valve. However, use of a check valve is not possible because of very rapid switching action required in operation. Also at higher pump speeds, the frequency response of the valve may limit its switching performance. Hence, it is ineffective at high delivery pressure and pump speed. (5) In spite of the reservations expressed above, the principle of using a check valve ahead of a delayed delivery port is promising. An alternative to check valve is the heavily damped check valve (HDCV) which prevents the rapid switching action, tunes itself according to the changing operating conditions and reduces the flow ripple. This technique seems promising and is under more investigation. Typically two check

valves are used in series. The positions of the HDCVs relative to a delayed kidney port are shown in Figure 1-3.

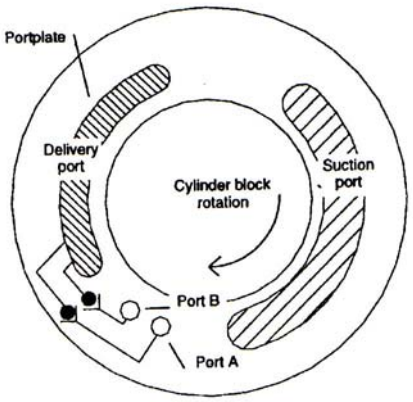

Figure 1-3 Check valve portplate positions
(Source: Edge and Darling [3])

In order to reduce the flow ripple, it is extremely important to know the mechanism of source flow ripple. Kojima et al. [5] introduced the '2 Pressures/ 2 System' method to predict the flow ripple and experimentally verified the same to a great accuracy. This model includes the compressibility of the fluid, the fluid momentum in the chamber and relief grooves, and the pressure dependent effective bulk modulus of the fluid containing air. The results supports the development of quieter pumps with better fluid borne noise characteristics.

Ivantysynova et al. [6] presents a new computer based design method for valve plate design using the simulation program CASPAR and the extension tool AVAS. The valve plate design strongly affects the instantaneous cylinder pressure, the profile of oscillating forces applied on the machine parts and the effective flow and pressure

pulsation. Having known that these oscillating forces exerted on machine parts cause structure borne noise and the flow/pressure pulsation causes the fluid borne noise, these software tools could be used to evaluate the effectiveness of design measures for noise reduction during the design phase, i.e. before prototype production.

Petterson et al. [7] made a theoretical mapping of the noise and vibration associated and presented many schemes to attenuate noise. One very important conclusion from this research is that higher speed and higher pressure affects the dynamic flow component severely and increases the pump noise. Three schemes; namely, pressure relief groove, pre-compression and ideal compression suggested by Petterson are already discussed by Harrison. The fourth scheme requires a special mention. It has been suggested earlier that variable timing is one method to reduce the dynamic flow ripple. However it is expensive and causes other problems like reduced volumetric efficiency. Petterson proposes a new approach to variable timing wherein the mechanism pre-compresses the cylinder contents to the delivery pressure in time for communication with the delivery port. Variable cylinder pre-compression can be achieved by using a pre-compression filter volume (PCFV). At present results from the PCFV mechanisms have only been published for fixed-displacement pumps and its range of operation to work effectively has been questioned by Harrison and Edge [4].

In a conventional axial piston pump**,** the cylinders are equally spaced, circumferentially, and at the end of each cylinder, the cylinder barrel defines a cylinder port or kidney port, which provides fluid communication between its respective cylinder and the fluid inlet and fluid outlet in the adjacent valve plate. In a typical, axial piston

pump**,** each of the cylinder barrel kidney ports is the same size, in both the radial and circumferential dimension, with circumferential dimension of each kidney port being substantially equal to the diameter of the cylinder. Schutten et al. [8] suggests putting kidney ports at different circumferences and thereby varying the timing of the communication between the leading edges of the kidney ports and the fluid inlet and fluid outlet. This design called ‘random porting’ shifts the sound energy from high to low frequency. Since high frequency noise is more annoying than low frequency; even though sound energy remains same, noise quality is improved. Figure 1-4 shows one example of random porting. Another way of achieving the same is keeping cylinders at different circumferential dimensions but it encounters the balancing problem and hence may not be of practical importance.

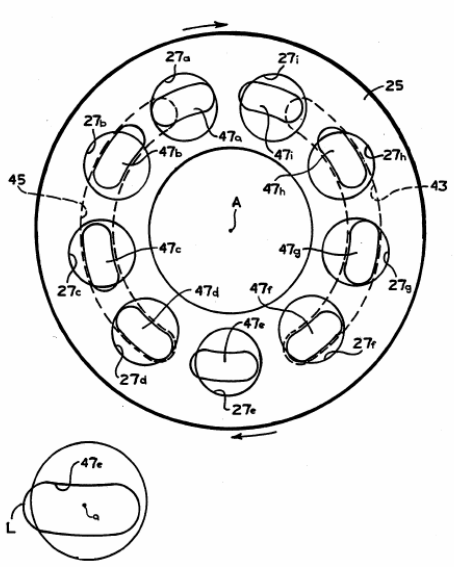

Figure 1-4 Random porting
(Source: Schutten [8])

In a very different concept, Achten et al. [9, 10, 11] proposes a ‘floating cup principle’ where in two pumps connected by a through shaft make a tandem pump. The pistons are arranged in two rings of twelve pistons each with both rings connected to the central rotor in a mirrored back-to-back configuration. There are two rotating groups consisting of twelve pistons on each side and the first pistons of both rotating groups are separated by 15^{o}. It is shown that the flow and pressure pulsations are greatly reduced resulting in low noise. However, it can be argued that the resulting reduction in these amplitudes could be due to a very large number of pistons. It has been a well accepted fact that since the total flow is summation of individual piston flows, more pistons produce a smoother flow. Also pumps with odd number of pistons generate lesser flow fluctuations while pumps with even number of pistons generate more. This will be demonstrated in Chapters 5 and 6.

Along with a few general recommendations for noise reduction earlier summarized, Wilkes [12] proposes the use of an ‘in-line nitrogen charged noise suppressor’ right at the outlet of the pump. It is common knowledge that introducing a compressible medium of nitrogen into the relatively incompressible medium of hydraulic fluid will help reduce pulsations. Traditional hydraulic accumulators that are fitted in the hydraulic lines have been found ineffective as they pose problems like the flow pulsations not entering the accumulator, sizing the accumulator and cost of this fixture. However, an ‘in-line nitrogen charged noise suppressor’ has been found to reduce noise level of a pump from 82 dBA to 78 dBA.

Strunk [13] developed a new type of reactive silencer called a cross-loop attenuator which is essentially a side branch resonator but differs in design from other side-branch resonators. Any kind of reactive silencer changes the load impedance and reflects the pulsations back to the pump. Here the cross-loop line has resonant frequencies which are defined by the length of the cross-loop line and the speed of wave propagation in the line. When the resonant frequency of the cross-loop line matches that of the fluid pulsations, the pressure pulsations are reflected back to the pump. This in turn reduces the amplitude of the pressure oscillations that are transmitted into the line connected to the down stream hydraulic circuit.

1.3.5 Summary of Literature

In summary, positive displacement piston pumps generate a flow ripple that is created by the pumping action of the pistons and the valve in the pump. The total flow is composed of summation of flows from individual pistons and is a periodic function of time with a fundamental frequency that corresponds to the piston pass frequency and higher harmonics. The most effective method of reducing pump noise is by reducing the amplitude of the flow and pressure ripple by a better design of port-plate geometry. The other common approach to this problem is use of reactive silencers. The reactive silencers have been used effectively in many applications and have many different configurations such as accumulators, in-line silencers and side-branch resonators. However, there is a limited success in lowering down the noise level. Also, pumps with relief groove can generate a significant increase in fluid borne noise (FBN) when operated away from the

design point. It is possible to alleviate this problem further if new methods are employed. This work basically proposes a new theory for noise generation phenomenon, different from what the academic and industrial community have accepted and designs two methods to reduce the pump noise.

1.4 Correlation Between the Noise and the Input Shaft Torque

A recent industrial study [15] shows that the torque acting on the input shaft of the hydrostatic pump correlates with the noise. Like flow variation, this torque ripple results from the discrete piston locations within the pump that create oscillating moments on the shaft. To attempt an improved pump design, it is necessary to understand the details of the pump noise. When is the pump noise level high, from where does the noise radiate, what caused that part to vibrate, and from where does the energy originate that sustains the vibration? In this study, two 250cc/rev pumps were tested where the pump speed was swept from low to high. The pump was hard mounted to a frame while all other connections were flexible. Instrumentation included were microphones and accelerometers on the pump and frame. The input shaft torque and pump speed and output fluid flow and pressure were measured. Test runs were performed at a cross-section of discharge pressures and pump displacements. Test runs were speed sweeps from low idle to maximum operating speed.

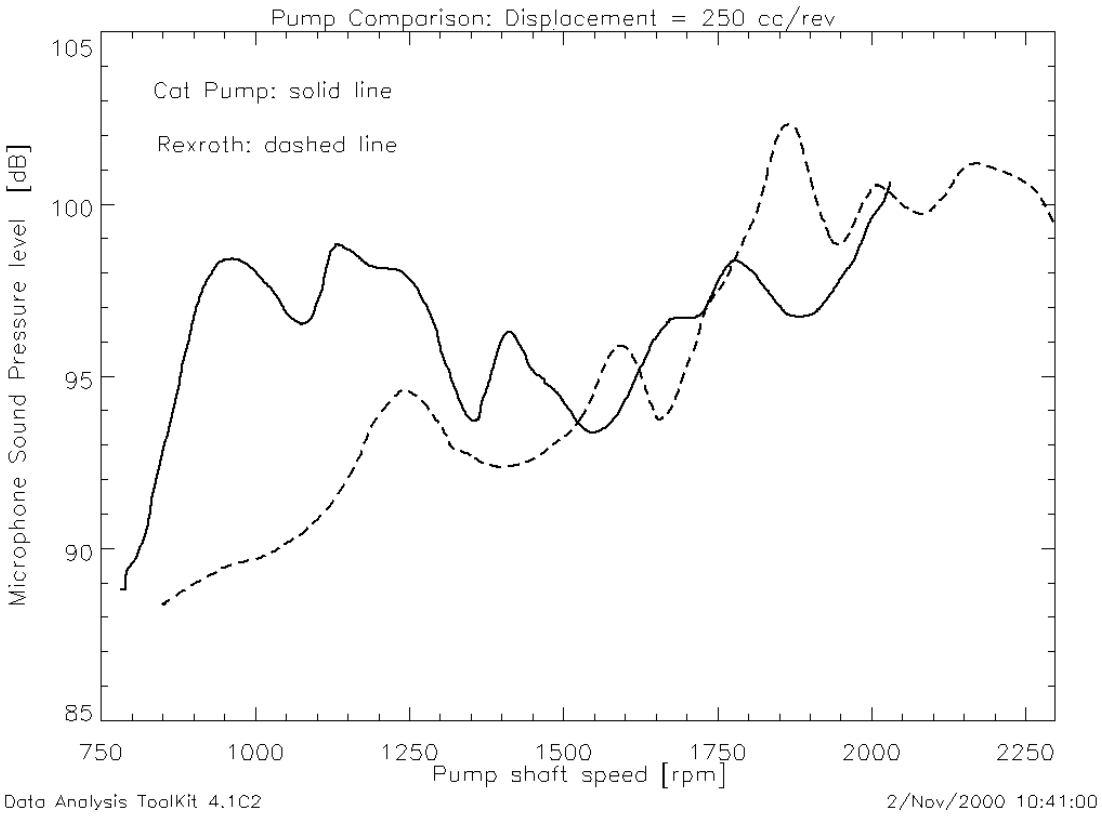

Figure 1-5 Comparison of pump sound pressure levels
(Source: Landsberger [15])

Figure 1-5 compares the sound level of two different pumps during a speed sweep at maximum displacement and high discharge pressure. It can be seen that the sound level for the pump shown in the solid line has a prominent high noise operating region from 1000 to 1250 RPM. The investigation looked at that operating region as an opportunity to improve the pump performance. As mentioned earlier, it is important to know from where the noise was radiating, was it driven or resonant, and what was causing the radiating surface to vibrate?

There are usual suspects for the source of the sound. With a hydraulic pump the case of the pump can vibrate, radiating sound. Also, the pulsations in the fluid, transmitted through the hydraulic hoses, at a mounting point can cause other surfaces to vibrate, radiating sound. Among other parameters case vibration and sound were recorded. A first-look observation of the waveforms of the sound pressure and fluid pressure (not shown here) supported the popular theory of fluid pulsation as the main source of noise but a look at the excitation levels for the entire sweep told a different story.

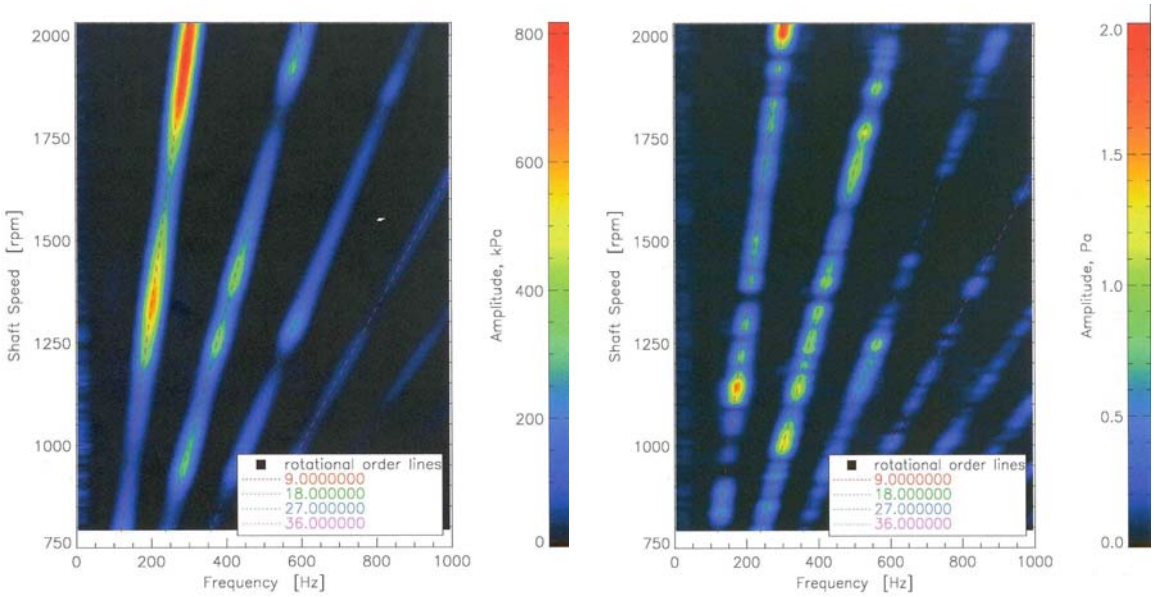

Figure 1-6 Discharge delta pressure and sound pressure
(Source: Landsberger [15])

The plots in Figure 1-6 show excitation levels of the discharge fluid pressure on the left and the sound pressure on the right. The plot has frequency on the horizontal axis

and shaft velocity on the vertical axis. The plot is made by taking a DFT of segments of the time signal from the speed sweep. The lines radiating from the lower left are areas of higher intensity that correspond to the orders of the pump rotation. The order being cycles per revolution as compared to cycles per unit time. The first order line is the 9th order which corresponds to the fundamental piston pass frequency as the pump has nine pistons. Higher intensities are shown in yellow and red progressively. One can see on the right side plot of the sound pressure, the high noise region between 1000 and 1250 RPM in the 9th and 18th order lines. In contrast, the discharge pressure is relatively calm there.

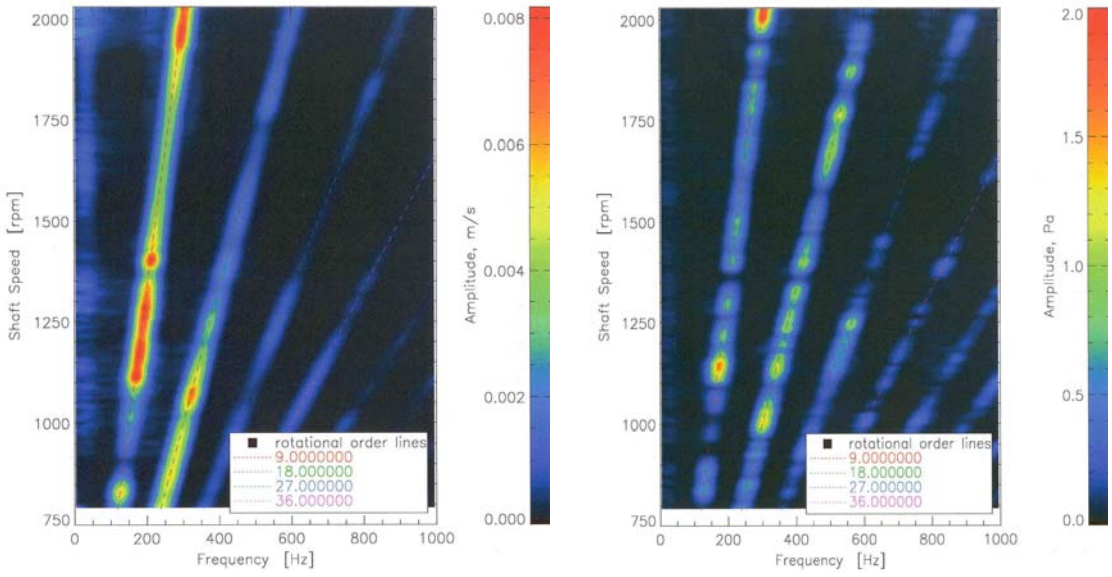

Figure 1-7 Case vibration and sound pressure
(Source: Landsberger [15])

The plots in Figure 1-7 show excitation levels of the case vibration on the left and the sound pressure on the right. Here we see close correlation between the high levels of

both plots. These plots then indicate that case vibration is likely to be the cause of the noise. Hence, at excitation level, waveform of the case acceleration confirmed to the waveform of the sound pressure. Subsequently, it was also proved that case vibration is driven by the input shaft velocity fluctuations. The shaft velocity fluctuations also show a peak (not shown here) that correlate very well with sound pressure. The fluid pressure fluctuation, however, do not. A follow on test showed an in-phase correlation between velocity fluctuations and torque fluctuations. This then showed a path of torque fluctuations to velocity fluctuations to case vibration to sound emission. The fluid pressure fluctuations did not have any physical path like that and are therefore not a significant cause of the case noise. The fluid fluctuations are normally a significant cause of noise in the structure where a hose or valve is hard mounted to the frame.

This experiment suggests a possible connection between the input shaft torque ripple and pump noise. The research conducted by this author is based on this very important conclusion that the torque ripple, and not the flow ripple, is the main source of the noise in pumps. Hence, the goal is to find out new methods to reduce the torque ripple amplitude. Also, by attenuating the amplitude of the torque ripple, the other vibrational characteristics of the pump will also be reduced thereby providing a machine that operates more smoothly with less noise generation.

1.5 Dissertation Outline

This remaining dissertation is organized into 8 chapters in following order. Chapter 2 describes composition and function of a typical axial piston pump with detailed

descriptions of major components such as pistons, swash plate, cylinder block etc. It basically familiarizes the reader with basic geometry of the pump and nomenclatures used in this work. Again this description is helpful for the kinematic and dynamic analysis given in Chapter 3. A second pump design that has two rotating groups of pistons on a common shaft and popularly known as the tandem pump, is also described. So, with the laws of motion, Chapter 3 details derivations of governing equations for pump components like cylinder block, swash plate, pistons, slippers etc. Chapter 4 presents numerical and closed form approximation for the pressure within a single piston-bore. Important phenomena like pressure undershoot and overshoot are also described. Chapter 5 details the derivation of the pump shaft torque for one and two rotating groups. It also includes two new methods to reduce pump noise from its current level. The relationship between the flow ripple problem and torque ripple problem is given in Chapter 6. This is very important in establishing the fact that this work is valid for even the case when the source of noise is considered to be the pump flow ripple instead of torque ripple. Chapter 7 presents and discusses analytical and numerical results for a pump with one rotating group of pistons for continuous swash plate adjustment method. Chapter 8 presents and discusses analytical and numerical results for a tandem pump design with optimal index angle. Chapter 9 summarizes the important conclusions and limitation of this work and some ideas that could be explored to continue this project. Finally, appendix A includes a numerical code as described in Chapter 5.

CHAPTER 2. HYDROSTATIC PISTON PUMP: COMPONENT DESCRIPTION

2.1 Introduction

This chapter introduces the reader with the basic configuration of an axial piston swash plate type hydrostatic pump. The functions, the basic geometry of the pump and other important design features are described for a few important components. It also familiarizes the reader with the nomenclatures used in this work. The tandem pump design with two rotating groups of pistons on a common shaft is also discussed. The descriptions prepare the reader for the kinematic analysis and subsequent discussion presented in later chapters. This chapter is based on the discussion presented by Manring [16] and Damtew [17].

2.2 Introduction to Hydrostatic Pump

A hydraulic pump converts rotating shaft power into fluid power. The pump does not create system pressure, since pressure can be created only by a resistance to the flow. This restriction is normally the work accomplished by the hydraulic system, but can also be restrictions of lines, fittings, and valves within the system. Thus the pressure is controlled by the load imposed on the system or the action of a pressure-regulating device. There are two ways to classify pumps e.g. a) hydrodynamic pumps (non-positive displacement pump and b) hydrostatic pumps (positive displacement pump). The positive-displacement pump delivers a definite volume of fluid for each cycle of

pump operation, regardless of the resistance offered, provided the capacity of the power unit driving the pump is not exceeded. If the outlet of a positive-displacement pump were completely closed, the pressure would instantaneously increase to the point at which the unit driving the pump would stall or something would break. Since, this work deals with a piston type hydrostatic pump, next sections are dedicated to describing the piston pump configuration, typical components and functions of each component in broad sense.

2.3 General Pump Configuration

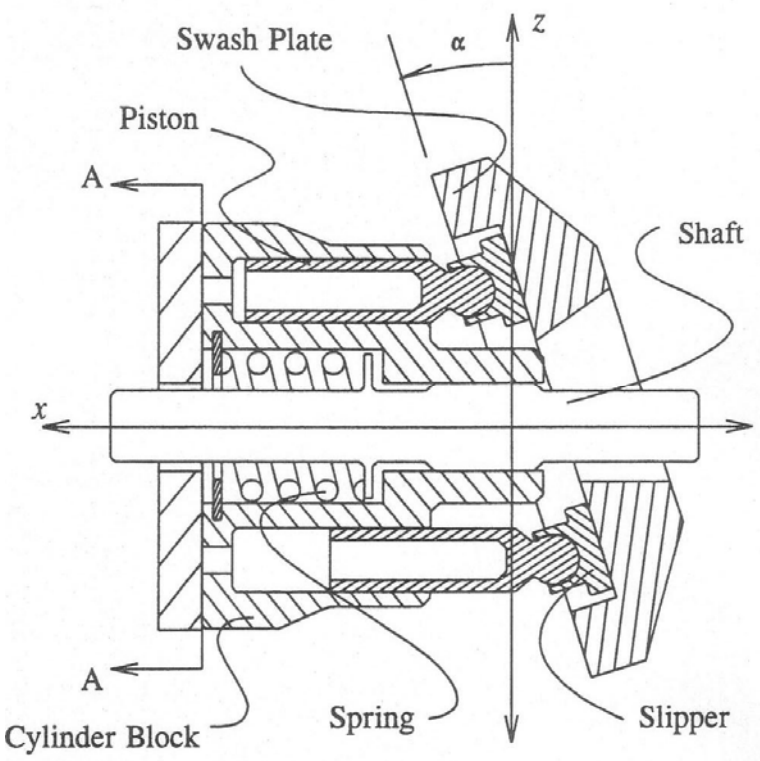

Figure 2-1 Axial piston pump – general configuration
(Source: Manring [16])

In axial piston pumps of the in-line type, where the cylinders and the drive shaft are parallel as shown in Figure 2-1, the pistons are nested in a circular array within a common cylindrical block at equal intervals about the *x*-axis. Here, the reciprocating motion is created by the swash plate which is sometimes referred as cam plate or wobble plate as well. The swash plate lies in a plane that cuts across the center line of the drive shaft and cylinder barrel and does not rotate. In a fixed-displacement pump, the swash plate will be rigidly mounted in a position so that it intersects the center line of the cylinder barrel at an angle approximately 18^o from perpendicular. Variable-delivery axial piston pumps are designed so that the angle that the swash plate makes with a perpendicular to the center line of the cylinder barrel may be varied from 0 to 18^o to one or both sides.

A cylinder block is held tightly against a valve plate using the force of compressed cylinder-block springs. The shaft, piston, cylinder block, and swash plate together is also referred to as the rotating group or assembly. A thin film of oil separates the valve plate from the block forming a hydrodynamic bearing between the two parts. The valve plate provides a bearing surface for the cylinder block and is also used to separate the discharge and intake ports that are more crudely defined by the manifold (not shown in Figure 2-1). A ball and socket joint connects the base of each piston to a slipper, which are kept in reasonable contact with the swash plate. Hydrostatic and hydrodynamic lubrication mechanisms are used to provide adequate bearing conditions between the slippers and the swash plate.

While the valve plate is held in a fixed position, the splined input shaft is used to drive the cylinder block about the *x*-axis at a constant angular velocity ω. When the drive shaft is rotated, it rotates the pistons and the cylinder block with it. The length of the piston stroke is proportional to the angle that the swash plate is set from perpendicular to the center line of the cylinder barrel. The swash plate placed at an angle causes the pistons to move back and forth in the cylinder block while the shaft, piston, cylinder block and swash plate rotate together. As the pistons reciprocate in the cylinder block, they pass over the intake and discharge ports in succession causing fluid to enter the piston chamber, compress and discharge at the high pressure side. This motion repeats itself for each pump revolution and the basic task of pumping fluid is then accomplished.

2.4 Port-Plate Geometry

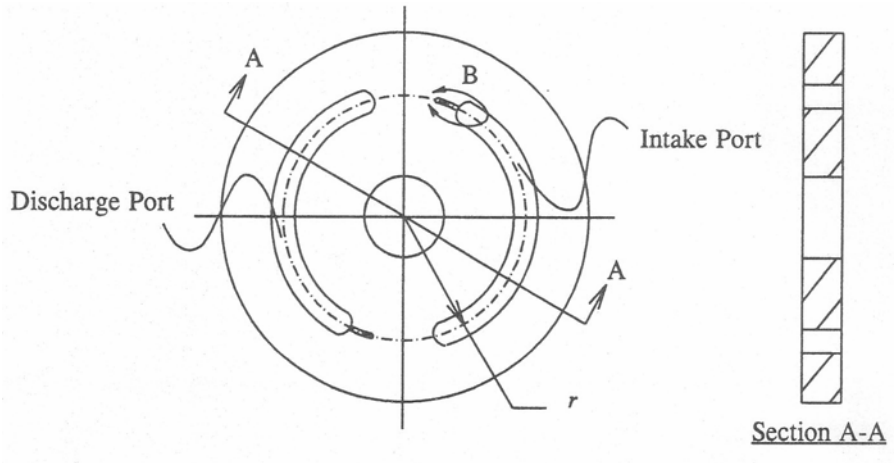

Figure 2-2 Port-plate Geometry
(Source: Manring [16])

As described earlier, axial piston pumps now come with relief grooves at the leading edges of the inlet and outlet ports as shown in Figure 2-2. They eliminate cylinder pressure undershoot at top dead center (TDC) and overshoot at bottom dead center (BDC) which help reduce the noise level. Even though, it is not very difficult to optimize pump geometry in order to reduce flow ripple for one specific operation condition, if the operational conditions are changed, the pump geometry will no longer guarantee the best flow ripple. Hence optimal slot geometries depend on the pump operating conditions.

2.5 Cylinder-Block Geometry

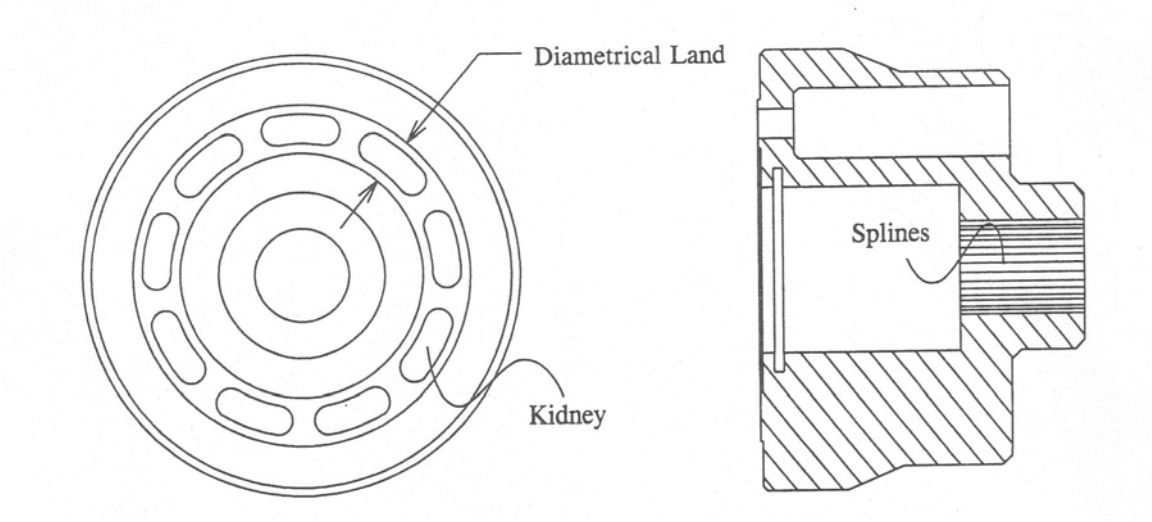

Figure 2-3 Cylinder-block geometry
(Source: Manring [16])

The rotating group of the axial piston pump results from an arrangement of a circular array of pistons in the common cylinder-block which is driven by the shaft

(connected by splines on the shaft). The opening of each piston chamber is designed to match the shape of the port-plate ports as shown in Figure 2-3. Due to inherent shape of these openings, they are often referred to as ‘kidneys’. The kidneys are contained within an elevated diametral-land which is machined onto the face of the cylinder block. The function of the land is to provide sealing and a running surface between the port-plate and the block.

2.6 Piston-Slipper Geometry

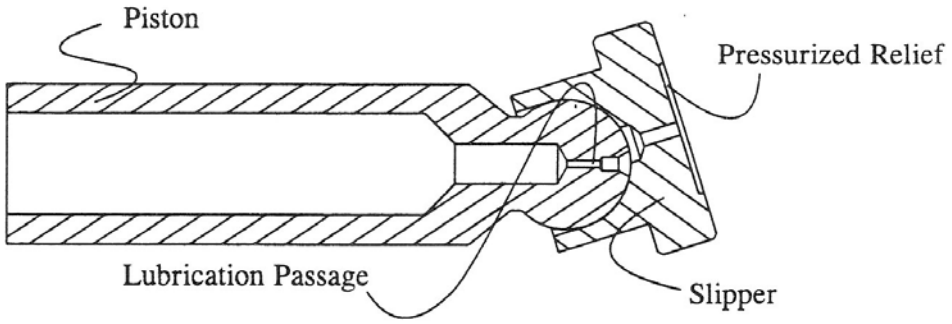

Figure 2-4 Piston-slipper geometry
(Source: Manring [16])

Typically, solid pistons represent the simplest and cheapest design however they add higher inertia forces especially at high speed. Since a hollow piston possesses high dead volume which leads to higher compression losses, hollow piston filled with plastic materials render pistons with lower dead volume and compression losses. The welded capped-piston is one the most modern design solution. As described earlier, a ball and

socket joint connects the base of each piston to a slipper as shown in Figure 2-4. The slippers are kept in reasonable contact with the swash plate. Figure 2-4 also shows a small lubrication passage to provide lubrication to the ball and socket joint and the slipper-swash plate surface. A shallow relief is cut into the running face of the slipper to provide pressurized fluid in the area generating a lifting force between the slipper and the swash plate.

2.7 Shaft Geometry

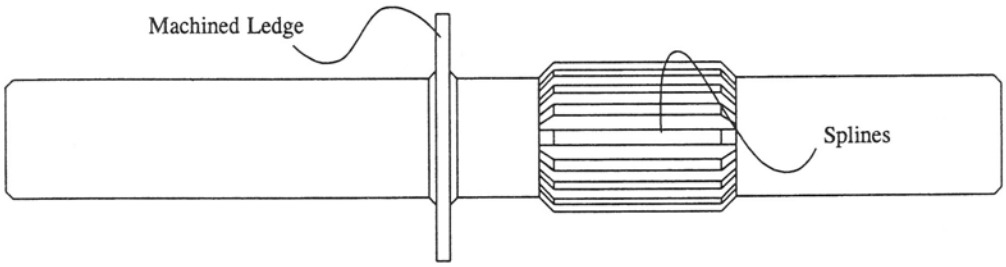

Figure 2-5 Shaft geometry
(Source: Manring [16])

Two main functions that the shaft performs in the axial piston pumps are transmitting the torque to the cylinder-block via a spline connection and maintaining the alignment of the cylinder-block with the port-plate. The shaft is supported at both ends by frictionless bearings. As shown in Figure 2-5, a typically shaft will have splines that run parallel to the shaft and connects the cylinder block to the shaft. The torque it transmits to the cylinder-block is the main focus of this work and will be described in later chapters.

2.8 Tandem Design: General Pump Configuration

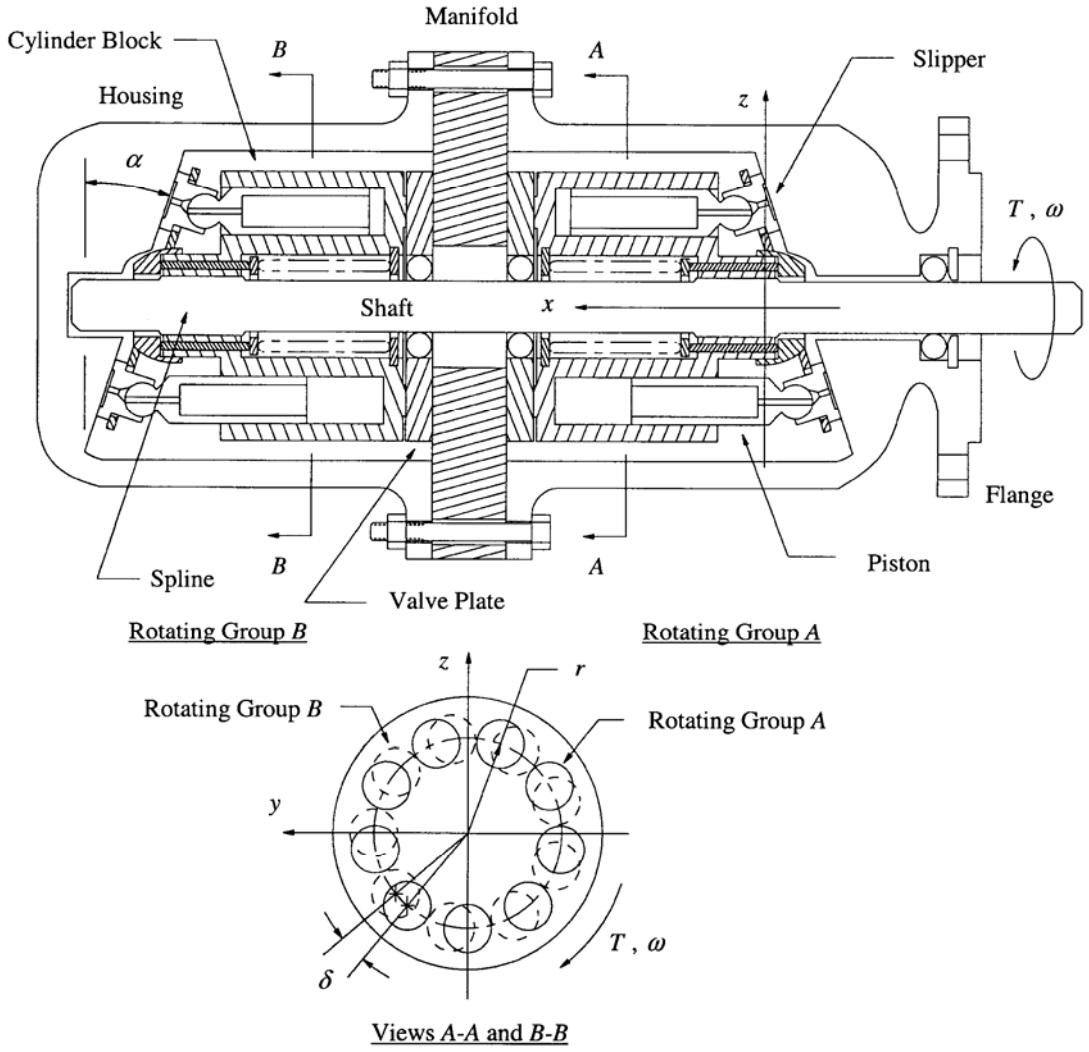

Figure 2-6 Tandem pump configuration
(Source: Manring and Mehta [2])

Figure 2-6 shows a schematic of a tandem pump design [2]. As shown in this figure, the tandem pump is comprised of two identical rotating groups that are designed to pump fluid through a mechanism that will be described shortly. Each rotating group in

Figure 2-6 is used to produce a specified volumetric displacement per revolution of the input shaft. Used together, these two rotating groups produce twice the volumetric flow rate as compared to a single rotating group.

The rotating groups in Figure 2-6 are connected to each other using a single shaft and a manifold. The shaft is used to turn both rotating groups at an angular velocity ω while the manifold provides a common intake and discharge port for both rotating groups. The torque on the input shaft of the tandem pump is shown in Figure 2-6 by the symbol T. Again, the attenuation of the magnitude of this torque is the main goal of this work. The flange in Figure 2-6 is used to bolt the tandem pump assembly to a prime mover such as an electric motor or an internal combustion engine. Each rotating group consists of several pistons that are evenly spaced within a circular array about the centerline of the cylinder block. This centerline of the cylinder block is shown in by the *x*-axis which also corresponds to the centerline of the input shaft. The shaft and the cylinder blocks are connected to each other through the use of a spline that transmits torque and angular displacement from the shaft to the cylinder blocks. The pumping mechanism described earlier for one rotating group is identical for both rotating groups shown in Figure 2-6 and the flow contribution from each rotating group is added together to achieve the net discharge flow for the assembled tandem pump design.

Views *A*-*A* and *B*-*B* of Figure 2-6 show a sectional view taken through the cylinder block of Rotating Groups *A* and *B* respectively. This view shows that when the tandem pump is assembled, the discrete pumping elements for each rotating group may be indexed slightly relative to each other. This index angle is shown in Figure 2-6 by the

symbol δ. In other words the angular position of the pistons may or may not be coincident with one another depending upon where the shaft spline connection happens to place each rotating group. As it turns out, this angular difference δ between the two rotating groups shown in View *A-A* and *B-B* of Figure 2-6 is very important in determining the magnitude and frequency of the torque ripple that is generated on the pump shaft and it will be discussed in detail in Chapter 5.

2.9 Summary

This chapter introduced the reader with a few of the most important components of a piston pump. The designs have been described in general sense noting that the individual components' design may vary based on the pump configuration and output requirements. Also components with lack of generality have been excluded but will be introduced later in this work if needed. Next, Chapter 3 is dedicated to describing the kinematic analysis of the components described in Chapter 2.

CHAPTER 3. MECHANICAL ANALYSIS

3.1 Introduction

In this chapter, the governing equations of the cylinder block, the pistons and the slippers of an axial piston swash plate type hydrostatic pump are derived by relating the kinematics of each component to the forces that act upon them using the laws of mechanics. In the concluding section of this chapter, the equations that describe significant physical quantities are written in their most primitive forms for the cylinder block, the piston and the slippers. Any simplifications to these quantities based upon symmetry are also performed. This analysis has been based on similar analysis by Manring [16] and Damtew [17] and modified for this work.

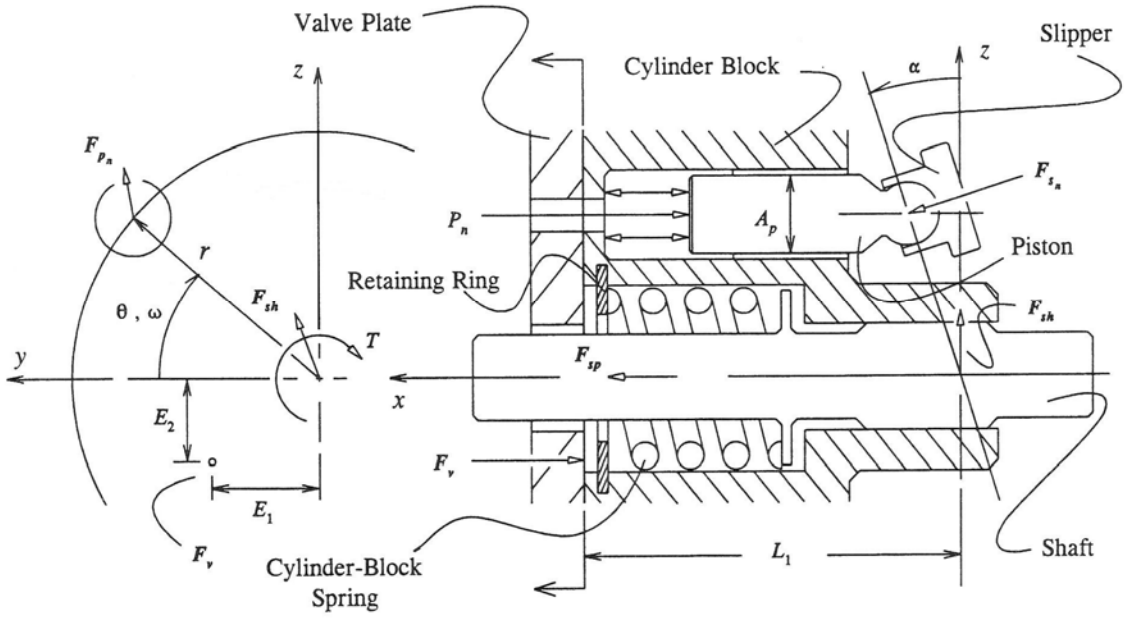

Figure 3-1 A sparse schematic of forces that coexist within the axial-piston pump (Source: Modified from Manring [16])

Figure 3-1 introduces the reader to several forces that coexist within the axial piston pump under normal operating conditions. However, only the forces pertinent to the analysis and not all the forces within the machine are represented here. More detail will be added to this figure as the analysis in this chapter progresses.

3.2 Cylinder Block Free-Body Diagram

Figure 3-2 shows the free-body diagram of the cylinder block. The forces acting on the cylinder block come from the block spring ($\boldsymbol{F}_{sp}$), the reaction of the shaft ($\boldsymbol{F}_{sh}$), the reaction of the valve plate ($\boldsymbol{F}_{v}$), the spring force from the piston-bore springs within each piston-bore ($\boldsymbol{F}_{B_n}$) the clamping force from the pressure within each piston-bore ($\boldsymbol{F}_{c_n}$), the reaction of the piston against the side-wall of each piston-bore ($\boldsymbol{F}_{p_n}$). Using standard mechanical analysis, these forces are summed and set equal to the translation inertia of the cylinder block, $M_b \ddot{\boldsymbol{X}}_b$ to derive the following equation of motion as,

$$M_b \ddot{\boldsymbol{X}}_b = \boldsymbol{F}_{sp} + \boldsymbol{F}_{sh} + \boldsymbol{F}_{v} + \sum_{n=1}^{N} \boldsymbol{F}_{B_n} + \sum_{n=1}^{N} \boldsymbol{F}_{c_n} + \sum_{n=1}^{N} \boldsymbol{F}_{p_n}. \tag{3-1}$$

In general, each force on the cylinder block generates a corresponding moment about the location of the shaft reaction. Summing these moments, and setting them equal to the time rate of change of angular momentum of the cylinder block, $\boldsymbol{I}_b \ddot{\boldsymbol{\Theta}}_b + \dot{\boldsymbol{\Theta}}_b \times \boldsymbol{I}_b \dot{\boldsymbol{\Theta}}_b$, it can be shown that

$$\boldsymbol{I}_b \ddot{\boldsymbol{\Theta}}_b + \dot{\boldsymbol{\Theta}}_b \times \boldsymbol{I}_b \dot{\boldsymbol{\Theta}}_b = \boldsymbol{M}_{sp} + \boldsymbol{M}_{sh} + \boldsymbol{M}_v + \sum_{n=1}^{N} \boldsymbol{M}_{B_n} + \sum_{n=1}^{N} \boldsymbol{M}_{c_n} + \sum_{n=1}^{N} \boldsymbol{M}_{p_n} . \qquad (3\text{-}2)$$

Equations (3-1) and (3-2) provide the basis for determining the equations of motion for the cylinder block. The following subsection will examine the components of equations (3-1) and (3-2) in closer details.

3.2.1 Cylinder Block Kinematics and Inertia

Figure 3-3 shows the cylinder block forced against the valve plate by the cylinder block spring which is compressed between the retaining ring mounted within the cylinder block and the machined ledge on the shaft. Furthermore, a pressure force exists within each piston-bore that clamps the cylinder block against the valve plate. Due to these constraints, under normal operating conditions, the cylinder block is not able to move in the *x*-direction. Furthermore, the shaft passing through the center of the cylinder block keeps the cylinder block from moving in either the *y* or *z*-directions; therefore the translational inertia of the cylinder block is given by ,

$$M_b \ddot{\boldsymbol{X}}_b = 0 . \qquad (3\text{-}3)$$

In this analysis, it is assumed that the cylinder block rotates about the *x*-axis at a constant angular speed, ω (i.e. there is no angular acceleration in the *x*-direction). Since, under normal operating conditions, the face of the cylinder block remains reasonably parallel with the face of the valve plate, there is no angular acceleration in either the *y* or

z-directions. Due to symmetry there are no products of inertia for the cylinder block and therefore time rate of change of angular momentum of the cylinder block is written as,

$$\boldsymbol{I}_b \ddot{\boldsymbol{\Theta}}_b + \dot{\boldsymbol{\Theta}}_b \times \boldsymbol{I}_b \dot{\boldsymbol{\Theta}}_b = 0 \,. \tag{3-4}$$

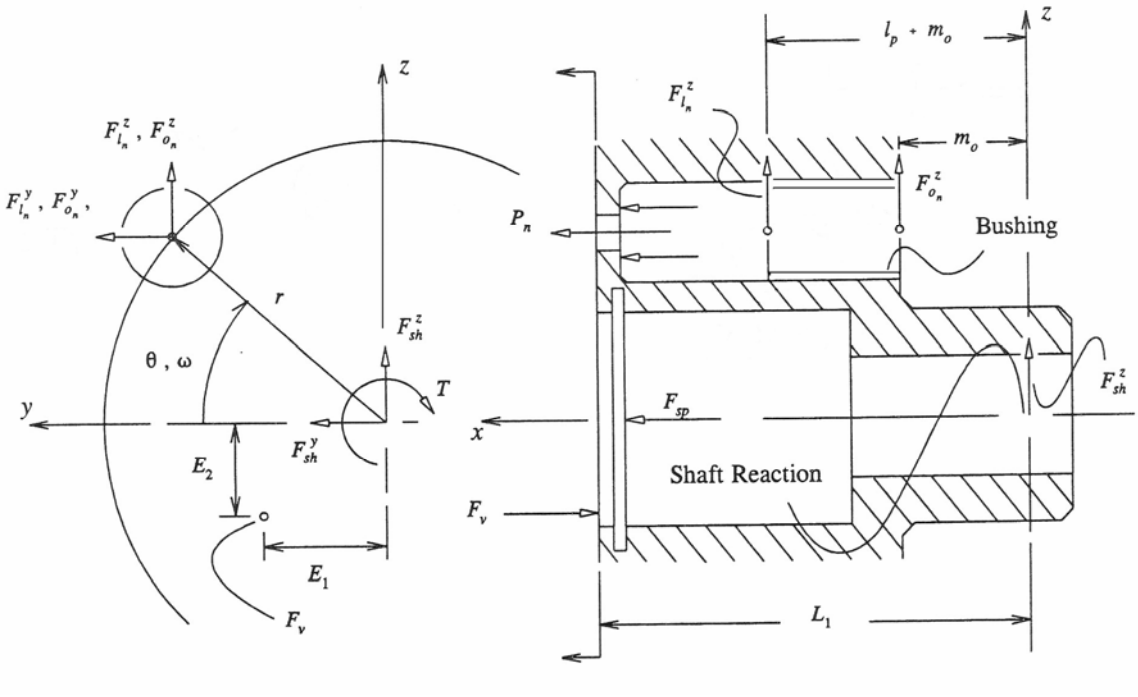

Figure 3-2 Free-body diagram of a cylinder block
(Source: Modified from Manring [16])

3.2.2 Cylinder Block Spring Force

As previously mentioned, the cylinder block spring is compressively assembled between a retaining ring, mounted within the cylinder block and a machined ledge on the shaft. The cylinder block spring is used to hold the cylinder block against the valve plate and acts only in the x-direction. Hence, this force is written as,

$$\boldsymbol{F_{sp}} = F_{sp}\,\hat{\boldsymbol{i}} + 0\,\hat{\boldsymbol{j}} + 0\,\hat{\boldsymbol{k}}\ , \tag{3-5}$$

where $\boldsymbol{F_{sp}}$ is the assembled load of the cylinder block spring. The distance of this force away from the shaft reaction is given by $L_1\,\hat{\boldsymbol{i}} + 0\,\hat{\boldsymbol{j}} + 0\,\hat{\boldsymbol{k}}$. Taking the cross product of this distance with equation (3-5) it can be seen that the net moment generated about the shaft reaction from the block spring is

$$\boldsymbol{M_{sp}} = 0\ . \tag{3-6}$$

3.2.3 Shaft Reaction

The shaft is used to drive the cylinder block about the *x*-axis and to maintain the alignment of the cylinder block with the valve plate. The connection between the cylinder block and the shaft is accomplished through a set of splines that run parallel to the shaft, as such the spline interaction allows for no resultant force along the *x*-axis. In general, the forces from the shaft acting on the cylinder block may be written as,

$$\boldsymbol{F_{sh}} = 0\,\hat{\boldsymbol{i}} + F_{sh}{}^{y}\,\hat{\boldsymbol{j}} + F_{sh}{}^{z}\,\hat{\boldsymbol{k}}\ . \tag{3-7}$$

Since moments are conventionally being summed about the shaft reaction for this research, it is clear that $\boldsymbol{F_{sh}}$ exerts no moment about itself, however, the torque on the cylinder block, $\boldsymbol{T}$ is present at this location and therefore the net moment on the cylinder block, generated by the shaft is given by,

$$\boldsymbol{M_{sh}} = T\,\hat{\boldsymbol{i}} + 0\,\hat{\boldsymbol{j}} + 0\,\hat{\boldsymbol{k}}\ . \tag{3-8}$$

This torque is the quantity of interest for this research and will be discussed in detail in subsequent chapters.

3.2.4 Valve Plate Reaction

The valve plate is set rigidly within the pump and exerts a keeping force on the cylinder block in the negative *x*-direction. In general, this force is distributed over the contact area between the valve plate and the cylinder block. However for the purpose of this analysis, this force will be treated as a point-load located at the centroid of the actual distributed-load. This force is then written,

$$\boldsymbol{F}_v = -F_v\,\hat{\boldsymbol{i}} + 0\,\hat{\boldsymbol{j}} + 0\,\hat{\boldsymbol{k}}\ . \tag{3-9}$$

From Figure 3-2 it can be seen that the distance of this force away from the shaft reaction is given by $L_1\,\hat{\boldsymbol{i}} + E_1\,\hat{\boldsymbol{j}} - E_2\,\hat{\boldsymbol{k}}$, where E_1 and E_2 locate the centroid of the distributed load between the cylinder block and the valve plate. Taking the cross product of this distance with equation (3-9), the net moment generated on the cylinder block by the valve plate may be expressed as,

$$\boldsymbol{M}_v = 0\,\hat{\boldsymbol{i}} - F_v E_2\,\hat{\boldsymbol{j}} - F_v E_1\,\hat{\boldsymbol{k}}\ . \tag{3-10}$$

3.2.5 Piston-Bore Spring Force

The piston-bore springs are assembled within the piston-bores in a pre-loaded condition and are always in compression. Due to the motion of the pistons within the

piston chambers, the force exerted on the cylinder block by each piston-bore spring is different. The force from the n^{th} piston-bore spring can be given by,

$$\boldsymbol{F}_{\boldsymbol{B}_n} = F_{B_n}\,\hat{\boldsymbol{i}} + 0\,\hat{\boldsymbol{j}} + 0\,\hat{\boldsymbol{k}}\ . \tag{3-11}$$

At any given time, the magnitude of the spring force depends on the position of the piston within the piston chamber. The n^{th} piston-bore spring force can be given as a function of the position of the n^{th} piston-slipper ball-joint center as follows,

$$F_{B_n} = F_{B_o} + k\ x_n\ , \tag{3-12}$$

where F_{B_o} represents the nominal load and k the stiffness of the spring. Equation (3-12) can be also written as,

$$F_{B_n} = F_{B_o} + k\ (e + r\sin(\theta_n))\tan(\alpha) + a\sec(\alpha))\ , \tag{3-13}$$

where $x_n = e + r\sin(\theta_n))\tan(\alpha) + a\sec(\alpha)$ gives the position of the piston. The point of action of the nth piston-bore spring force relative to the origin is given by $L_1\,\hat{\boldsymbol{i}} + y_n\,\hat{\boldsymbol{j}} + z_n\hat{\boldsymbol{k}}$ where (y_n, z_n) is $(r\cos(\theta_n), r\sin(\theta_n))$ and the moment generated by this force is,

$$\boldsymbol{M}_{\boldsymbol{B}_n} = 0\,\hat{\boldsymbol{i}} + F_{B_n}\,z_n\,\hat{\boldsymbol{j}} - F_{B_n}\,y_n\,\hat{\boldsymbol{k}}\ . \tag{3-14}$$

3.2.6 Pressure Clamping Force

The cylinder block is designed so that the pressure within the n^{th} piston-bore forces the block in the positive x-direction. This effect is often called pressure-clamping

because it ‘clamps’ the block onto the valve plate. See Figure 3-2. Because each piston-bore contains fluid under different pressures, each piston-bore exerts a different pressure-clamping force on the cylinder block. For the n^{th} piston-bore the pressure-clamping force may be written as,

$$\boldsymbol{F}_{c_n} = A_b P_n \hat{\boldsymbol{i}} + 0\,\hat{\boldsymbol{j}} + 0\,\hat{\boldsymbol{k}}\ , \tag{3-15}$$

where A_b is the effective pressurized area within a single piston-bore and P_n is the instantaneous pressure within the n^{th} piston-bore. An idealized piston-bore profile (P_n) and a numerical profile is presented in Chapter 4. The distance of the n^{th} clamping force away from the shaft reaction is given by $L_1 \hat{\boldsymbol{i}} + y_n \hat{\boldsymbol{j}} + z_n \hat{\boldsymbol{k}}$. Taking the cross product of this distance with equation (3-15) it may be shown that the moment acting on the cylinder block from the pressure-clamping force within the n^{th} piston-bore is given by,

$$\boldsymbol{M}_{c_n} = 0\hat{\boldsymbol{i}} + A_b P_n z_n \hat{\boldsymbol{j}} - A_b P_n y_n \hat{\boldsymbol{k}}\ . \tag{3-16}$$

3.2.7 Piston Reaction

The piston-bore of the cylinder block is lined with a metal bushing. The reaction forces of the piston within the piston-bore are placed along the centerline of the piston-bore at both the inner and out ends of the bushing. To simplify the analysis, the friction generated at the inner and outer edge of the bushing will be ignored here.

3.2.7.1 Reaction at the Inner Edge of the Bushing

From Figure 3-2 it can be seen that the forces exerted on the inner edge of the n^{th} bushing by the n^{th} piston may be expressed as,

$$\boldsymbol{F}_{l_n} = F_{l_n}{}^{y}\,\hat{\boldsymbol{j}} + F_{l_n}{}^{z}\,\hat{\boldsymbol{k}} \ . \tag{3-17}$$

The distance of the force $\boldsymbol{F}_{l_n}$ from the location of the shaft reaction is given by $(l_p + m_o)\,\hat{\boldsymbol{i}} + y_n\,\hat{\boldsymbol{j}} + z_n\,\hat{\boldsymbol{k}}$. Hence the moment exerted about the shaft reaction by the force F_{l_n} within the n^{th} piston-bore is given by,

$$\boldsymbol{M}_{l_n} = (F_{l_n}{}^{z} y_n - F_{l_n}{}^{y} z_n)\,\hat{\boldsymbol{i}} - (F_{l_n}{}^{z}(l_p + m_o))\,\hat{\boldsymbol{j}} + (F_{l_n}{}^{y}(l_p + m_o))\,\hat{\boldsymbol{k}} \ . \tag{3-18}$$

3.2.7.2 Reaction at the Outer Edge of the Bushing

Similarly, the force exerted on the outer edge of the n^{th} bushing by the n^{th} piston may be expressed as,

$$\boldsymbol{F}_{o_n} = F_{o_n}{}^{y}\,\hat{\boldsymbol{j}} + F_{o_n}{}^{z}\,\hat{\boldsymbol{k}} \ . \tag{3-19}$$

The distance of this force from the location of the shaft reaction is given by $m_o\,\hat{\boldsymbol{i}} + y_n\,\hat{\boldsymbol{j}} + z_n\,\hat{\boldsymbol{k}}$. Hence, the moment exerted about the shaft reaction by the force F_{o_n} within the n^{th} piston-bore is given by,

$$\boldsymbol{M}_{o_n} = (F_{o_n}{}^{z}\, y_n - F_{o_n}{}^{y}\, z_n)\,\hat{\boldsymbol{i}} + (F_{o_n}{}^{z}\, m_o)\,\hat{\boldsymbol{j}} + (F_{o_n}{}^{y}\, m_o)\,\hat{\boldsymbol{k}} \ . \tag{3-20}$$

3.2.7.3 Summary of Piston Reaction

By adding the results of equations (3-17) and (3-19), the net piston force acting on the bushing can be calculated as,

$$\boldsymbol{F}_{\boldsymbol{p_n}} = (F_{o_n}{}^{y} + F_{l_n}{}^{y})\,\hat{\boldsymbol{j}} + (F_{o_n}{}^{z} + F_{l_n}{}^{z})\,\hat{\boldsymbol{k}} \ . \tag{3-21}$$

Similarly, the net moment generated by the n^{th} piston within the n^{th} piston-bore about the shaft reaction is given by,

$$\begin{aligned}\boldsymbol{M}_{\boldsymbol{p_n}} = {} & [(F_{l_n}{}^{z} + F_{o_n}{}^{z})\,y_n - (F_{o_n}{}^{y} + F_{l_n}{}^{y})\,z_n]\,\hat{\boldsymbol{i}} \\ & -[F_{l_n}{}^{z}(l_p + m_o) + F_{o_n}{}^{z} m_o)]\,\hat{\boldsymbol{j}} + (F_{l_n}{}^{y}(l_p + m_o) + F_{o_n}{}^{y} m_o)]\,\hat{\boldsymbol{k}} \ .\end{aligned} \tag{3-22}$$

3.2.8 Summary of Cylinder Block Reactions

Collecting the forces acting on the cylinder block by substituting equations (3-3), (3-5), (3-7), (3-9), (3-15), (3-21) into equation (3-1), the forces exerted on the cylinder block are summarized by,

$$\begin{aligned}0 = {} & (F_{sp} - F_v + \sum_{n=1}^{N}(F_{B_n} + A_b\,P_n))\,\hat{\boldsymbol{i}} + (F_{sh}{}^{y} + \sum_{n=1}^{N}(F_{l_n}{}^{y} + F_{o_n}{}^{y}))\,\hat{\boldsymbol{j}} \\ & + (F_{sh}{}^{z} + \sum_{n=1}^{N}(F_{l_n}{}^{z} + F_{o_n}{}^{z}))\,\hat{\boldsymbol{k}} \ .\end{aligned} \tag{3-23}$$

Similarly, by substituting equations (3-4), (3-6), (3-8), (3-10), (3-16) and (3-22) into equation (3-2), the moments exerted on the cylinder block are summarized as in equation (3-24). Equations (3-23) and (3-24) contain quantities that depend upon the behavior of

the pistons. In following section, the influence of the pistons will be analyzed in closer detail.

$$
\begin{aligned}
0 = & \left[T + \sum_{n=1}^{N} ((F_{l_n}{}^{y} + F_{o_n}{}^{y})\, y_n - (F_{l_n}{}^{y} + F_{o_n}{}^{y}) z_n \right] \hat{\boldsymbol{i}} + \\
& \left[\sum_{n=1}^{N} (A_b\ P_n\ z_n + F_{B_n}\, z_n - F_{l_n}{}^{z} (l_p + m_o) - F_{o_n}{}^{z}\ m_o - F_v\ E_2 \right] \hat{\boldsymbol{j}} + \\
& \left[\sum_{n=1}^{N} (A_b\ P_n\ y_n - F_{B_n}\, y_n - F_{l_n}{}^{y} (l_p + m_o) - F_{o_n}{}^{y}\ m_o - F_v\ E_1 \right] \hat{\boldsymbol{k}}\ .
\end{aligned}
\tag{3-24}
$$

3.3 Piston Free-Body Diagram

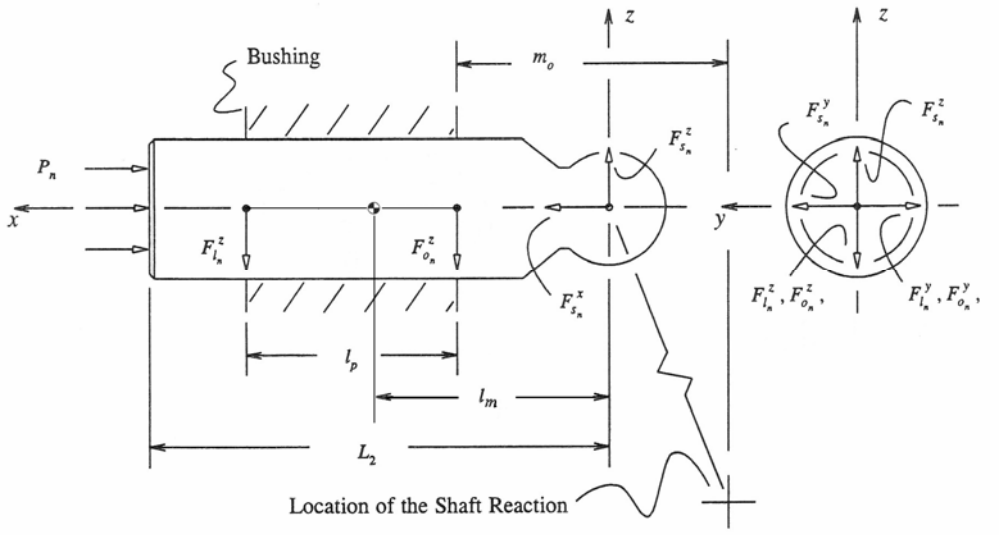

Figure 3-3 Free-body diagram of a single piston
(Source: Modified from Manring [16])

Figure 3-3 shows the free-body diagram of a single piston. The forces acting on the n^{th} piston come from the reaction of the n^{th} slipper at the piston/slipper ball-joint ($\boldsymbol{F}_{s_n}$),

the equal and opposite reaction of the piston against the cylinder block ($-\boldsymbol{F}_{p_n}$), the equal and opposite reaction of the piston-bore spring force acting on the cylinder block ($-\boldsymbol{F}_{B_n}$) and the pressure within the n^{th} piston-bore acting on the face of the piston ($\boldsymbol{F}_{pr_n}$). Summing these forces and setting them equal to the inertia of the piston, $M_p \ddot{\boldsymbol{X}}_{p_n}$ give,

$$M_p \ddot{\boldsymbol{X}}_{p_n} = \sum_{n=1}^{N} (\boldsymbol{F}_{s_n} - \boldsymbol{F}_{p_n} - \boldsymbol{F}_{B_n} + \boldsymbol{F}_{pr_n}) \,. \tag{3-25}$$

In general, each force on the piston generates a corresponding moment about the mass-center of the piston. Summing these moments and setting them equal to the time rate-of-change of angular momentum of the piston yields,

$$\boldsymbol{I}_p \ddot{\boldsymbol{\Theta}}_{p_n} + \dot{\boldsymbol{\Theta}}_{p_n} \times \boldsymbol{I}_p \dot{\boldsymbol{\Theta}}_{p_n} = \sum_{n=1}^{N} (\boldsymbol{M}_{s_n} + \boldsymbol{M}_{p_n} + \boldsymbol{M}_{B_n} + \boldsymbol{M}_{pr_n}) \,. \tag{3-26}$$

Equation (3-25) and (3-26) provide a basis for fully determining the equations that describe the behavior of a single piston.

3.3.1 Piston Kinematics and Inertia

From geometry, it can be shown that the position of the n^{th} piston is given by,

$$\boldsymbol{X}_{p_n} = (x_n + l_m)\,\hat{\boldsymbol{i}} + (y_n)\,\hat{\boldsymbol{j}} + (z_n)\,\hat{\boldsymbol{k}} \,. \tag{3-27}$$

where (x_n, y_n, z_n) is $((e + r\sin(\theta_n))\tan(\alpha) + a\sec(\alpha), \cos(\theta_n), \sin(\theta_n))$. Differentiating equation with respect to time twice and multiplying this result by the mass of a single piston, the final translational inertia of the piston is given by

$$M_p \ddot{\boldsymbol{X}}_{p_n} = M_p \ddot{x}_n \hat{\boldsymbol{i}} + M_p \ddot{y}_n \hat{\boldsymbol{j}} + M_p \ddot{z}_n \hat{\boldsymbol{k}} \ . \tag{3-28}$$

However, due to the constraining nature between the piston and the piston-bore, and due to the symmetry of the piston time rate of change of angular momentum is,

$$\boldsymbol{I}_p \ddot{\boldsymbol{\Theta}}_{p_n} + \dot{\boldsymbol{\Theta}}_{p_n} \times \boldsymbol{I}_p \dot{\boldsymbol{\Theta}}_{p_n} = 0 \ . \tag{3-29}$$

3.3.2 Slipper Reaction

The slipper is connected to the spherical end of the piston using a forming process called swaging. The final result of this process is a connection that allows for three degrees of rotational freedom and zero degrees of a translational freedom within the ball joint. In general, the forces exerted on the piston by the slipper may be express as,

$$\boldsymbol{F}_{s_n} = F_{s_n}{}^x \hat{\boldsymbol{i}} + F_{s_n}{}^y \hat{\boldsymbol{j}} + F_{s_n}{}^z \hat{\boldsymbol{k}} \ . \tag{3-30}$$

From geometry, it can be shown that the distance of this force from the mass-center of the piston is given by $-l_m \hat{\boldsymbol{i}} + 0 \hat{\boldsymbol{j}} + 0 \hat{\boldsymbol{k}}$. Taking the cross product of this distance with equation (3-30), the moment generated by the slipper reaction at the ball of the piston is given by,

$$\boldsymbol{M}_{s_n} = 0 \hat{\boldsymbol{i}} + (F_{s_n}{}^z \ l_m) \hat{\boldsymbol{j}} - (F_{s_n}{}^y \ l_m) \hat{\boldsymbol{k}} \ . \tag{3-31}$$

3.3.3 Piston Reaction

The force and moment generated on the cylinder block by the piston also exerts an equal and opposite force and moment against the piston itself. These quantities are already described in section 3.2.7. The point of action of the force at the inner edge of the bushing is given by the expression $(m_o + l_p - (l_m + x_n))\,\hat{\boldsymbol{i}} + 0\,\hat{\boldsymbol{j}} + 0\,\hat{\boldsymbol{k}}$ while the point of action of the force at the outer edge of the bushing is given by the expression $(m_o - (l_m + x_n))\,\hat{\boldsymbol{i}} + 0\,\hat{\boldsymbol{j}} + 0\,\hat{\boldsymbol{k}}$. Taking the cross product of these distances with the negative of equations (3-17) and (3-19) and adding them the net moment generated by these forces is given as,

$$\begin{aligned}\boldsymbol{M}_{\boldsymbol{p_n}} = 0\,\hat{\boldsymbol{i}} + [(F_{l_n}{}^{z} + F_{o_n}{}^{z})(m_o - (l_m + x_n)) + F_{o_n}{}^{z} l_p]\,\hat{\boldsymbol{j}} \\ -[(F_{l_n}{}^{y} + F_{o_n}{}^{y})(m_o - (l_m + x_n)) + F_{o_n}{}^{y} l_p]\,\hat{\boldsymbol{k}}\ .\end{aligned} \tag{3-32}$$

3.3.4 Piston-Bore Spring Force

The equal and opposite piston-bore spring force given in equation (3-11) acts on the n^{th} piston. Since the line of action of this force passes through the mass-center of piston, it does not create any moment about the piston mass-center. Hence,

$$\boldsymbol{M}_{\boldsymbol{B_n}} = 0\ . \tag{3-33}$$

3.3.5 Piston-Bore Pressure Force

The pressure acting on the face of the piston within the bore tends to drive the piston in the negative *x*-direction. This force is simply given as,

$$\boldsymbol{F}_{pr_n} = -A_p\ P_n\,\hat{\boldsymbol{i}} + 0\,\hat{\boldsymbol{j}} + 0\,\hat{\boldsymbol{k}}\ . \tag{3-34}$$

Since, the line of action of this force passes through the mass-center of the piston; the moment exerted about the mass-center of the piston due to the piston-bore pressure on the face of the n^{th} piston is given by,

$$\boldsymbol{M}_{pr_n} = 0\,. \tag{3-35}$$

3.3.6 Summary

By substituting the results of equations (3-28), (3-30), (3-21), (3-11) and (3-34) into equation (3-25) the net force acting on the n^{th} piston may be written as,

$$\begin{aligned} &M_p\,\ddot{x}_n\,\hat{\boldsymbol{i}} + M_p\,\ddot{y}_n\,\hat{\boldsymbol{j}} + M_p\,\ddot{z}_n\,\hat{\boldsymbol{k}} = \\ &(F_{s_n}{}^x - A_p\,P_n - F_{B_n})\,\hat{\boldsymbol{i}} + (F_{s_n}{}^y - F_{l_n}{}^y - F_{o_n}{}^y)\,\hat{\boldsymbol{j}} + (F_{s_n}{}^z - F_{l_n}{}^z - F_{o_n}{}^z)\,\hat{\boldsymbol{k}}\ . \end{aligned} \tag{3-36}$$

Similarly by substituting equations (3-29), (3-31), (3-22), (3-14) and (3-35) into equation (3-26) the net moment about the location of the shaft reaction due to the forces acting on the n^{th} piston may be summarized as,

$$\begin{aligned} 0 &= [0]\,\hat{\boldsymbol{i}} \\ &+\Big[l_m\ F_{s_n}{}^z + F_{l_n}{}^z(l_p + m_o - (x_n + l_m)) + F_{o_n}{}^z(m_o - (x_n + l_m))\Big]\,\hat{\boldsymbol{j}} \\ &+\Big[l_m\ F_{s_n}{}^y + F_{l_n}{}^y(l_p + m_o - (x_n + l_m)) + F_{o_n}{}^y(m_o - (x_n + l_m))\Big]\,\hat{\boldsymbol{k}}\ . \end{aligned} \tag{3-37}$$

Equations (3-36) and (3-37) are dependent upon forces that are exerted by the slipper on the n^{th} piston. The following section investigates these forces in detail.

3.4 Slipper Free-Body Diagram

The free-body diagram of a single slipper is shown in Figure 3-4. The forces acting on the slipper come from the mechanical hold-down force exerted on the slipper ($\boldsymbol{F}_{hd}$), the equal and opposite reaction of the slipper against the piston ($-\boldsymbol{F}_{s_n}$), the reaction of the swash plate against the slipper ($\boldsymbol{F}_{sw_n}$) and the pressure balance acting between the slipper and the swash plate ($\boldsymbol{F}_{bal_n}$). Summing these forces and setting them equal to the translational inertia of the slipper it can be seen that,

$$M_s \ddot{\boldsymbol{X}}_{s_n} = \boldsymbol{F}_{hd} - \sum_{n=1}^{N} \boldsymbol{F}_{s_n} + \sum_{n=1}^{N} (\boldsymbol{F}_{sw_n} + \boldsymbol{F}_{bal_n}) \; . \tag{3-38}$$

In general, each force on the slipper generates a corresponding moment about the location of the shaft reaction. Summing these moments and setting them equal to the time rate-of-change of angular momentum,

$$\boldsymbol{I}_s \ddot{\boldsymbol{\Theta}}_{s_n} + \dot{\boldsymbol{\Theta}}_{s_n} \times \boldsymbol{I}_s \dot{\boldsymbol{\Theta}}_{s_n} = \boldsymbol{M}_{hd} + \sum_{n=1}^{N} \boldsymbol{M}_{s_n} + \sum_{n=1}^{N} (\boldsymbol{M}_{sw_n} + \boldsymbol{M}_{bal_n}) \; . \tag{3-39}$$

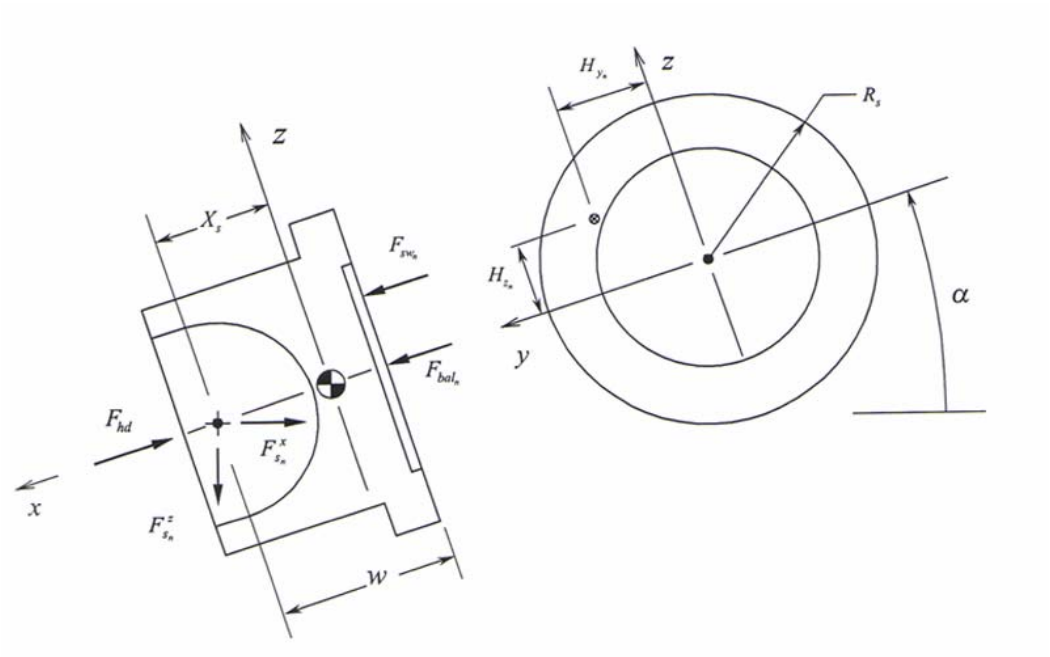

Figure 3-4 Free-body diagram of a single slipper
(Source: Modified from Manring [16])

Equations (3-38) and (3-39) provide the basis for describing the behavior of the slipper. The following subsection examines the components of these equations in more details.

3.4.1 Slipper Kinematics and Inertia

The n^{th} slipper is connected to the n^{th} piston. The mass-center of the n^{th} slipper relative to the fixed origin is given by,

$$\boldsymbol{X}_{s_n} = (x_n - X_s \cos(\alpha))\,\hat{\boldsymbol{i}} + y_n\,\hat{\boldsymbol{j}} + (z_n + X_s \sin(\alpha))\hat{\boldsymbol{k}}\ . \tag{3-40}$$

Differentiating this vector twice and multiplying it with the mass of the slipper gives the translation inertia of the slipper and can be written as,

$$M_s \ddot{\boldsymbol{X}}_{s_n} = M_s(\ddot{x}_n \cos(\alpha) - \ddot{z}_n \sin(\alpha) + X_s \dot{\alpha}^2)\,\hat{\boldsymbol{i}} + M_s \ddot{y}_n \hat{\boldsymbol{j}} + M_s(\ddot{x}_n \sin(\alpha) + \ddot{z}_n \cos(\alpha) + X_s \ddot{\alpha})\,\hat{\boldsymbol{k}} \ . \tag{3-41}$$

During normal operation, the angular acceleration of the n^{th} slipper is zero in all directions. Due to the angular rotation of the slipper about the *y*-axis a product of inertia is induced. Because of this, the time rate of change of angular momentum of the slipper is strictly not zero, however since the angle α is small, this contribution is considered negligible and the time rate of change of angular momentum of the n^{th} slipper is written as,

$$\boldsymbol{I}_s \ddot{\boldsymbol{\Theta}}_{s_n} + \dot{\boldsymbol{\Theta}}_{s_n} \times \boldsymbol{I}_s \dot{\boldsymbol{\Theta}}_{s_n} = 0 \ . \tag{3-42}$$

3.4.2 Slipper Hold-Down Force

The design of an axial piston hydrostatic pump always includes a mechanism to insure that the slippers remain in reasonable contact with the swash plate. In general, this mechanism takes on many different forms and is there for not included in the general drawings of this study. However it is usually classified as one of two types: 1) a fixed clearance hold-down or 2) a positive force hold-down. See Figure 3-5. A fixed clearance hold-down allows for a controlled gap or clearance between the slipper and the swash plate. Note, this clearance is allowed, not required. It is expected that applied loads will force the slipper against the swash plate during normal operating conditions. A positive force hold down exerts a separate force on the slipper that insures the slipper's contact with the swash plate. Usually this force is generated by a compressed spring and remains

constant throughout the cycle of operation. In this analysis, the more general case is assumed where the slipper is in constant contact with the swash plate and is held down by a positive force hold down mechanism.

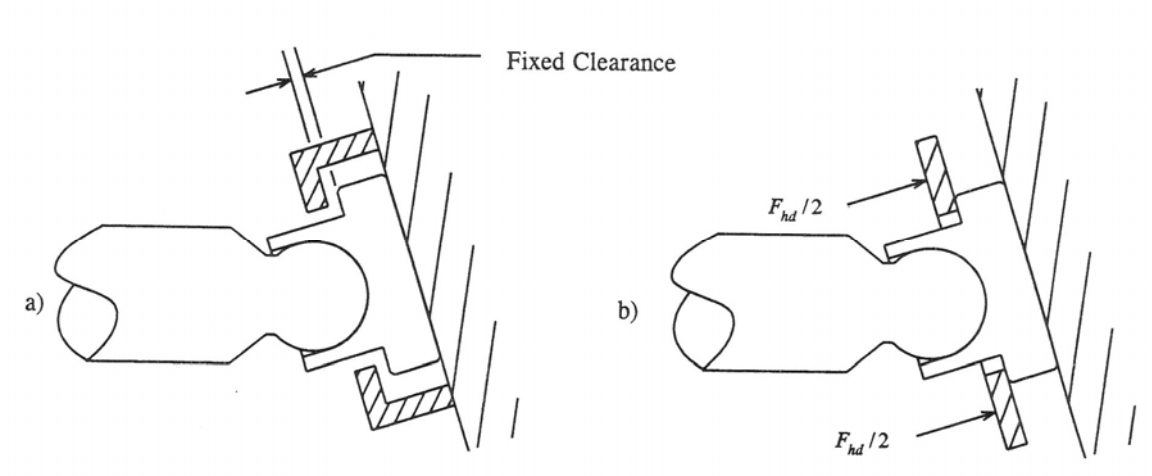

Figure 3-5 Schematic of two types of slipper hold-down mechanism: a) fixed clearance b) positive force
(Source: Modified from Manring [16])

The force from the slipper hold down mechanism acts on the slipper normal to the swash plate and is expressed by,

$$\boldsymbol{F}_{hd} = -F_{hd}\,\hat{\boldsymbol{i}} + 0\,\hat{\boldsymbol{j}} + 0\,\hat{\boldsymbol{k}}\ . \tag{3-43}$$

Since this force is applied symmetrically about the slipper, line of action of this force is passing through the mass-center of the slipper, therefore this force does not generate any moment about the mass-center of the slipper.

$$\boldsymbol{M}_{hd} = 0\ . \tag{3-44}$$

3.4.3 Slipper Reaction

The force and moment of the slipper acting on the piston is applied equally and oppositely against the slipper. These force and moment are already described in section 3.3.2. This force can be written in terms of the new coordinate system as,

$$\boldsymbol{F}_{s_n} = (-F_{s_n}{}^{x}\cos(\alpha) + F_{s_n}{}^{z}\sin(\alpha))\,\hat{\boldsymbol{i}} - F_{s_n}{}^{y}\,\hat{\boldsymbol{j}} - (F_{s_n}{}^{x}\sin(\alpha) + F_{s_n}{}^{z}\cos(\alpha))\,\hat{\boldsymbol{k}}\ . \quad (3\text{-}45)$$

The point of action of this force relative to the slipper mass-center is given by $X_s\,\hat{\boldsymbol{i}} + 0\,\hat{\boldsymbol{j}} + 0\,\hat{\boldsymbol{k}}$ with X_s as shown in Figure 3-4. Again the moment generated by this force on the slipper about the slipper mass-center is obtained by the cross product of the force and the distance as,

$$\boldsymbol{M}_{s_n} = 0\,\hat{\boldsymbol{i}} + (F_{s_n}{}^{x}\sin(\alpha)\,X_s + F_{s_n}{}^{z}\cos(\alpha)\,X_s)\,\hat{\boldsymbol{j}} - (F_{s_n}{}^{y}\,X_s)\,\hat{\boldsymbol{k}}\ . \quad (3\text{-}46)$$

3.4.4 Swash-Plate Reaction

The reaction of the swash plate against the slipper is described with two forces: 1) the centroid of the load distributed across the area of contact between the slipper and the swash plate, ($\boldsymbol{F}_{sw_n}$) and 2) the friction force that results from the relative sliding between the swash plate and the slipper ($\boldsymbol{F}_{s_n}$), which will be ignored in this analysis for simplicity reason. After a careful look at Figure 3-5 it can be seen that this force may be expressed as,

$$\boldsymbol{F}_{sw_n} = F_{sw_n}\,\hat{\boldsymbol{i}} + 0\,\hat{\boldsymbol{j}} + 0\,\hat{\boldsymbol{k}}\ . \quad (3\text{-}47)$$

Using geometry, the distance of this force away from the mass-center of the slipper is shown to be $-(w - X_s)\,\hat{\boldsymbol{i}} + H_{y_n}\,\hat{\boldsymbol{j}} + H_{z_n}\,\hat{\boldsymbol{k}}$. Taking the cross product of this distance with equation (3-47), the net moment generated about the mass-center by this force is,

$$\boldsymbol{M}_{sw_n} = 0\,\hat{\boldsymbol{i}} + F_{sw_n} H_{z_n}\,\hat{\boldsymbol{j}} - F_{sw_n} H_{y_n}\,\hat{\boldsymbol{k}} \;. \tag{3-48}$$

3.4.5 Slipper-Balance Force

To provide hydrostatic lubrication to the slipper, it is customary to drill a small hole through the slipper and the piston to ensure that fluid from the piston-bore is supplied to the slipper/swash-plate interface. A shallow relief is cut into the slipper face and for this analysis, it is assumed that the fluid occupying this shallow volume is pressurized to the same level as the piston-bore (P_n). (If the leakage from the slipper is excessive this assumption may be invalid). The pressure P_n acts on the effective pressurized area of the slipper (A_s) to force the slipper away from the swash plate. Since it is not desirable for the slipper to actually lift from the swash plate (A_s) must be designed properly so as to balance the forces that are trying to move the slipper toward the swash plate, thus the resultant force is often called the 'slipper-balance' force. This force may generally be expressed as,

$$\boldsymbol{F}_{bal_n} = A_s\, P_n\,\hat{\boldsymbol{i}} + 0\,\hat{\boldsymbol{j}} + 0\,\hat{\boldsymbol{k}} \;. \tag{3-49}$$

Again the line of action of this force is passing through the mass-center of the slipper, therefore this force does not generate any moment about the mass-center of the slipper,

$$\boldsymbol{M}_{bal_n} = 0 \ . \tag{3-50}$$

3.4.6 Summary

By substituting the results of equations(3-41), (3-43), (3-45), (3-47) and (3-49) into equation (3-38) the net force acting on the n^{th} slipper may be written as,

$$\begin{aligned} & M_s(\ddot{x}_n \cos(\alpha) - \ddot{z}_n \sin(\alpha) + X_s \dot{\alpha}^2)\, \hat{\boldsymbol{i}} + M_s \ddot{y}_n \hat{\boldsymbol{j}} \\ & \qquad + M_s(\ddot{x}_n \sin(\alpha) + \ddot{z}_n \cos(\alpha) + X_s \ddot{\alpha})\, \hat{\boldsymbol{k}} = \\ & (-F_{s_n}{}^x \cos(\alpha) + F_{s_n}{}^z \sin(\alpha) - F_{hd} + F_{sw_n} + A_s P_n)\, \hat{\boldsymbol{i}} \\ & \qquad - F_{s_n}{}^y \hat{\boldsymbol{j}} - (F_{s_n}{}^x \sin(\alpha) + F_{s_n}{}^z \cos(\alpha))\, \hat{\boldsymbol{k}} \ . \end{aligned} \tag{3-51}$$

Similarly, by substituting equations (3-42), (3-44), (3-46), (3-48) and (3-50) into equation (3-39) it can be shown that the net moment about the shaft reaction point, due to forces acting on a single slipper is given by,

$$0 = 0\, \hat{\boldsymbol{i}} + (F_{s_n}{}^x \sin(\alpha)\, X_s + F_{s_n}{}^z \cos(\alpha)\, X_s + F_{sw_n} H_{z_n})\, \hat{\boldsymbol{j}} - (F_{s_n}{}^y\, X_s + F_{sw_n} H_{y_n})\, \hat{\boldsymbol{k}}. \tag{3-52}$$

3.5 Swash Plate Free-Body Diagram

The free-body diagram of a swash plate is shown in Figure 3-6. The forces acting on the swash plate are, the equal and opposite reaction of the swash plate against the slipper ($-\boldsymbol{F}_{sw_n}$) and the equal and opposite pressure balance acting between the slipper and the swash plate ($-\boldsymbol{F}_{bal_n}$) and the external control and containment force ($\boldsymbol{F}'_c$).

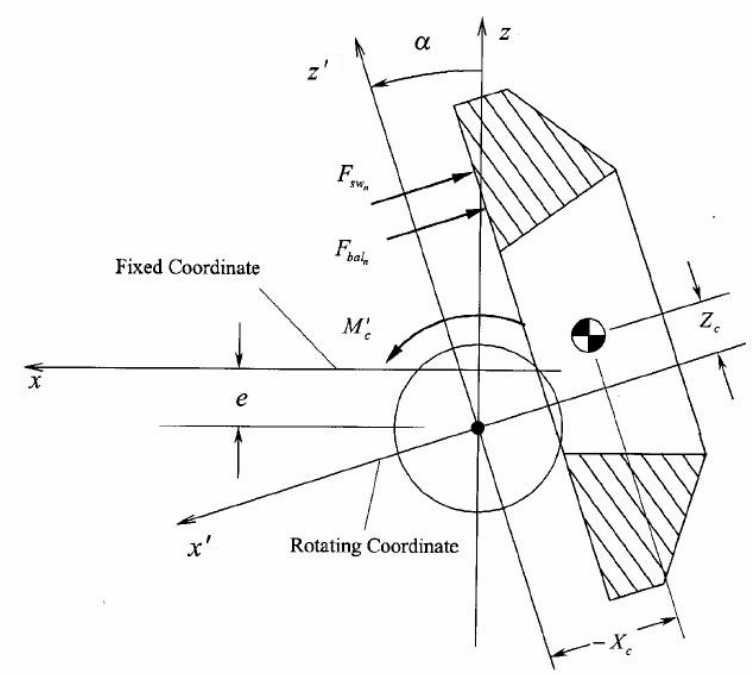

Figure 3-6 Free-body diagram of a swash-plate
(Source: Modified from Damtew [17])

A new coordinate system (x, y and z) which is fixed at the swash plate pivot point and which is rotating together with the swash plate is considered. In this analysis, all the forces and moments acting on the swash plate are given in terms of this coordinate system. Also, since this systems stays in parallel with the original system, the unit vectors associated with them are considered the same. Summing these forces and setting them equal to the translational inertia of the swash plate, it can be seen that

$$M_{sw}\,\ddot{\boldsymbol{X}}_{sw_n} = -\sum_{n=1}^{N}\boldsymbol{F}_{sw_n} - \sum_{n=1}^{N}\boldsymbol{F}_{bal_n} + \boldsymbol{F}'_c \ . \tag{3-53}$$

In general, each force on the swash plate generates a corresponding moment about the pivot point. Summing these moments and setting them equal to the time rate of change of angular momentum gives,

$$\boldsymbol{I}_{sw}\,\ddot{\boldsymbol{\Theta}}_{sw_n} + \dot{\boldsymbol{\Theta}}_{sw_n} \times \boldsymbol{I}_{sw}\,\dot{\boldsymbol{\Theta}}_{sw_n} = \sum_{n=1}^{N} (\boldsymbol{M}_{sw_n} + \boldsymbol{M}_{bal_n}) + \boldsymbol{M}'_c \ . \tag{3-54}$$

3.5.1 Swash Plate Kinematics and Inertia

The analysis considers a case where the mass-center of the swash plate does not coincide with the pivot point as shown in Figure 3-6 by the eccentricity dimension e. (X_c, Y_c, Z_c) locates the mass-center with respect to the pivot point as,

$$\boldsymbol{X}_{sw} = -X_c\,\hat{\boldsymbol{i}} + Y_c\,\hat{\boldsymbol{j}} + X_c\,\hat{\boldsymbol{k}} \ . \tag{3-55}$$

For most reasonable designs, X_c is most likely a negative number. Taking the derivate of this location twice and multiplying the result by the mass of the swash plate, yield the time rate of change of angular momentum of the swash plate as,

$$M_{sw}\ddot{\boldsymbol{X}}_{sw} = M_{sw}\,(Z_c\ddot{\alpha} + X_c\dot{\alpha}^2)\,\hat{\boldsymbol{i}} + 0\,\hat{\boldsymbol{j}} + M_{sw}\,(X_c\ddot{\alpha} - Z_c\dot{\alpha}^2)\,\hat{\boldsymbol{k}} \ . \tag{3-56}$$

The swash plate's time rate of change of momentum about the swash plate's pivot point can be given as,

$$\dot{\boldsymbol{H}}'_{sw} = (I'_{xy_{sw}}\ddot{\alpha} + I'_{yz_{sw}}\dot{\alpha}^2)\,\hat{\boldsymbol{i}} + I'_{yy}\ddot{\alpha}\,\hat{\boldsymbol{j}} + (I'_{yz_{sw}}\ddot{\alpha} - I'_{xy_{sw}}\dot{\alpha}^2)\,\hat{\boldsymbol{k}} \ . \tag{3-57}$$

3.5.2 Slipper Reaction

The reaction between the swash plate and the slipper has been already described in equation (3-47). The point of action of this force relative to the swash plate pivot point is given by $(a-w)\,\hat{\boldsymbol{i}} + (y_n + H_{y_n})\,\hat{\boldsymbol{j}} + ((z_n+e)\,\sec(\alpha) + a\,\tan(\alpha) + H_{z_n})\,\hat{\boldsymbol{k}}$. Taking the cross product of this distance with the negative of equation (3-47) gives the moment by this reaction force around the swash plate pivot point as,

$$\boldsymbol{M}'_{sw_n} = 0\,\hat{\boldsymbol{i}} - F_{sw_n}((z_n+e)\,\sec(\alpha) + a\,\tan(\alpha) + H_{z_n})\,\hat{\boldsymbol{j}} + F_{sw_n}(y_n + H_{y_n})\,\hat{\boldsymbol{k}}\,. \quad (3\text{-}58)$$

3.5.3 Slipper Balance Force

The slipper balance force has been already described in equation (3-49). It acts at the distance of $(a-w)\,\hat{\boldsymbol{i}} + y_n\,\hat{\boldsymbol{j}} + ((z_n+e)\,\sec(\alpha) + a\,\tan(\alpha))\,\hat{\boldsymbol{k}}$ from the swash plate pivot point. Taking the cross product of this distance with the negative of equation (3-49) gives the moment generated by the slipper balance force about the swash plate pivot point as,

$$\boldsymbol{M}'_{bal_n} = 0\,\hat{\boldsymbol{i}} - A_s\,P_n\,((z_n+e)\,\sec(\alpha) + a\,\tan(\alpha) + H_{z_n})\,\hat{\boldsymbol{j}} + A_s\,P_n\,y_n\,\hat{\boldsymbol{k}}\,. \quad (3\text{-}59)$$

3.5.4 External Control and Containment Forces

Since, the control and containment mechanisms for the swash plate are design specific, the forces exerted on the swash plate by these devices are considered in a general sense in this analysis and expressed as,

$$\boldsymbol{F}'_{c} = F^{x'}{}_{c}\ \hat{\boldsymbol{i}} + F^{y'}{}_{c}\ \hat{\boldsymbol{j}} + F^{z'}{}_{c}\ \hat{\boldsymbol{k}}\ . \tag{3-60}$$

The moments generated about the swash plate pivot by these forces may be generalized as well and written as,

$$\boldsymbol{M}'_{c} = T^{x'}{}_{c}\ \hat{\boldsymbol{i}} + T^{y'}{}_{c}\ \hat{\boldsymbol{j}} + T^{z'}{}_{c}\ \hat{\boldsymbol{k}}\ . \tag{3-61}$$

3.5.5 Summary

Substituting equations (3-56), (3-47), (3-49) and (3-60) into equation (3-53) yields the following equation,

$$\begin{aligned} M_{sw}\ (Z_c\ddot{\alpha} + X_c\dot{\alpha}^2)\ \hat{\boldsymbol{i}} + 0\,\hat{\boldsymbol{j}} + M_{sw}\ (X_c\ddot{\alpha} - Z_c\dot{\alpha}^2)\ \hat{\boldsymbol{k}} = \\ (F_{sw_n} + A_s\ P_n + F^{x'}{}_{c})\ \hat{\boldsymbol{i}} + F^{y'}{}_{c}\ \hat{\boldsymbol{j}} + F^{z'}{}_{c}\ \hat{\boldsymbol{k}}\ . \end{aligned} \tag{3-62}$$

Similarly, substituting equation (3-57), (3-58), (3-59), (3-61) into equation (3-54) yields the following equation,

$$\begin{aligned} (I'_{xy_{sw}}\ddot{\alpha} + I'_{yz_{sw}}\dot{\alpha}^2)\ \hat{\boldsymbol{i}} + I'_{yy}\ddot{\alpha}\ \hat{\boldsymbol{j}} + (I'_{yz_{sw}}\ddot{\alpha} - I'_{xy_{sw}}\dot{\alpha}^2)\ \hat{\boldsymbol{k}} = T^{x'}{}_{c}\ \hat{\boldsymbol{i}} \\ + \begin{bmatrix} T^{y'}{}_{c} - F_{sw_n}((z_n + e)\ \sec(\alpha)\ + a\ \tan(\alpha) + H_{z_n}) \\ -A_s\ P_n\ ((z_n + e)\ \sec(\alpha)\ +\ a\ \tan(\alpha) + H_{z_n} \end{bmatrix} \hat{\boldsymbol{j}} \\ + [F_{sw_n}(y_n + H_{y_n}) + A_s\ P_n\ y_n + T^{z'}{}_{c}\ ]\ \hat{\boldsymbol{k}}\ . \end{aligned} \tag{3-63}$$

3.6 Summary of Equations with Symmetry Considerations

In this section, the results of this chapter are gathered to describe specific physical quantities within the pump. This part of the chapter begins by presenting several

symmetry relationships that are used to simplify the result of this analysis. Finally, the analytical results are summarized using categories specific to the cylinder block, pistons and the slippers.

3.6.1 Symmetry Considerations

Because the pistons are evenly spaced in a circular array within the cylinder block, several simplifications arise due to symmetry. These symmetry relationships are called Lagrange's Trigonometric Identities as identified by Damtew [17];

$$\sum_{n=1}^{N} \sin\left(\frac{\xi\ \pi}{N}(n-1)\right) = 0 \tag{3-64}$$

and

$$\sum_{n=1}^{N} \cos\left(\frac{\xi\ \pi}{N}(n-1)\right) = 0 \tag{3-65}$$

Equations (3-64) and (3-65) are always valid for $N > 1$ and $\xi = 2, 4, 6...$

If the angular position of each piston is referenced from piston one, the circular position of the n^{th} piston may be expressed as $\theta_n = \theta_1 + 2\ \pi\ (n-1)/N$. Using this relationship and equation (3-64) and (3-65) with the identities $\sin(a+b) = \sin(a)\ \sin(b) + \cos(a)\ \cos(b)$ and $\cos(a+b) = \cos(a)\ \cos(b) - \sin(a)\ \sin(b)$ it can be shown that for $N > 1$,

$$\sum_{n=1}^{N} \sin(\theta_n) = 0\ . \tag{3-66}$$

$$\sum_{n=1}^{N} \cos(\theta_n) = 0 \ . \tag{3-67}$$

Similarly, using other mathematical identities following result could be easily proved for $N > 1$.

$$\sum_{n=1}^{N} \sin(\theta_n)\ \cos(\theta_n) = 0 \ . \tag{3-68}$$

$$\sum_{n=1}^{N} \sin^2(\theta_n) = \frac{N}{2} \ . \tag{3-69}$$

$$\sum_{n=1}^{N} \cos^2(\theta_n) = \frac{N}{2} \ . \tag{3-70}$$

3.6.2 Piston Location

As earlier mention that piston location (x_n, y_n, z_n) is given by $((e + r\sin(\theta_n))\tan(\alpha) + a\sec(\alpha),\ \cos(\theta_n),\ \sin(\theta_n))$. Differentiating x_n vector twice with respect to time gives the acceleration of the n^{th} piston-slipper ball-joint in the *x*-direction as,

$$\begin{aligned} \ddot{x}_n = &[\frac{r\ddot{\alpha}}{\cos^2(\alpha)} + \frac{2r\dot{\alpha}^2\sin(\alpha)}{\cos^3(\alpha)} - r\omega^2\tan(\alpha)]\sin(\theta_n) + [\frac{\ddot{\alpha} + 2\dot{\alpha}^2\tan(\alpha)}{\cos^2(\alpha)}]e \\ &+[\frac{2r\dot{\alpha}\omega}{\cos^2(\alpha)} + 2\dot{\omega}\tan(\alpha)]\cos(\theta_n) + [\frac{(1+2\tan^2(\alpha))\dot{\alpha}^2}{\cos(\alpha)} + \frac{\dot{\alpha}^2\sin(\alpha)}{\cos^2(\alpha)}]a \ . \end{aligned} \tag{3-71}$$

Differentiating the location components in *y* and *z* direction respectively gives the acceleration in *y* and *z* directions as follows,

$$\ddot{y}_n = -r\ \dot{\omega}\ \sin(\theta_n) - r\ \omega^2 \cos(\theta_n)\ . \tag{3-72}$$

$$\ddot{z}_n = r\ \dot{\omega} \cos(\theta_n) - r\ \omega^2 \sin(\theta_n)\ . \tag{3-73}$$

3.6.3 Cylinder-Block Equations

Cylinder block results are summarized by using equations (3-13), (3-23), (3-36), (3-51), (3-71), (3-72) and (3-73) to show that the force exerted by the shaft on the cylinder block in the *y*-direction is,

$$F_{sh}{}^{y} = 0\ . \tag{3-74}$$

Similarly, using same equations the force exerted by the shaft on the cylinder block in the *z*-direction is,

$$F_{sh}{}^{z} = [N\ F_{B_o} + N\ k\ (e\ \tan(\alpha) + a\ \sec(\alpha)) + \sum_{n=1}^{N} A_p\ P_n\ ]\ \tan(\alpha)\ . \tag{3-75}$$

Using equations (3-13), (3-23), (3-24), (3-71), (3-72) and (3-73) the torque exerted on the cylinder block by the shaft in the positive *x*-direction is given by,

$$T = \sum_{n=1}^{N} A_p\ P_n\ r\ \tan(\alpha)\ \cos(\theta_n)\ . \tag{3-76}$$

Using equations (3-13) and (3-23) it can be show that the force exerted on the cylinder block by the valve plate is expressed as,

$$F_v = N\ F_{B_o} + N\ k\ (e\ \tan(\alpha) + a\ \sec(\alpha)) + F_{sp} + \sum_{n=1}^{N} A_b\ P_n\ . \tag{3-77}$$

3.6.4 Pistons Equations

Using equations (3-13), (3-36), (3-37) and (3-51) the reaction in the *y*-direction of the n^{th} piston against the inner edge of the bushing within the n^{th} piston-bore may be expressed as,

$$F_{l_n}{}^{y} = -\left[\left(M_p + M_s\right)\frac{m_o - (e + r\ \sin(\theta_n))\tan(\alpha) - a\sec(\alpha)}{l_p} - M_p\frac{l_m}{l_p}\right] r\ \omega^2\cos(\theta_n)\ . \quad (3\text{-}78)$$

Similarly, the reaction in *z*-direction of the n^{th} piston against the inner edge of the bushing within the n^{th} piston-bore is shown to be,

$$\begin{aligned} &F_{l_n}{}^{z} = \\ &\left[\begin{array}{l}(k - (M_p + M_s))\omega^2 r\ \sin(\theta_n)\tan(\alpha) \\ +k(e\tan(\alpha) + a\sec(\alpha)) + A_p P_n + F_{B_o}\end{array}\right]\frac{m_o - (e + r\ \sin(\theta_n))\tan(\alpha) - a\sec(\alpha)}{l_p}\tan(\alpha) \quad (3\text{-}79) \\ &-\left[\left(M_p + M_s\right)\frac{m_o - (e + r\ \sin(\theta_n))\tan(\alpha) - a\sec(\alpha)}{l_p} - M_p\frac{l_m}{l_p}\right] r\omega^2\sin(\theta_n)\ . \end{aligned}$$

Continuing in this same fashion for the reaction of the n^{th} piston against the outer edge of the bushing, using the same set of equations, the reaction in the *y*-direction of the n^{th} piston against the outer edge of the bushing within the n^{th} piston-bore may be expressed as,

$$F_{o_n}{}^{y} = \left[\left(M_p + M_s\right)\frac{m_o + l_p - (e + r\ \sin(\theta_n))\tan(\alpha) - a\sec(\alpha)}{l_p} - M_p\frac{l_m}{l_p}\right] r\ \omega^2\sin(\theta_n)\ . \quad (3\text{-}80)$$

Again, the reaction in the *z*-direction of the n^{th} piston against the outer edge of the bushing within the n^{th} piston-bore is shown to be,

$$F_{o_n}{}^{z} =$$
$$-\left[\begin{array}{l}(k-(M_p+M_s))\omega^2 r\ \sin(\theta_n)\tan(\alpha)\\ +k(e\tan(\alpha)+a\sec(\alpha))+A_pP_n+F_{B_o}\end{array}\right]\frac{l_p+m_o-(e+r\ \sin(\theta_n))\tan(\alpha)-a\sec(\alpha)}{l_p}\tan(\alpha) \quad (3\text{-}81)$$
$$+\left[\left(M_p+M_s\right)\frac{l_p+m_o-(e+r\ \sin(\theta_n))\tan(\alpha)-a\sec(\alpha)}{l_p}-M_p\frac{l_m}{l_p}\right]r\omega^2\sin(\theta_n)\ .$$

3.6.5 Slipper Equations

From equations (3-36), (3-37), (3-78) to (3-81) it can be seen that the force in the *x*-direction from the n^{th} slipper against the n^{th} piston is simply given as,

$$F_{s_n}{}^{x} = (k - M_p\omega^2)\ r\ \tan(\alpha)\ \sin(\theta_n) + A_p\ P_n + F_{B_o} + k\ (e\ \tan(\alpha) + a\ \sec(\alpha))\ . \quad (3\text{-}82)$$

Similarly, the force in the *y*-direction from the n^{th} slipper against the n^{th} piston is expressed as,

$$F_{s_n}{}^{y} = M_s\ r\ \omega^2\ \cos(\theta_n)\ . \quad (3\text{-}83)$$

Using the same set of equations, the force in the *z*-direction from the n^{th} slipper against the n^{th} piston may be written as,

$$F_{s_n}{}^{z} = -\left[\begin{array}{l}(k-(M_p+M_s)\ \omega^2)\ r\ \tan(\alpha)\ \sin(\theta_n)+\\ k\ (e\ \tan(\alpha)+a\ \sec(\alpha))+A_p\ P_n\end{array}\right]\tan(\alpha)+F_{B_o}+M_s\ r\ \omega^2\ \sin(\theta_n)\ . \quad (3\text{-}84)$$

From equations (3-13), (3-36), (3-51), (3-52), (3-71), (3-72) and (3-73), the swash plate reaction against the n^{th} slipper is given by,

$$F_{sw_n} = \begin{bmatrix} (k - (M_p + M_s)\ \omega^2)\ r\ \tan(\alpha)\ \sin(\theta_n) + F_{B_o} \\ k\ (e\ \tan(\alpha) + a\ \sec(\alpha)) + A_p\ P_n \end{bmatrix} \sec(\alpha) - A_s\ P_{s_n} + F_{hd}\ . \quad (3\text{-}85)$$

3.7 Summary

In this chapter, the governing equations for the cylinder block, the pistons, and the slippers are derived using the free body diagrams of each components and kinematic analysis. The most important result of this chapter is the torque acting on the cylinder block (equation (3-76)) which is same as the shaft torque. The objective of this work is to attenuate the amplitude of this shaft torque and hence it will be analyzed in later chapters. Next Chapter 4 details the numerical pump model and also describes the pressure profile of the pump and important phenomenon like pressure undershoot and overshoot.

CHAPTER 4. NUMERICAL PRESSURE PROFILE

4.1 Introduction

As discussed earlier in Chapter 2, during one piston cycle, it continuously passes from the discharge port to the intake port and accordingly pressure changes very rapidly from a high discharge pressure to a low intake pressure, which is bridged by some intermediate pressure in the transition regions. It will be interesting to study the actual pressure behavior during the pumping cycle and hence a numerical and an ideal pressure profiles have been discussed in the chapter. The analysis begins by deriving the pressure rise rate equation using the control volume approach and conducts a simplified approximation of this pressure.

4.2 Piston Pressure

If the mass of the fluid within the bore is M, the instantaneous fluid density is ρ and instantaneous fluid volume is V, for a control volume the fluid mass time rate of change is given by,

$$\frac{dM}{dt} = \left(\frac{d\rho}{dt} V + \rho \frac{dV}{dt} \right). \tag{4-1}$$

Noting P as the instantaneous fluid pressure within the piston-bore, from the definition of the fluid bulk modulus β, the time-rate of change of fluid density is,

$$\frac{d\rho}{dt} = \frac{\rho}{\beta}\frac{dP}{dt}. \tag{4-2}$$

Also, the conservation of mass within the piston-bore gives,

$$\frac{dM}{dt} = \rho\,(Q - Q_l), \tag{4-3}$$

where Q is the volumetric flow rate into the piston-bore and Q_l is the leakage that occurs due to the clearance between the piston and bore and/or any other leak paths that may exist in the design of the piston chamber and leakage is modeled as,

$$Q_l = K\,P_d\,, \tag{4-4}$$

where P_d is the pressure on the discharge side and K is the leakage coefficient.

By substituting equations (4-2), (4-3) and (4-4) into equation (4-1), equations for pressure time rate of change (equation (4-5)) is given as,

$$\frac{dP}{dt} = \frac{\beta}{V}\left(Q - Q_l - \frac{dV}{dt}\right). \tag{4-5}$$

4.3 Piston Kinematics and Control Volume Analysis

The instantaneous volume V of each piston-bore is determined using the piston kinematics. As noted in Chapter 3, the position of each piston is described by the equation,

$$x_n = r\,\tan(\alpha)\,\sin(\theta). \tag{4-6}$$

With V_o as the reference volume and A_P as the area of the piston, the instantaneous volume V can be given as,

$$V = V_o - A_P\, r\, \tan(\alpha)\, \sin(\theta). \tag{4-7}$$

The flow in and out of the piston chamber occurs at high velocity and thus at high Reynold's number and hence Q is modeled using the classical orifice equation where the 'sign' function takes on the value ± 1 depending upon the sing of its argument.

$$Q = sign\,(P_b - P)\, C_d\, A_o \sqrt{\frac{2|P_b - P|}{\rho}}. \tag{4-8}$$

P_b is the boundary pressure outside the control volume (either P_i or P_d). Again, A_o is the varying discharge area of the control volume and has been show in Figure 4-1 along with the pressure variation.

4.4 Model Parameters

A piston pump model is made in Simulink® where some of the assumptions made during theoretical analysis are relaxed. In this model instantaneous pressure, fluid compressibility and leakage are considered. Manring [18] also describes a numerical model of a piston pump with odd and even number of pistons. Table 1 lists the design parameters used in this model [18] and explained earlier. Pump is assumed to be operating at 2250 rpm.

Table 1 Model parameters

Design Parameter	Value
Piston pitch circle radius- r (m)	0.05982
Area of the piston- A_P (m)	7.144e-4
Piston chamber volume V_o when $\alpha = 0$, (m^3)	17.46e-6
Discharge Pressure- P_d (MPa)	25
Intake Pressure - P_i (MPa)	2
Pump speed ω (rad/s)	235.6
Leakage coefficient- K	2e-11
Coefficient of discharge- C_d	0.62
Density of fluid- ρ (kg/m^3)	850
Bulk modulus- β (N/m^2)	14 GPa

4.5 Numerical Pressure Profile

Figure 4-1 shows a typical numerical pressure as θ varies from 0 to 2π (one pump revolution). Here, both instantaneous piston pressure and port area are plotted. As the piston passes over either the intake port or the discharge port of the valve plate, the port area remains at a maximum constant. Within these regions, the pressure within the n^{th} piston chamber also appears to remain fairly constant. The two ports on the valve plate are bridged by transition regions where area goes from a maximum value to a minimum value, slowly grows within the transition slot and then quickly returns to the

original maximum value. Pressure transition occurs almost linearly when a piston passes over the transition regions.

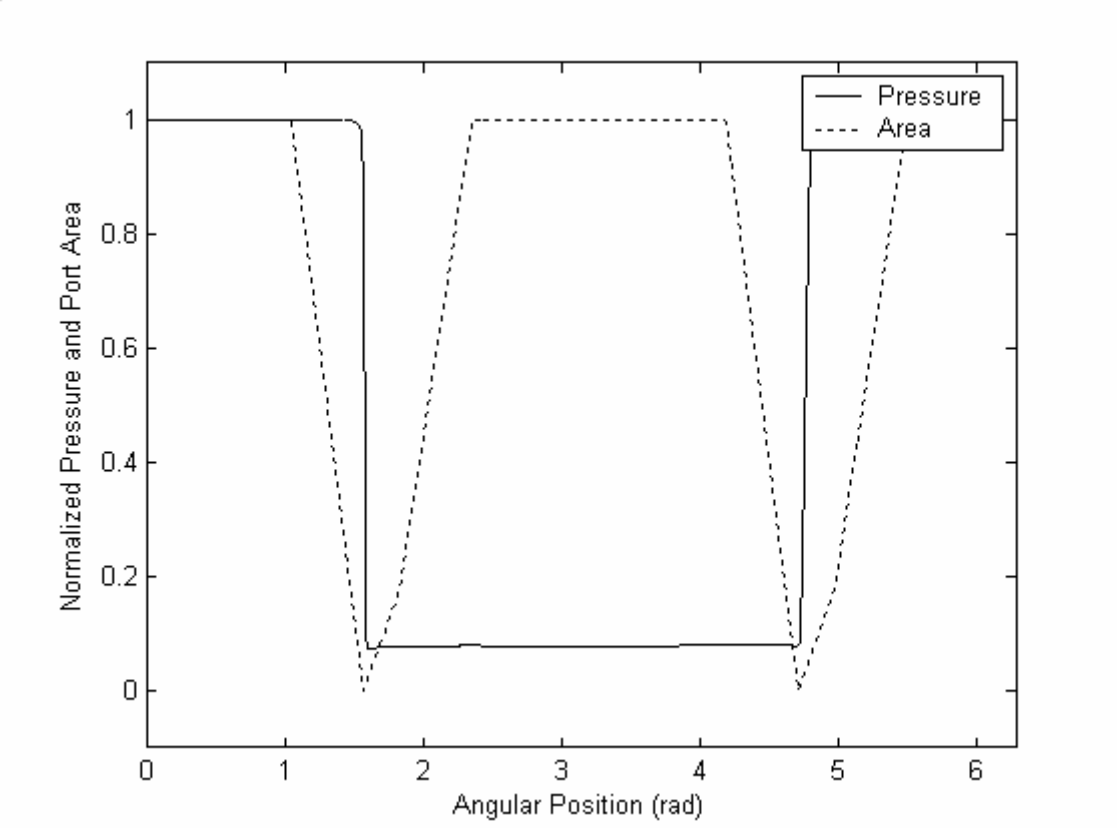

Figure 4-1 Numerical pressure-profile

A smaller pressure drop across the ports tends to create either overshoot and/or undershoot within the transition region which is sometimes evident as significant pressure spikes in the same region as shown in Figure 4-2. This is a result of the volumetric compression and expansion of the fluid [18]. When the volumetric compression occurs at the piston chamber, the chamber volume decreases at a rate faster than fluid can squeeze out through the port. If boundary pressure is not sufficiently large

compared to the starting pressure, the volumetric compression of the fluid will cause the pressure within the piston-bore to overshoot the approaching boundary condition.

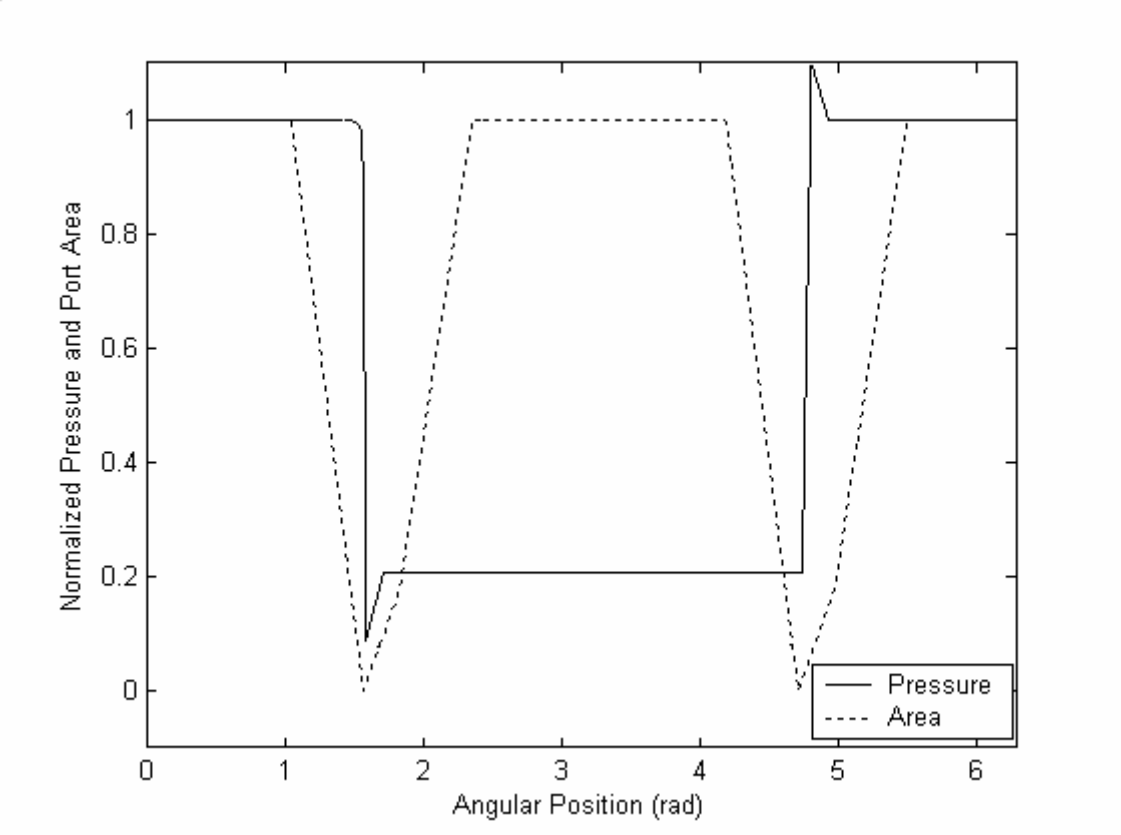

Figure 4-2 Numerical pressure profile with undershoot and overshoot

Similarly, when the volumetric expansion occurs at the piston chamber, the chamber volume increases at a rate faster than the fluid can enter the piston-bore. If boundary pressure is not sufficiently small compared to the starting pressure, the volumetric compression of the fluid will undershoot the approaching boundary condition. In either case, the pressure relaxes itself back to the appropriate boundary condition once sufficient flow is permitted by an increase in discharge or intake area. Earlier in Chapter

1 the role of pressure relief groove at the leading edges of intake and discharge ports is outlined. These relief grooves also help reduce the pressure undershoot and overshoot.

4.6 Ideal Pressure Profile

Equation (4-5) describes the pressure rise-rate for an axial piston pump as a function of time. The equation is non-linear and difficult to solve analytically. Hence, a numerical model is employed to investigate the pressure profile and they are shown in Figures 4-1 and 4-2. The pressure profile shown in Figure 4-2 is much less encountered than the one in Figure 4-1 which is plain. Therefore, most of the industries represent the pressure profile using an approximate scheme shown in Figure 4-3.

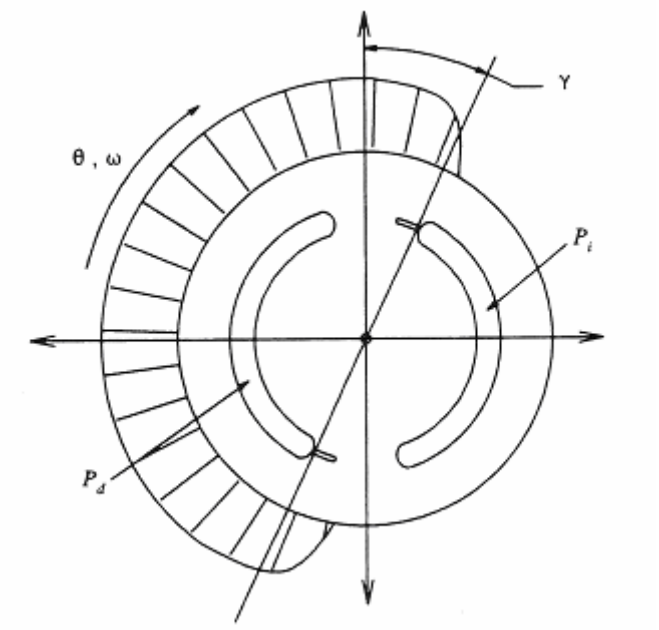

Figure 4-3 Ideal pressure profile
(Source: Manring [16])

In this schematic, it can be seen that the piston experiences a constant pressure as it directly passes over either port and that it undergoes a transition in pressure as it passes over the relief grooves. The transition occurs through some average angular distance which is known as pressure carry-over angle γ as shown Figure 4-3. Mathematically this pressure distribution can be represented as,

$$P_n = \begin{cases} P_d & 3\pi/2+\gamma < \theta_n < \pi/2 \\ P_d - m(\theta_n - \pi/2) & \pi/2 < \theta_n < \pi/2+\gamma \\ P_i & \pi/2+\gamma < \theta_n < 3\pi/2 \\ P_i + m(\theta_n - 3\pi/2) & 3\pi/2 < \theta_n < \pi/2+\gamma \end{cases}, \qquad (4\text{-}9)$$

where $m = (P_d - P_i)/\gamma$. Manring [18] derives the equation for γ and notes that it is twice as sensitive to percent changes in pump speed as compared to percent changes in pressure. Also, increased fluid volumes tend to increase the pressure carry-over angle as well.

4.7 Summary

In this chapter, a non-linear, first order, differential equation that describes the rate of pressure change with each piston chamber as function of time has been derived using the continuity equation. To investigate the behavior of this equation, a numerical technique was employed. Phenomena such as piston pressure undershot and overshoot are discussed. An ideal pressure profile is also discussed and compared with the numerical pressure profile. Next, Chapter 5 includes the derivation of the input shaft

torque for one and two rotating groups, two methods to attenuate the torque amplitude and finding the optimized index angle for a tandem pump configuration.

CHAPTER 5. SHAFT TORQUE ANALYSIS AND METHODS FOR TORQUE ATTENUATION

5.1 Introduction

In this chapter, the equations for the input shaft torque for pumps with one rotating group and two rotating groups will be derived. The analysis begins by deriving the equation of the shaft torque as a function of the average torque and the total number of pistons that are used within the rotating group. A control law is derived according to which if the swash plate is adjusted continuously, would give a constant shaft torque. In a second method, two pumps are used in tandem, separated by an angle, which is shown to amplify or attenuate the torque ripple amplitude depending on its value.

5.2 Shaft Torque of an Axial Piston Pump with One Rotating Group

In Chapter 3, the kinematic analysis for a swash plate type axial piston pump is given. A key equation describing the instantaneous torque that is exerted on the shaft of an axial-piston pump by a single rotating group has been presented. Previously Manring [18] and Ivantysyn and Ivantysynova [19] also present some of the discussions and analysis. In this study the torque on the shaft of a swash plate type axial piston pump is derived from the component level of the machine. The net input torque is calculated by summing all the idealized forces exerted on the components. Here the frictional losses resulting due to the sliding conditions within the pump have been neglected. Also piston inertia is ignored since the pistons are evenly spaced in a pump and inertia effectively

cancels out. The other assumptions are: fluid flow is considered incompressible and leakage is negligible. A constant pressure profile is assumed for this analysis as pressure is constant in the cylinder except at the TDC and BDC where compression and expansion occurs. While the dynamic component is concerned with pressure variation in the system, the aim here is to minimize the kinematic component of torque ripple. Similarly the effects of true port plate geometry are not considered. This analysis has been already published elsewhere [20] by this author and it is presented here.

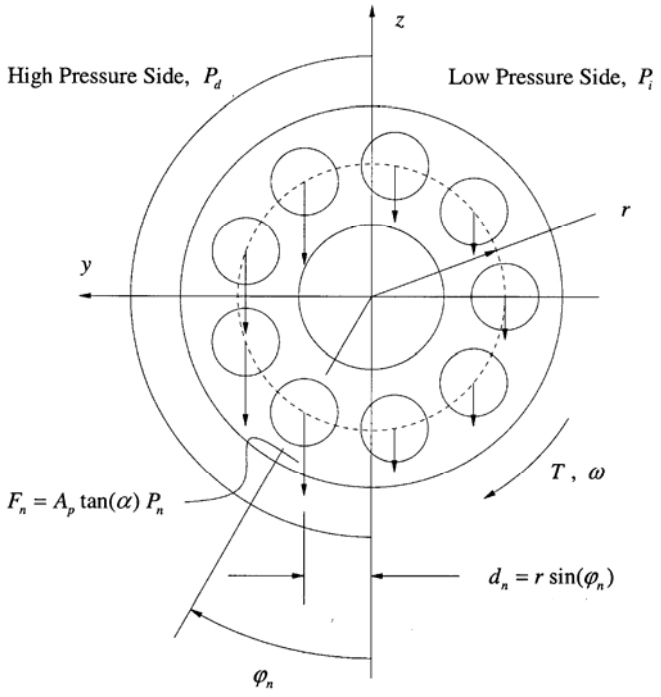

Figure 5-1 Reaction forces acting on the pump
(Source: Mehta and Manring [2])

Figure 5-1 shows a sectioned view AA of Figure 2-1 showing the horse-shoe porting and reaction forces. Earlier, each piston position is identified with the angle θ,

however in this chapter a new angle φ is introduced as the locator for each piston position. This transition is important as all the previous literature used θ which locates the piston in the middle of discharge port but it is logical to use φ as it locates the piston in reference to the bottom dead center just before discharge port. It is also worth noting here that $\varphi = \theta + 90^0$.

From the section view it can be shown that the torque exerted on the input shaft by a single piston is,

$$T_n = R_n \sin(\alpha)\, d_n , \tag{5-1}$$

where, $R_n \sin(\alpha)$ is the vertical component of the swash plate reaction R_n and d_n is the horizontal distance of the n^{th} piston away from the *z*-axis. R_n and d_n are given by the equations (5-2) and (5-3),

$$R_n = \frac{P_n A_p}{\cos(\alpha)} , \tag{5-2}$$

where, P_n is the pressure acting on the n^{th} piston while A_p is the area of a single piston. Also it can be shown that,

$$d_n = r \sin(\varphi_n) , \tag{5-3}$$

where r is the piston pitch radius and φ_n is the angular position of the n^{th} piston as shown in Figure 8. From equations (5-1), (5-2) and (5-3) the net instantaneous torque is,

$$T = A_P \tan(\alpha)\, r \sum_{n=1}^{N} P_n \sin(\varphi_n) , \tag{5-4}$$

where N is the total number of pistons in the pump. This equation is similar to equation (3-76) derived in Chapter 3 with the angular position of pistons located by θ.

5.2.1 Closed-Form Expression for Average Torque

Assuming that n' is the number of pistons over the discharge port, equation for the torque at the discharge side T_d and equation for the torque at the intake side T_i can be written as,

$$T_d = A_p \tan(\alpha)\, r\, P_d \sum_{n=1}^{n'} \sin(\varphi_n) \tag{5-5}$$

and,

$$T_i = A_p \tan(\alpha)\, r\, P_i \sum_{n=1}^{n'} \sin(\varphi_n)\,. \tag{5-6}$$

Also if the pistons are evenly spaced in a circular array about the center line of the pump shaft, then equation (5-7) describes the angular position of the n^{th} piston.

$$\varphi_n = \varphi_1 + \frac{2\pi}{N}(n-1)\,, \tag{5-7}$$

where φ_1 is the position of the first piston. It can be easily shown that the closed-form expression of $\sin(\varphi_n)$,

$$\sum_{n=a}^{b} \sin(\varphi_n) = \csc\left(\frac{\pi}{N}\right) \sin\left(\frac{\pi}{N}(1-a+b)\right) \sin\left(\varphi_1 + \frac{\pi}{N}(a+b-2)\right). \tag{5-8}$$

For the high pressure side, $a = 1$ and $b = n'$ while for the low pressure side $a = n' + 1$ and $b = n$. Summing T_d and T_i to give the total torque,

$$T = A_p \tan(\alpha)\, r \csc\left(\frac{\pi}{N}\right) \sin\left(\frac{\pi n'}{N}\right) P_d \left(\begin{array}{l} \sin\left(\varphi_1 + \frac{\pi}{N}(n'-1)\right) \\ + \varsigma \sin\left(1 + \frac{\pi}{N}(N + n'-1)\right) \end{array} \right), \quad (5\text{-}9)$$

where, $\varsigma = \frac{P_i}{P_d}$. The integral average of equation (5-9), as shown in equation (5-10) produces average torque acting on the input shaft $\bar{T}$ (equation (5-11)).

$$\bar{T} = \frac{N}{2\pi} \int_0^{2\pi/N} T \, d\varphi \,. \quad (5\text{-}10)$$

$$\bar{T} = \frac{N}{\pi} A_p \tan(\alpha)\, r\, P_d\, (1-\varsigma) \,. \quad (5\text{-}11)$$

5.2.2 Torque for Pumps with Odd and Even Number of Pistons

For a pump with odd number of pistons the number of pistons passing over the intake and discharge port is repeatedly fluctuating and depends upon the rotational position of the pump itself. The quantity is expressed by equations (5-12) and (5-14) and the torque is given by equations (5-13) and (5-15) respectively.

$$n' = \frac{N_o + 1}{2} \quad (5\text{-}12)$$

$$T_{o1} = A_p \tan(\alpha)\, r\, P_d \frac{(1-\varsigma)}{2} \csc\left(\frac{\pi}{2N_o}\right) \cos\left(\frac{\pi}{2N_o} - \varphi_1\right), \quad (5\text{-}13)$$

which is valid for $0 < \varphi_1 < \frac{\pi}{N_o}$. Similarly,

$$n' = \frac{N_o - 1}{2} \tag{5-14}$$

$$T_{o2} = A_p \tan(\alpha)\, r\, P_d \frac{(1-\varsigma)}{2} \csc\left(\frac{\pi}{2N_o}\right) \cos\left(\frac{\pi}{2N_o} - (\varphi_1 - \frac{\pi}{N_o})\right), \tag{5-15}$$

which is valid for $\frac{\pi}{N_o} < \varphi_1 < \frac{\pi}{2N_o}$.

Similarly for a pump with even number of pistons, the quantity is given by equation (5-16) and the torque value is given by (5-17) respectively.

$$n' = \frac{N_e}{2} \tag{5-16}$$

$$T_e = A_p \tan(\alpha)\, r\, P_d\, (1-\varsigma) \csc\left(\frac{\pi}{N_e}\right) \cos\left(\frac{\pi}{N_e} - \varphi_1\right), \tag{5-17}$$

which is valid for $0 < \varphi_1 < \frac{2\pi}{N_e}$. These torque equations (5-13), (5-15) and (5-17) when combined can also be written as equation (5-18) with the definitions of ξ given in equations (5-19) ,

$$T = \bar{T}\, \xi \csc(\xi) \cos(\xi - \varphi_1) \quad \text{for} \quad 0 < \varphi_1 < 2\xi \quad , \tag{5-18}$$

$$\xi = \begin{cases} \frac{\pi}{2\, N_o} & \text{odd number of pistons} \\ \frac{\pi}{N_e} & \text{even number of pistons} \quad . \end{cases} \tag{5-19}$$

The average torque $\bar{T}$ for odd and even number of pistons is given in equations (5-20) and (5-21) respectively.

$$\bar{T}_o = \frac{N_o}{\pi} A_p \, r \tan(\alpha) \, P_d (1-\varsigma) \quad , \tag{5-20}$$

$$\bar{T}_e = \frac{N_e}{\pi} A_p \, r \tan(\alpha) \, P_d (1-\varsigma) \quad . \tag{5-21}$$

Equation (5-18) defines the input shaft torque for a pump with an even or odd number of pistons as a function of average shaft torque and number of pistons. This ripple is periodic and repeats itself continuously as the pump shaft rotates. As shown in Figure 5-2 the period of the pulse width is 2ξ. ΔT is the amplitude of the flow ripple and is a very important characteristic for the pump since it has been already established that the goal here is to minimize the torque ripple amplitude to reduce the noise.

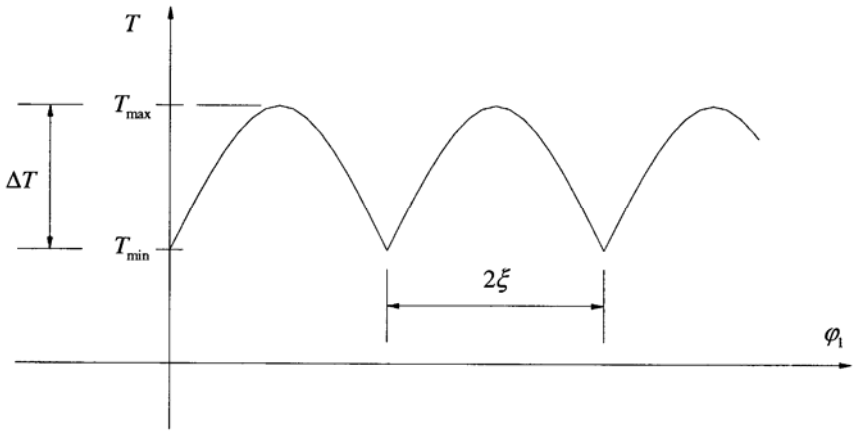

Figure 5-2 Schematic of net torque ripple for one rotating group

5.3 Control Law Derivation for One Rotating Group

The input shaft torque for an axial piston swash plate type hydrostatic pump is given by equation (5-18). The torque is a function of average shaft torque and number of pistons in the pump. Since the torque depends on the angular position of each piston, it is a function of φ_1 as well. Then, taking the derivative of T with respect to φ_1 and setting it to zero would yield conditions that pertain to minimum value for T. Setting $\frac{\partial T}{\partial \varphi_1} = 0$ gives,

$$\frac{\partial \bar{T}}{\partial \varphi_1} \; \xi \; \csc(\xi) \cos(\xi - \varphi_1) \; + \; \bar{T} \; \xi \; \csc(\xi) \sin(\xi - \varphi_1) = 0. \tag{5-22}$$

Then using the separation of variables principle and integrating both side as shown in equation (5-23),

$$\int_{\bar{T}_s}^{\bar{T}} \frac{1}{\bar{T}} \, \partial \bar{T} = -\int_0^{\varphi_1} \tan(\xi - \varphi_1) \, \partial \varphi_1 \, , \tag{5-23}$$

and then,

$$\ln\left(\frac{\bar{T}}{\bar{T}_s}\right) = -\int_0^{\varphi_1} \tan(\xi - \varphi_1) \, \partial \varphi_1. \tag{5-24}$$

Upon integration of right hand side of equation (5-24) and after simplification,

$$\bar{T} \; = \; \bar{T}_s \; \cos(\xi) \; \sec(\xi - \varphi_1), \tag{5-25}$$

where $\bar{T}_s$ is the starting torque when swash plate angle α is zero. From equation (5-20) the average starting torque evaluated at $\alpha = \alpha_s$ can be defined as in equation (5-26).

$$\bar{T}_s = \frac{A_p\, r\, \tan(\alpha_s)\, P_d\, (1-\varsigma)}{\xi} \,. \tag{5-26}$$

Equations (5-25) and (5-26) yield,

$$\bar{T} = \frac{1}{\xi} A_p\, r\, \tan(\alpha_s)\, P_d\, (1-\varsigma)\, \cos(\xi)\, \sec(\xi - \varphi_1) \,. \tag{5-27}$$

Equation (5-27) gives an alternative solution to average shaft torque. Equating equations (5-20) and (5-27) yields,

$$\tan(\alpha) = \tan(\alpha_s)\, \cos(\xi)\, \sec(\xi - \varphi_1) \,. \tag{5-28}$$

Equation (5-28) defines a swash plate control law. If the swash plate is continuously adjusted according to the control law described in equation (5-28), theoretically it should eliminate the ripple effect and generate a constant shaft torque. Adjusting the swash plate continuously creates a ripple that counters the original torque ripple. However, this may not be true when compressibility and leakage are considered as well as friction forces neglected in the theoretical analysis. Regardless, this control action should reduce the magnitude of the torque ripple by a considerable amount.

5.4 Shaft Torque of an Axial Piston Pump with Two Rotating Groups (Tandem Design)

This analysis has been already published [2] by this author and it is presented here. In practical tandem pump designs, two identical rotating groups are typically used on a single shaft to generate twice as much pump flow as compared to the flow produced by a single rotating group. In this case, both rotating groups exert a torque on the pump shaft that is governed by equation (5-18). The only difference between the two rotating groups used in a tandem pump design is the angular position of piston one φ_1 that may be indexed relative to the other rotating group by an amount δ. As shown in Figure 2-6, this angular index results from a difference in the assembled positions of each rotating group on the shaft. In other words, the spline connection between the cylinder block and the rotating shaft may not be aligned perfectly so as to position piston one in the same place for each rotating group. To account for this potential angular difference, the following equations are written to describe the torque exerted on the pump shaft by each rotating group:

$$\begin{aligned} T_A &= \bar{T}\ \xi \csc(\xi)\cos(\xi-\varphi_1) \quad \text{for} \quad 0<\varphi_1<2\xi \quad , \\ T_B &= \bar{T}\ \xi \csc(\xi)\cos(\xi-\varphi_1-\delta) \quad \text{for} \quad -\delta<\varphi_1<2\xi-\delta \ . \end{aligned} \tag{5-29}$$

In this equation, the subscript A and B refers to Rotating Groups A and B respectively and ξ and $\bar{T}$ are given in equations (5-19) and (5-20) respectively. By adding these two results together, the following torque pulsation is described for the tandem pump design:

$$T = 2\,\overline{T}\;\xi\,\csc(\xi)\cos(\delta/2)\cos(\delta/2-\xi+\varphi_1) \quad \text{for} \quad 0<\varphi_1<2\xi-\delta \quad , \qquad (5\text{-}30)$$

where $0<\delta<\xi$ for an examination of the largest pulsation of the torque ripple.

5.5 Optimized Index Angle for Tandem Design

It is already stated that it is known that the index angle δ the key to the torque ripple amplitude. Hence, the objective of this exercise is to identify the index angle δ that produces the smallest amplitude of the torque ripple. As shown in Figure 5-2, the maximum torque exerted on the shaft will occur at the middle of the pulse which, for the tandem pump design, is given by $\varphi_1 = \xi - \delta/2$. See equation (5-30). This maximum torque value is,

$$T_{\max} = 2\,\overline{T}\;\xi\,\csc(\xi)\cos(\delta/2)\,. \qquad (5\text{-}31)$$

Also shown in Figure 5-2, the minimum torque exerted on the shaft will occur at the ends of the pulse. These ends are identified when $\varphi_1 = 0$ or when $\varphi_1 = 2\xi - \delta$ for the tandem pump design. Evaluating equation (5-30) at one of these points produces the following result for the minimum torque:

$$T_{\min} = 2\,\overline{T}\;\xi\,\csc(\xi)\cos(\delta/2)\cos(\xi-\delta/2)\,. \qquad (5\text{-}32)$$

Subtracting equation (5-32) from equation (5-31) produces the following result for the torque ripple amplitude of the tandem pump:

$$\Delta T = 2\,\overline{T}\;\xi\,\csc(\xi)\cos(\delta/2)\left[1-\cos(\xi-\delta/2)\right] \quad , \qquad (5\text{-}33)$$

where ΔT is schematically shown in Figure 5-2. This is a very important equation in identifying the optimum index angle that would give the minimum torque amplitude. This equation will be further analyzed in Chapter 8.

5.6 Best Tandem Pump Design

A Matlab® program was written to find out the best tandem pump design. This program models equation (5-33) and calculates torque amplitude for different design configuration. Four design variables chosen are: number of pistons N_1 and N_2 for rotating group 1 and 2 respectively, ratio of average torques $\bar{T}$ for rotating group 1 and 2 and index angle δ. It is worth noting here that all four design variables are non-dimensional. This program basically assigns different values to these four variables from a range, calculates the torque amplitude for each design and gives design values that yields the smallest torque ripple amplitude. Table 2 lists the range attributed to each design variable.

Table 2 Range of design variables

Design Variable	**Range**	**Increment**	**Best Design**
N_1	5 to 15	1	15
N_2	5 to 15	1	15
$\bar{T}$	1 to 3	0.1	1
δ	0 to $2\pi / \min(N_1, N_2)$	0.1^o	6^o

Table 2 also lists the values corresponding to the best design. A tandem pump design with 15 pistons on each rotating group with the average torque ratio of 1 and index angle of 6^o should give the smallest torque ripple amplitude. The Matlab program used to generate this result is provided in its entirety in Appendix. This program can be used to find the optimum index angle for any tandem pump configuration. It also can be used for other purposes such as making FFT diagrams with some modification.

5.7 Summary

In this chapter, the equation for the shaft torque of a hydrostatic pump is derived from the component level. A second equation is derived for the tandem design. These equations are further analyzed to find the optimum operating condition that would render minimum torque amplitude. Result of a program to identify the optimum index angle is given. Next, Chapter 6 includes the flow ripple analysis for swash plate type piston pumps. This will be analogous to the torque ripple derivation and a very important conclusion will be drawn based on the similarities between non-dimensional forms of the torque and flow equations.

CHAPTER 6. RELATIONSHIP BETWEEN TORQUE RIPPLE AND FLOW RIPPLE

6.1 Introduction

Earlier it was highlighted that our understanding of how different sources contribute to pump noise is not clear. Hence the central difference between the research presented in this dissertation and the research done by other researchers is the understanding of the source of noise. It was pointed that many researches believe that the flow pulsation in the pump is the main cause of noise and vibrations. However, this work presented a new theory that the shaft torque pulsation is the dominant source of noise, supported by some lab experiments done at Caterpillar Inc. This Chapter presents the derivation for the flow ripple and compares it with the torque equation.

The other difference lies in the solution technique. It is evident from the methods listed in the literature review section that researchers rely on use of CAD to design a perfect port plate geometry and use of auxiliary components common to many pumps, to suppress noise. However, this work uses a pure mathematical approach to solve the problem. Having defined the closed-form equation for a torque ripple, use of some basic calculus and mathematical manipulation proved effective in finding two new methods to reduce noise. The effectiveness of this technique is that it can be applied to any similar problem and an optimal solution can be found.

6.2 A Closed-form Expression for Flow Ripple

Manring [21] examined the idealized and actual flow ripple of an axial piston pump. Again with the assumptions of no leakage and incompressible fluid a closed-form expression which describes the characteristics of the idealized flow ripple is derived. The instantaneous value of volumetric flow Q of an axial piston pump is determined by summing the instantaneous volumetric flows of the individual pistons Q_n.

$$Q = \sum_{n=1}^{N} Q_n . \tag{6-1}$$

The flow rate generated by a single piston is equal to the time rate of change of the instantaneous volume of the piston chamber V_n. V_n is already defined in equation (4-7).

$$Q_n = \frac{-dV_n}{dt} . \tag{6-2}$$

Equation (6-3), the theoretical discharge flow generated by the n^{th} piston is obtained by substituting equation (4-7) into equation (6-2). The total discharge flow may then be expressed by equation (6-4).

$$Q_n = A_p \, r \, \tan(\alpha) \, \omega \, \sin(\varphi_n) , \tag{6-3}$$

$$Q = A_p \, r \, \tan(\alpha) \, \omega \sum_{n=1}^{n'} \sin(\varphi_n) , \tag{6-4}$$

where n' is the total number of pistons instantaneously pressurized by the discharge port of the pump. As explained in derivation of the closed-form expression of the torque ripple, for a rotating group with an odd number of pistons, $n' = (N \pm 1)/2$ and for a

rotating group with an even number of pistons, $n' = N/2$. Earlier the average shaft torque was derived using the integral average concept, similarly using the integral average of equation (6-4), the nominal discharge flow of the pump may be obtained as follows.

$$\bar{Q} = \frac{N}{2\pi} A_p \, r \, \tan(\alpha) \, \omega \int_0^{\pi} \sin(\varphi) \, d\varphi, \tag{6-5}$$

$$\bar{Q} = \frac{N}{\pi} A_p \, r \, \tan(\alpha) \, \omega \, . \tag{6-6}$$

Substituting the mathematical identities defined in equations (5-7) and (5-8) into equation (6-4) and dividing the same by equation (6-6) renders equation (6-7) defining the normalized discharge flow,

$$\hat{Q} = \xi \, \csc(\xi) \, \cos(\varphi_1 - \xi) \quad \text{for } 0 < \varphi_1 < 2\xi. \tag{6-7}$$

The normalized discharge flow is obtained by dividing the net instantaneous flow by the average discharge flow. Again ξ is defined in equation (5-19) for odd and even number of pistons. It is interesting to note here that equation (6-7) looks similar to equation (5-18), in fact if both the torque and discharge flow expressions are considered in the normalized form, they are identical. So torque and discharge flow both are the function of their nominal quantity and ξ. Having established this fact, it can be said that this entire research holds true even if the main source of noise is the flow pulsation and not the torque pulsations. Employing these techniques will reduce the amplitude of flow pulsation as well as torque pulsation. Hence, the pump discharge flow should be a constant value with no fluctuation when shaft torque is governed by the control law given

in equation (5-28). Similarly, the pump discharge for the tandem design would be the summation of flow from both the pumps.

$$\begin{aligned} Q_A &= \bar{Q}\,\xi\,\csc(\xi)\cos(\xi-\varphi_1) \quad \text{for} \quad 0<\varphi_1<2\xi \quad , \\ Q_B &= \bar{Q}\,\xi\,\csc(\xi)\cos(\xi-\varphi_1-\delta) \quad \text{for} \quad -\delta<\varphi_1<2\xi-\delta \quad . \end{aligned} \tag{6-8}$$

In this equation, the subscript A and B refers to Rotating Groups A and B respectively and ξ and $\bar{Q}$ are given in equations (5-19) and (6-6) respectively. By adding these two results together, the following flow pulsation is described for the tandem pump design:

$$Q = 2\,\bar{Q}\,\xi\,\csc(\xi)\cos(\delta/2)\cos(\delta/2-\xi+\varphi_1) \quad \text{for} \quad 0<\varphi_1<2\xi-\delta \quad . \tag{6-9}$$

However, as in the torque ripple problem, when the optimal index angle is used to separate the first piston of both pumps, the flow pulsation amplitude will be reduce by as much as 75% of its maximum value.

6.3 Summary

In this chapter, by comparing the closed-form expressions of torque and flow ripples, it is discovered that the torque ripple and flow ripple problems are in fact just one problem. Two methods discussed earlier to reduce the torque ripple amplitude will decrease the flow ripple amplitude as well. Next, Chapter 7 presents the results from analysis and modeling for one rotating group for two cases: without the application of swash plate control law and with the application of the swash plate control law.

CHAPTER 7. RESULTS AND DISCUSSION FOR ONE ROTATING GROUP WITH APPLICATION OF THE SWASH PLATE CONTROL LAW

7.1 Introduction

In this chapter the torque profiles for swash plate type axial piston pumps with only one rotating group of pistons are presented and discussed. These results are separated into two sections: the results of idealized analysis and the results from numerical modeling. In particular, the torque ripple profiles for the pumps with nine, ten and eleven pistons are shown with respective Fast Fourier Transforms (FFT). Finally, for the nine piston pump, the torque profiles are compared for two cases: the constant swash plate angle and the swash plate continuously being adjusted by the swash plate control law given in equation (5-28).

7.2 Results from the Idealized Analysis

Figure 7-1 shows a typical torque ripple for a nine piston pump as given in equation (5-18). It is evident that the torque varies by amplitude of only 1.5 percent; however, even this small repeating variation is capable of creating undesirable vibration effects. The frequency spectrum (FFT) of the torque ripple shown in Figure 7-1 is shown in Figure 7-2. Here the frequency axis is normalized by the piston pass frequency of the pump. Also, the piston pass frequency is given by,

$$f = \frac{N\ \omega}{2\ \pi}\ . \tag{7-1}$$

It is interesting to note here that the dominant frequency is twice the piston pass frequency for an odd number of pistons pump.

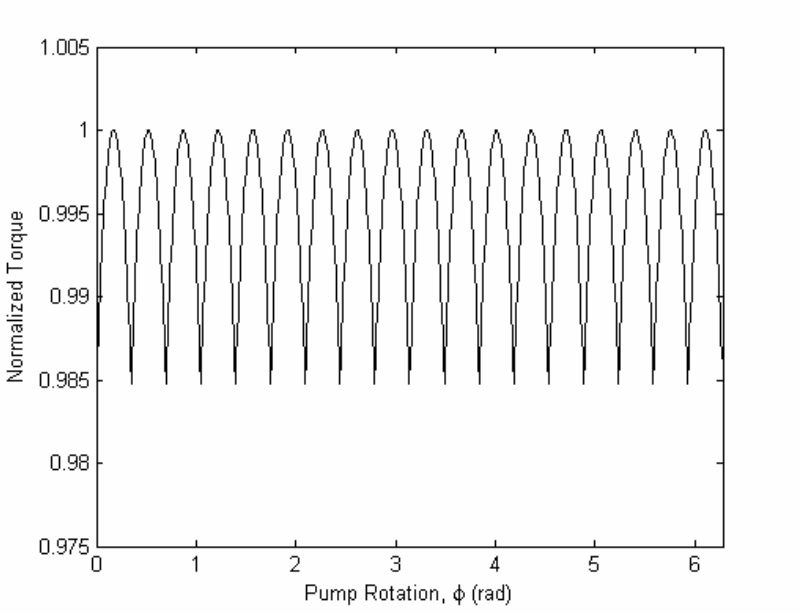

Figure 7-1 Shaft torque for one rotating group of nine pistons

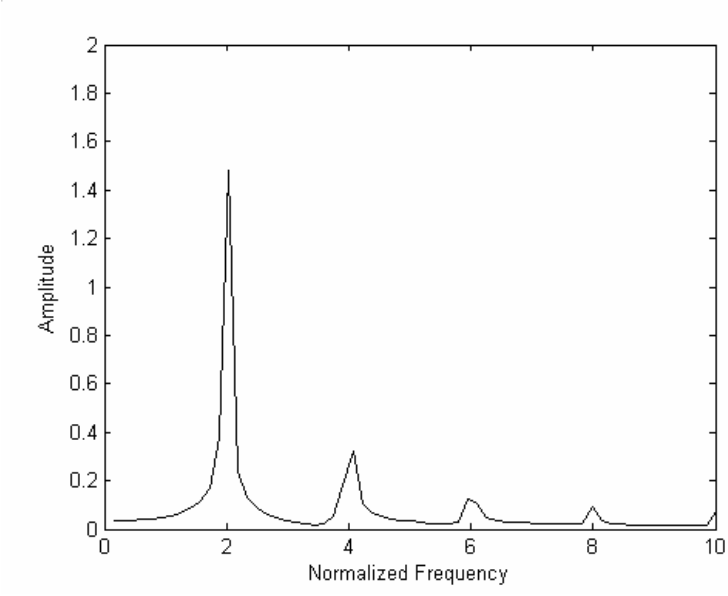

Figure 7-2 FFT of the idealized torque ripple for a nine piston pump

Figure 7-3 shows the torque ripple (equation (5-18)) over approximately 0.7 radians of rotation covering several cycles of the dominant frequency of the ripple. This plot shows the torque ripple for three different pump designs having 9, 10 and 11 pistons respectively. It is clearly evident that torque amplitude of pumps with odd number of pistons is smaller than the same with the even number of pistons. At the same time, 11 pistons pump has smaller amplitude then 9 pistons pump. This fact can be explained by considering only the kinematic torque ripple component. Since the total flow is made up of flows from different pistons, more pistons generate smaller amplitude.

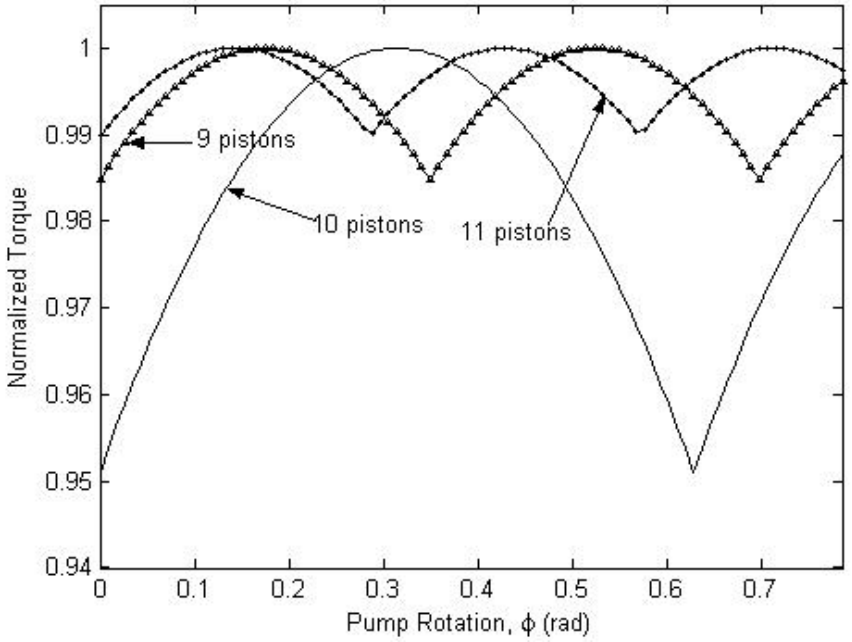

Figure 7-3 Shaft torque for pumps with 9, 10 and 11 pistons

The same fact can be seen in Figure 7-4 where the frequency spectrum (FFT) of these three pump configurations are shown. It is interesting to note that the dominant

frequency for the pump with even number of pistons equal to even and odd multiples of the piston pass frequency.

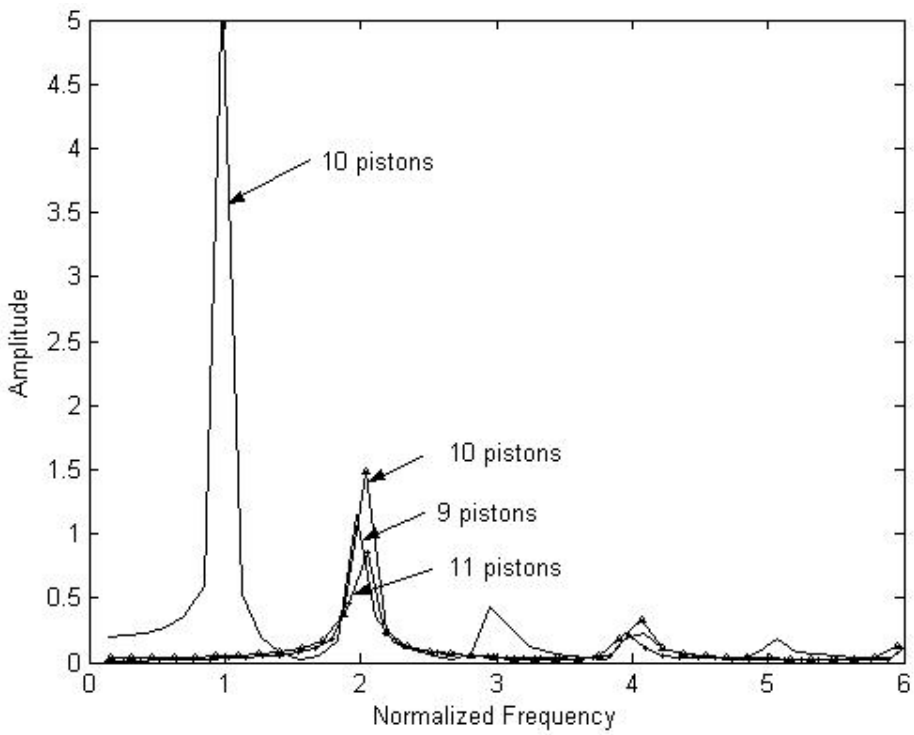

Figure 7-4 FFT of pumps with 9, 10 and 11 pistons

In earlier sections, two designs were discussed to attenuate the torque ripple. One of the designs involves a new control law governing the swash plate movement. This control (equation (5-28)) is plotted in Figure 7-5 for a half pump revolution. It can be seen that this swash plate adjustment is very small compared to the initial swash plate angle. However when the swash plate is governed by this control, ideally it removes the ripple effect and generates a constant shaft torque as shown in the torque profile of Figure 7-6. It is again needed to be emphasized that this holds true only for the idealized case of

no leakage in the port plate or anywhere else and in the case of incompressible fluid. Regardless, this control law should attenuate the torque ripple in actual pumping environment as well.

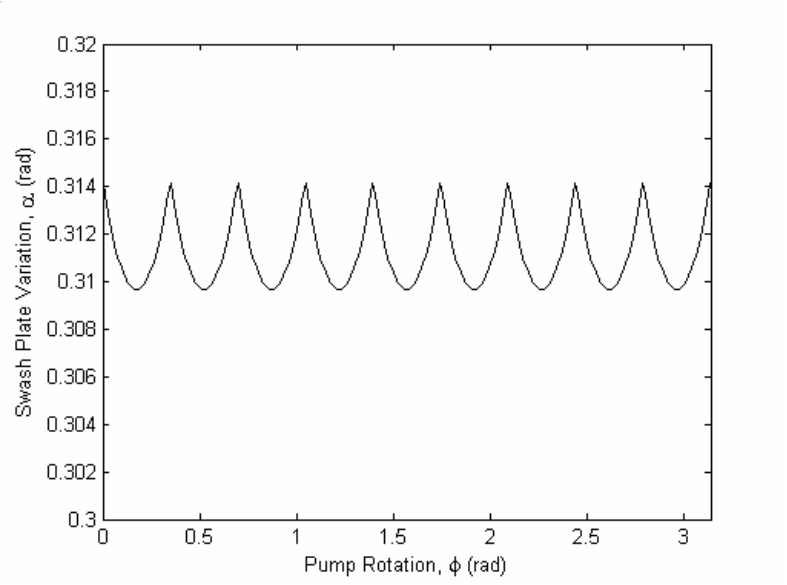

Figure 7-5 Swash plate variation

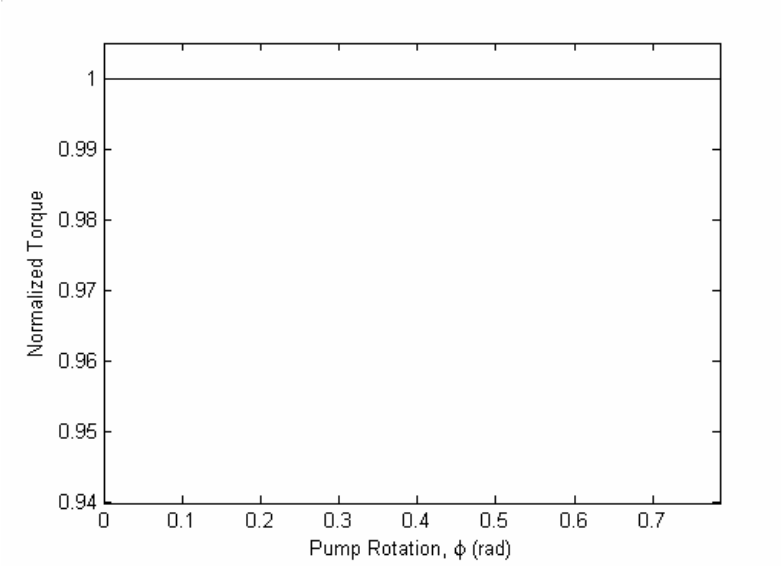

Figure 7-6 Shaft torque when control law applied

7.3 Results from the Numerical Analysis

A piston pump model was made in Matlab® Simulink® software. In this model instantaneous pressure, fluid compressibility and leakage are considered unlike the closed-form solution where they were neglected. Details of the model are given in Chapter 4.

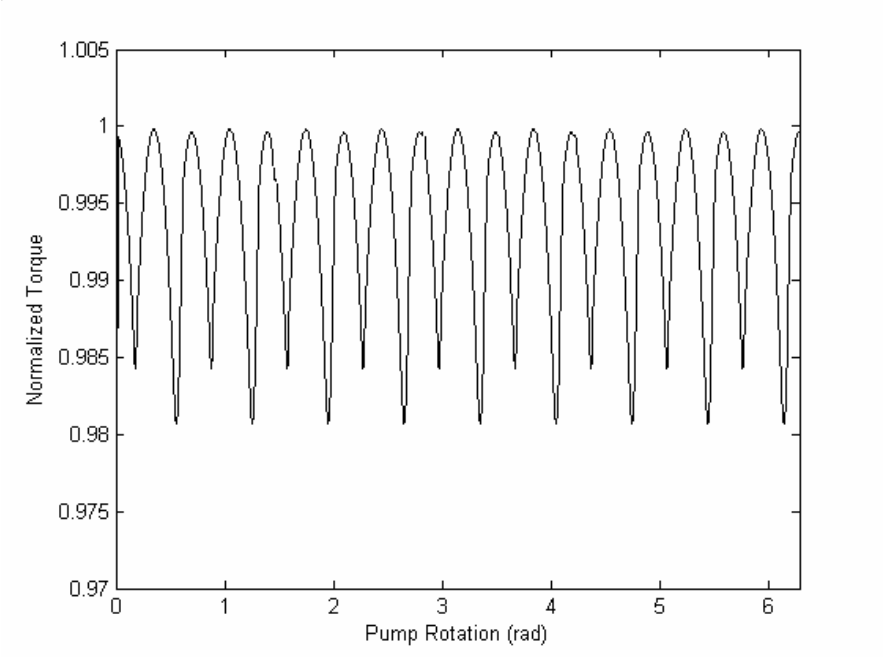

Figure 7-7 Numerical torque ripple for one rotating group of nine pistons

Figure 7-7 shows a numerical torque ripple. It is evident that the torque varies by amplitude of only 2 percent; compared to 1.5 percent as predicted in the analysis. This is due to the fact that there is a bigger torque variation in the transition region and it is governed by the fluid compression and decompression events.

Figure 7-8 shows a numerical torque ripple when the swash plate control law (equation (5-28)) is applied. As shown, the torque is mainly constant except spikes at regular intervals. The spikes in the torque ripple are due to the spikes in the pressure ripple.

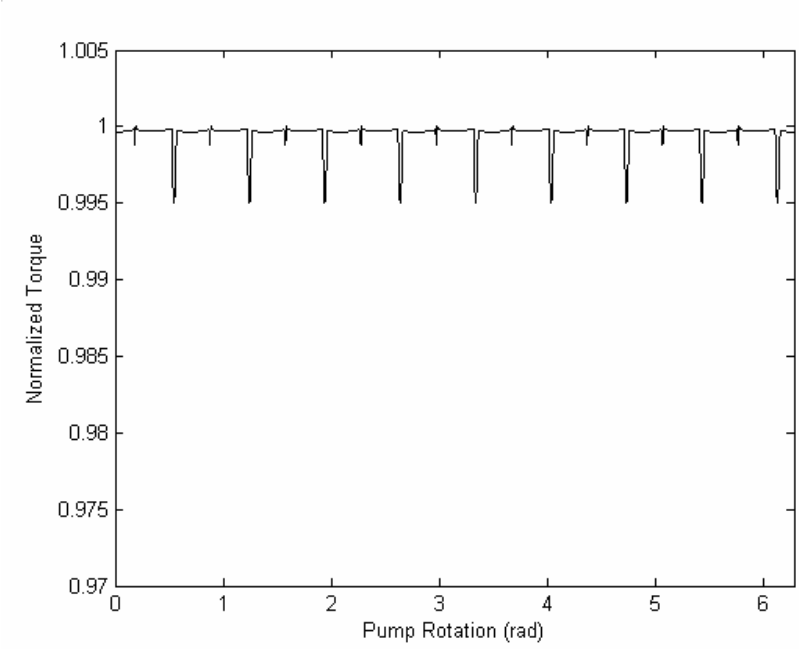

Figure 7-8 Numerical torque ripple when control law applied

7.4 Summary

In this chapter the results from the idealized analysis and numerical model are presented and discussed for piston pumps with only one rotating group. It is also shown that numerical findings support the theoretical analysis. It is important to note here that the shaft torque varies by only 1.5 percent from its maximum value; however this small change is enough to create loud noise and accompanying vibration in the system. It is

shown that application of the control law brings about 75 percent reduction in the torque amplitude.

CHAPTER 8. RESULTS AND DISCUSSION FOR TWO ROTATING GROUPS WITH OPTIMAL INDEX ANGLE DESIGN

8.1 Introduction

In this chapter the torque profiles for swash plate type axial piston pumps for the tandem design of two rotating group of pistons are presented and discussed. These results are separated into two sections again: the results of idealized analysis and the results from numerical modeling. In particular, the torque ripples for different index angle configurations to decide the optimum index angle are presented. Also, in a special case the torque ripples and respective frequency spectrums of tandem pumps with index angle of 10^o and 20^o are presented and discussed to demonstrate the effect of setting the pump at the optimal index angle.

8.2 Results from the Idealized Analysis

8.2.1 Torque Amplitude with Different Index Angle

The second design that would attenuate the torque ripple is the tandem pump design where in two rotating groups are connected by a common shaft in a mirrored back to back configuration. It is already stated that this design is used in industry as it posses many advantages over the conventional single rotating group design. One key design feature is that first pistons of both rotating groups are separated by an index angle. Typically this angle is either set by some experiments that would yield the lowest flow

ripple amplitude and noise or experience of the operator. However, this analysis proves that this practice does not index these pumps at the optimal angle. Following discussion will be helpful in understanding this concept.

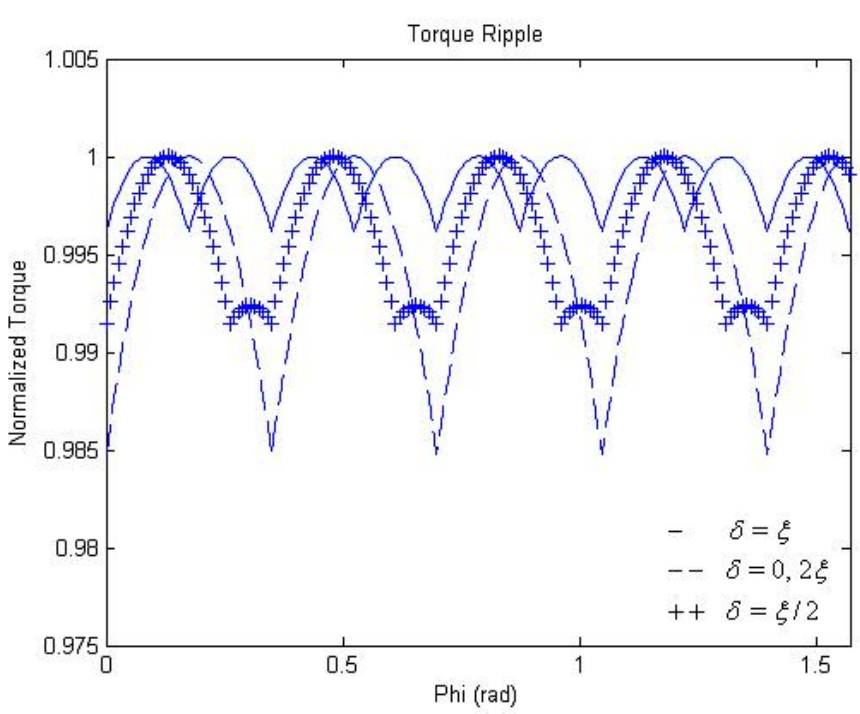

Figure 8-1 Torque ripple amplitude for different index angles

To illustrate the torque result of equation (5-30), the quantity $T/(2\bar{T})$ is plotted in Figure 8-1 for a tandem pump utilizing 9 pistons for each rotating group. As shown in this figure, the torque amplitude is a maximum when $\delta = 0$ and is a minimum when $\delta = \xi$. The reader will recall that δ is bounded between 0 and ξ for the examination of the largest pulsation of the tandem pump torque ripple. In other words, we have analytically identified the index angles that maximize and minimize the amplitude of the torque ripple. These analytical results are summarized as follows:

$$\Delta T_{\max} = 2\,\bar{T}\,\xi\,\csc(\xi)\left[1-\cos(\xi)\right] \quad \text{when} \quad \delta = 0 \quad ,$$

$$\text{and} \tag{8-1}$$

$$\Delta T_{\min} = 2\,\bar{T}\,\xi\,\csc(\xi)\cos(\xi/2)\left[1-\cos(\xi/2)\right] \quad \text{when} \quad \delta = \xi \quad .$$

8.2.2 Torque Amplitudes for Pumps with Odd and Even Number of Pistons

To illustrate the difference between these two results, Figure 8-2 shows a bar-chart comparison of the maximum and minimum torque amplitudes for tandem pumps utilizing rotating groups with a specified number of pistons in each group.

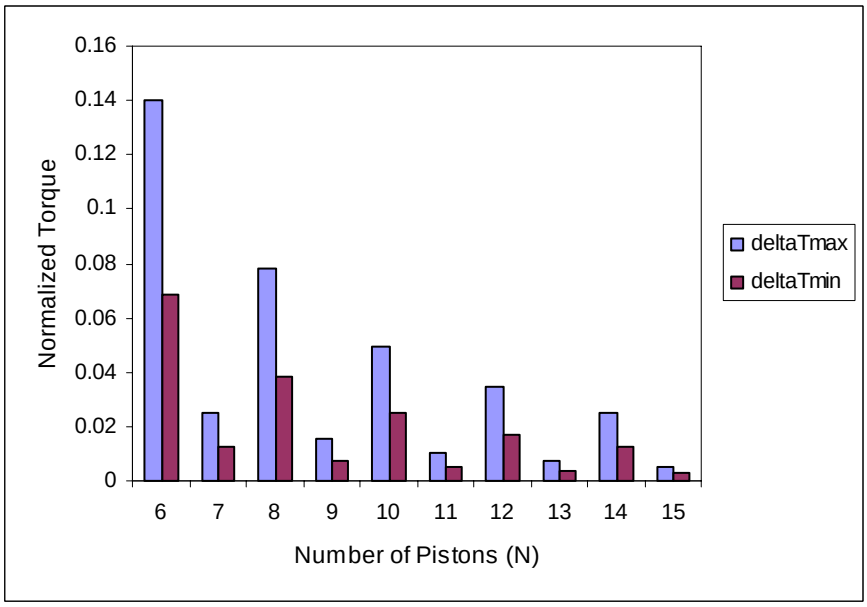

Figure 8-2 Maximum and minimum torque amplitudes for different tandem pump configuration

As shown in this figure, tandem pumps that use an even number of pistons within each rotating group exhibit the largest torque amplitude while tandem pumps that use an odd

number of pistons in each rotating group exhibit the lowest torque amplitude. This is a well-known feature of axial piston pumps and is the primary reason for using an odd number of pistons within most rotating group designs.

From equation (8-1), the percent difference between the maximum and minimum torque amplitude may be calculated as

$$\frac{\Delta T_{\max} - \Delta T_{\min}}{\Delta T_{\max}} \times 100\% = \frac{2 + \cos(\xi/2)}{4\cos^2(\xi/4)} \times 100\% \approx 75\% \quad . \tag{8-2}$$

In other words, by selecting the proper index angle for the assembly of the two rotating groups; i.e., setting $\delta = \xi$, the torque amplitude may be reduced by 75% from its largest possible value. As the reader can see, this reduction is significant. To achieve this smallest torque amplitude for the tandem pump, the index angles shown in Table 3 should be used for tandem pumps utilizing rotating groups with a specified number of pistons:

Table 3 Optimized index angles for different tandem pump configurations

N	6	7	8	9	10	11	12
δ	30.0°	12.9°	22.5°	10.0°	18.0°	8.2°	15.0°

The explanation for these results is as follows. For each rotating group used in the tandem pump design, the frequency of the torque ripple is equal to the piston pass frequency for a rotating group that utilizes an even number of pistons. For a rotating group that utilizes an odd number of pistons, the frequency of the torque ripple is equal to two times the piston pass frequency. To minimize the amplitude of the net torque ripple

for two rotating groups used on a tandem pump shaft, the minimum torque value for one of the rotating groups must coincide with the maximum torque value for the other rotating group. This means that the torque ripple for one of the rotating groups must be shifted (or indexed) by one fourth of the piston pass frequency for a pump utilizing an odd number of pistons for each rotating group; or, the torque ripple must be shifted by one half the piston pass frequency for a pump utilizing an even number of pistons for each rotating group. These shifted dimensions are shown in Table 3 by the angular dimension δ which is a physical index that may be designed into the assembly process of the tandem pump for the purposes of generating a torque ripple with the lowest possible amplitude.

8.2.3 Torque Profile for Tandem Pump with Index Angle of 20^o

Typically, in a pump with nine pistons, each piston separates the other piston by 40^o. Hence the index angle is set to be 20^o. Figure 8-3 shows the individual torque ripples (equation(8-3)) for two rotating groups with an index angle of 20^o, where as Figure 8-4 shows the total input shaft torque for the tandem pump design. It is to be noted here that the torque profiles of both rotating groups are identical in amplitude over the entire pump revolution i.e. maximum torque amplitude of one matches the maximum torque amplitude of the second group in the pumping cycle.

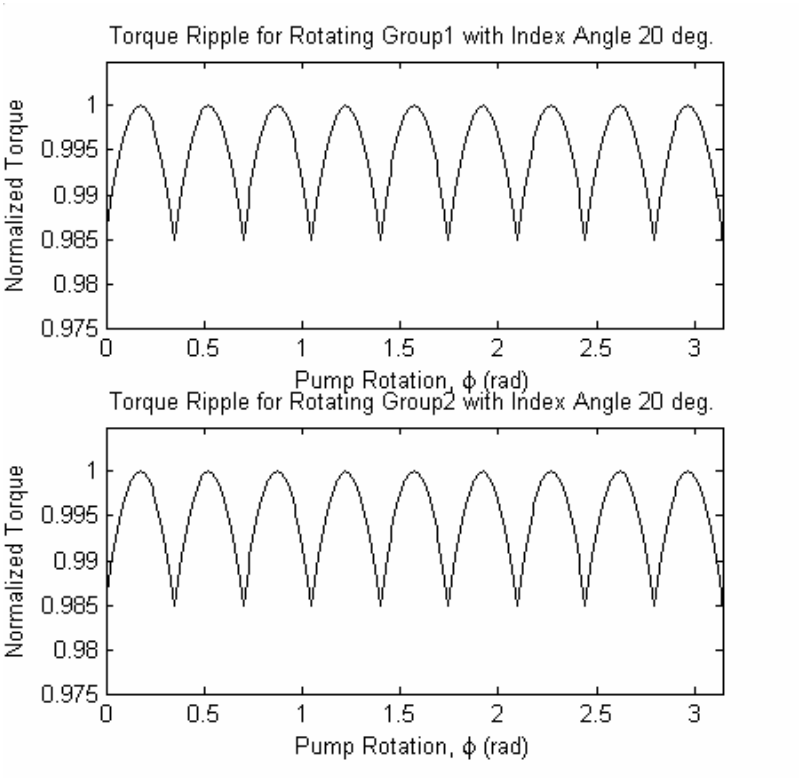

Figure 8-3 Torque ripples with index angle 20 deg.

So when these amplitudes are added (equation(8-4)) up for Figure 8-4, it shows the maximum variation of 1.5 percent as stated earlier. This however does not render any advantage over the convention single pump design. Here what we need is that at every point in one pump revolution, the maximum torque value on one rotating group should coincide with the minimum torque value on the other group to get the smallest net torque.

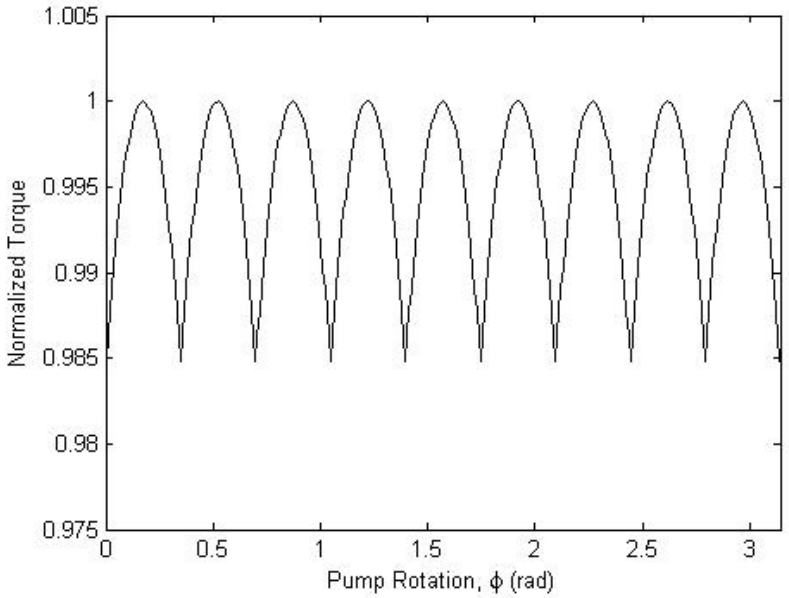

Figure 8-4 Total shaft torque with index angle of 20 deg.

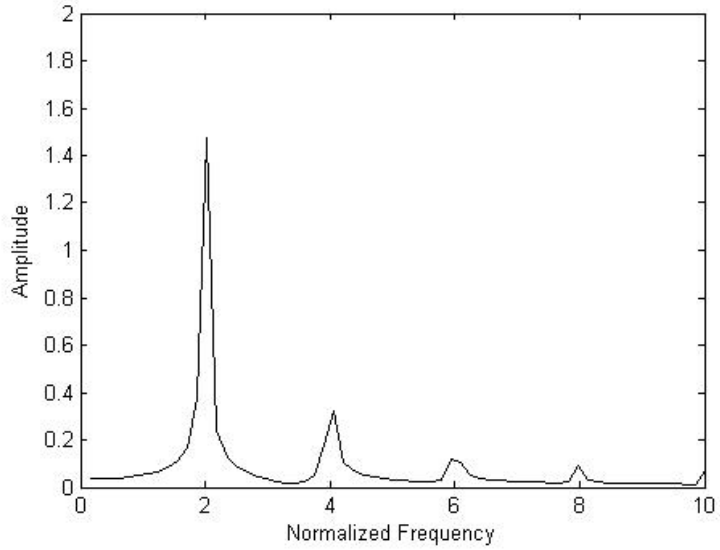

Figure 8-5 FFT of the idealized shaft torque with index angle of 20 deg.

The fact is that 20^o not an optimum index angle for this design, in fact it gives the worst design possible along with the index angle of 0^o. Figure 8-5, shows the frequency

spectrum of the tandem pump design with the index angle of 20^o. As one would expect, it is similar to the frequency spectrum for the single rotating group design as shown in Figure 7-2.

8.2.4 Torque Profile for Tandem Pump with Index Angle of 10^o

Earlier, it was stated that by selecting the proper index angle for the assembly of the two rotating groups; i.e., setting $\delta = \xi$, the torque amplitude may be reduced by 75% from its largest possible value. According to Table 3, for nine piston pump design the optimum index angle would be 10^o.

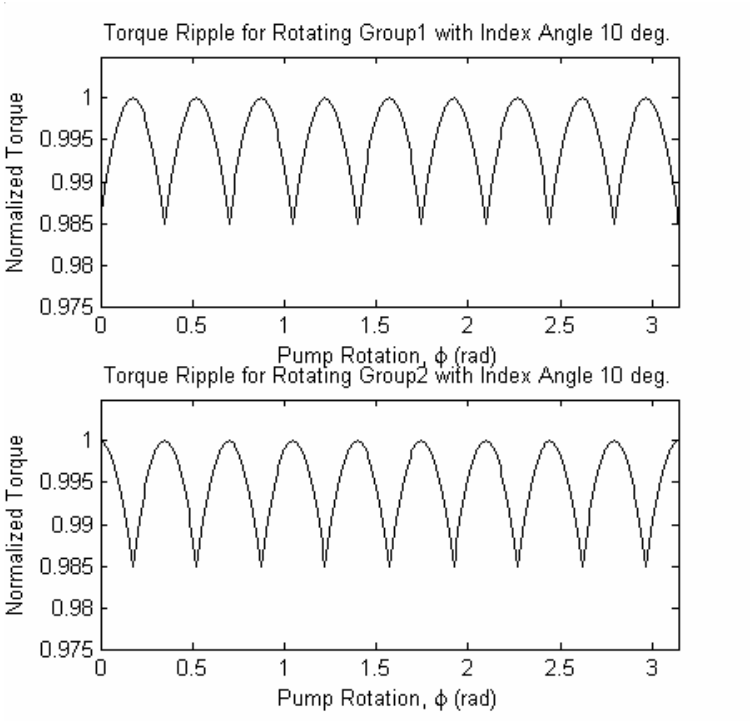

Figure 8-6 Torque ripples with index angle 10 deg.

Figure 8-6 shows the torque ripples for both the rotating groups when the index angle is 10^o. It is clearly evident that in this case, the torque profiles are such that maximum value on one corresponds to the minimum value on the other at every point in one pump revolution. This would lower down the overall torque amplitude as seen in Figure 8-7 by approximately 75%.

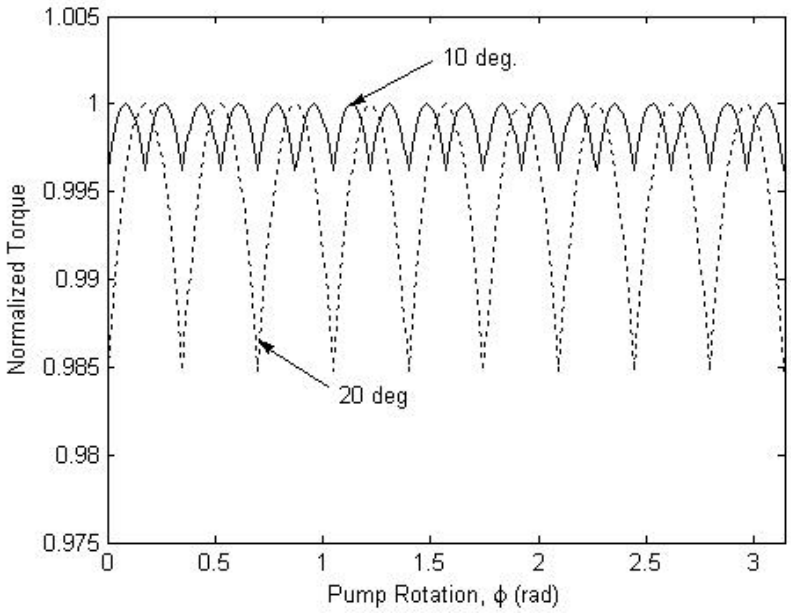

Figure 8-7 Shaft torque with index angle of 10 and 20 deg.

Figure 8-7 shows these two torque profile (equation(8-5)) on a common scale for comparison, while Figure 8-8 shows the FFT for two designs. It is very interesting to see here that when the index angle is set 10^o, it alters the frequency spectrum. Earlier the dominant frequencies were even multiple of the piston pass frequency. Now the dominant frequency is four times the piston pass frequency. Hence, not only it reduces the amplitude of the dominant frequencies but it also removes every other dominant

frequencies. This is very significant as it completely removes the first harmonics which is a big source of noise. As stated in the literature review, higher harmonics contain the maximum energy and they are responsible for the quality of noise as well.

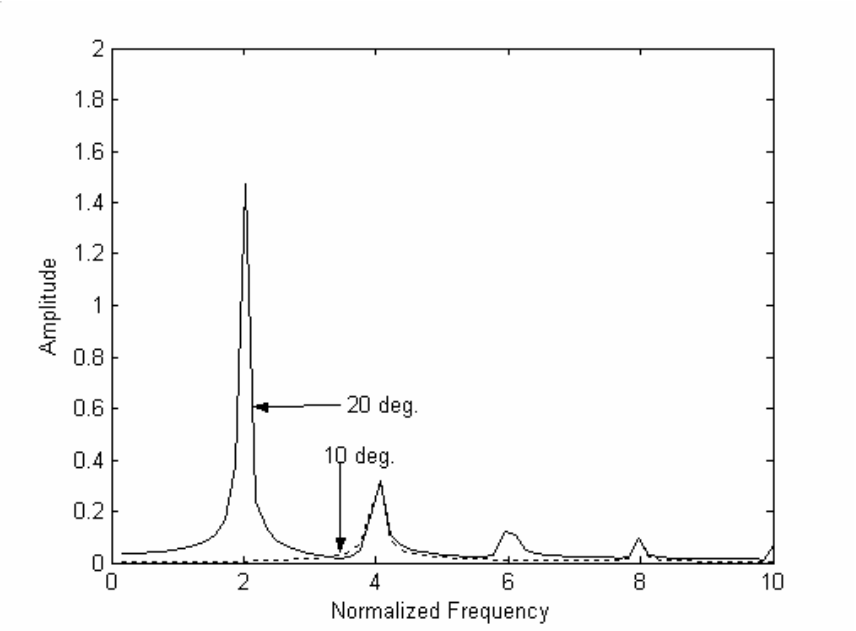

Figure 8-8 FFT of the idealized shaft torque with index angles of 10 and 20 deg.

8.3 Results from the Numerical Modeling

In the analysis section, it is highlighted that setting the first pistons on both the rotating groups with the separation angle of 10^o is more useful in curbing some of the amplitude of torque ripple than setting that angle at 20^o. Figure 8-9 shows the torque ripple for the tandem pump obtained by summing the instantaneous torque values for each piston from both rotating groups. When the leakage and compressibility are considered, the torque amplitude has maximum value of 1.6 percent.

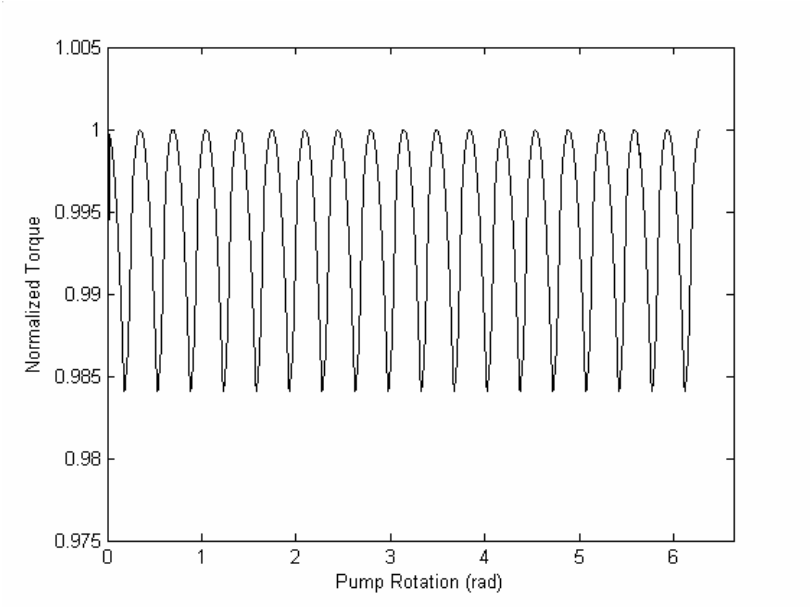

Figure 8-9 Shaft torque for a tandem pump with index angle of 20 deg.

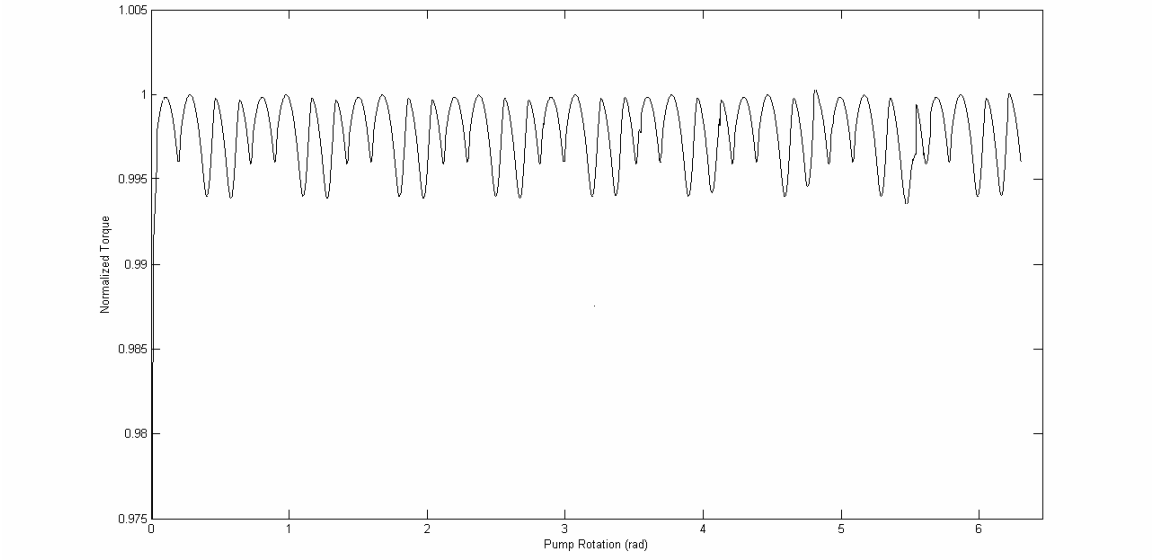

Figure 8-10 Shaft torque for a tandem pump with index angle of 10 deg.

Figure 8-10 shows the numerical torque profile of the tandem pump when the index angle is 10^{o}. Again the maximum torque amplitude generated by this model is 0.6 percent from its maximum, which confirms the analytical results.

8.4 Summary

Industrial practice of setting the index angle by trial or by experience in the case of the tandem pump could aggravate the noise problem. By comparing the torque ripples of two tandem designs with 20^{o} and 10^{o} index angles, it is shown here that setting the index angle according to the angles given in Table 3, will also reduce the torque amplitude by about 75%. Next, Chapter 9 summarizes important conclusions derived from the analysis and modeling results and recommendations for future work.

CHAPTER 9. CONCLUSIONS

9.1 Conclusions

The primary objective of this research is to describe new methods to reduce the axial piston pump noise. It has been accepted by many researchers that noise in an axial piston pump is generated by flow fluctuation and resulting pressure fluctuation at the pump discharge. The flow fluctuation is caused by the finite number of pistons and by the compressibility of the fluid. A good relief-groove design that delays the initiation of communication between the kidney port and the fluid inlet or fluid outlet in the valve plate has been the most effective way of reducing the flow pulsations. The other common method to attenuate the flow pulsation is to use a reactive silencer in forms such as accumulators, in-line silencers and side-branch resonators. However each design has limitations and pump noise still continues to be loud and annoying.

An alternative case is produced stating that the shaft torque ripple is the lead source of pump noise. This theory has been put forward after doing some laboratory experiments and logical reasoning. Therefore, instead of the flow ripple attenuation, the shaft torque attenuation should lower the noise level. A closed-form solution of the input shaft torque is produced as a function of the average shaft torque and total number of pistons. A swash plate control law is derived using the pump geometry and some mathematical manipulations. A few important conclusions are,

- A theoretical torque ripple has been shown to vary by 1.5 percent of the maximum torque input. Also, the amplitude is more for pumps with even number of pistons compared to pumps with odd number of pistons.
- The swash plate control law when applied to control the adjustment of the swash plate, is shown to wipe out the ripple effect theoretically.

Tandem axial-piston pumps produce an oscillatory torque ripple that is known to contribute to the noise and vibration characteristics of the machine. A closed-form solution of the input shaft torque is also produced as a function of the average shaft torque, total number of pistons and index angle δ. Some important conclusions regarding the behavior of the torque profile are,

- The torque ripple for the tandem pump is generally less for a pump that utilizes an odd number of pistons for each rotating group as compared to a pump that uses an even number of pistons for each rotating group.
- In order to minimize the amplitude of the tandem pump torque ripple, one rotating group must be indexed relative to the other rotating group by the angular dimension $\delta = \xi$. See equation (5-19) for the definition of ξ and Table 1 for tabulated values.
- By assembling the pump so that the index angle $\delta = \xi$ (i.e., according to the previous conclusion), the torque ripple amplitude may be reduced by 75% from is maximum possible value which exists when the index angle is zero. This result is explained by comparing two torque profiles. Torque ripple amplitude for a

tandem pump with the index angle of 10^o is smaller than the same with the index angle of 20^o.

A Matlab® program that models equation (5-33) and calculates torque amplitude for different design configuration is given. Four design variables chosen are: number of pistons N_1 and N_2 for rotating group 1 and 2 respectively, ratio of average torques $\bar{T}$ for rotating group 1 and 2 and index angle δ. A tandem pump design with 15 pistons on each rotating group with the average torque ratio of 1 and index angle of 6^o should give the smallest torque ripple amplitude.

Numerical models are made using Matlab® and Simulink® for the swash plate control law design and tandem pump design. These models consider the leakage and compressibility of fluid. Even after considering these effects, the both methods have shown a torque amplitude reduction of 65-75%.

It is shown that the flow equation and torque equation in their non-dimensional forms are identical. Hence, the research presented here holds true even if the original theory of the flow ripple being the main source of noise and vibrations. Two solution concepts outlined here should attenuate the flow ripple by as much amount as the torque ripple.

9.2 Flywheel Consideration

Following is a qualitative discussion about whether a flywheel could be used to reduce the torque fluctuations in the pump. Flywheels resist changes in their rotation speed, which helps steady the rotation of the shaft when an uneven torque is exerted on it

by its power source such as a piston-based (reciprocating) engine, or when the load placed on it is intermittent (such as a piston-based pump). It adds inertia to the system, thus reducing the velocity transients in the shaft, especially from the flywheel away from the shaft. If noise is coming from any component attached to the shaft after the flywheel, then this will help reduce that noise. The flywheel does nothing to reduce the uneven pumping torque caused by the pump design, rather it increases the pump impedance and the torque in the shaft from the flywheel to the pump will normally increase with a flywheel. That means the vibration in the pump case and the flow ripple from the pump will increase. The pump case is a major sound source so the flywheel will result in increased sound from that source.

9.3 Recommendation for Future Work

In Chapter 3 and 4 some of the assumptions considered in this analysis and modeling are listed. Even though the numerical models consider the leakage, the instantaneous piston pressure and compressibility effects, the frictional forces between sliding surfaces and centrifugal forces associating with rotating components are not considered. An improved model would consider these forces as well. Also, the features of true port plate geometry were not considered in the numerical model. However, the most important recommendation would be to conduct experiments involving these new methods and see if it reduces the pump noise. These methods were discussed with engineers of Caterpillar to check feasibility of conducting such experiments.

In order to attenuate the torque ripple by the swash plate dither design, the swash plate needs to be vibrated at its fundamental piston pass frequency, which in a typical design would be 300 Hz. It is a challenge to do so as current swash plate actuation methods could go up to only 50 Hz. The use of some fast servo valve enables the swash plate control to 100 Hz but that is still far from what is needed. One more requirement will be to locate the piston positions and mean discharge flow in real time and providing the feedback. However this is also a very difficult task at given frequencies. Use of a mechanical device like a multi-lobed cam controlling the swash plate, is still not conceived for axial piston pumps. Hence, it was decided that it would be extremely difficult and unaffordable to dither the swash plate according to the control law by any known swash plate control mechanism. However, it will be interesting to try the optimal index angle design to check its validity. Companies already make tandem pumps and as discussed earlier, they set the index angle by either experience or experiments. A splined shaft could be made in such a way that it separates pistons by the optimal index angle for the given design.

In another approach, Dr. Landsberger who initiated this project looked into a contoured swash plate design which could reduce the torque amplitude. He contributed with some interesting analysis however he left the project for another assignment. This idea could be explored further as well. Having said all, there is ample opportunity to expand this project and try putting them into practice.

REFERENCES

1) Manring N.D., Mehta V.S., Raab F.J., Graf K.J., "Shaft Torque of an Axial Piston Pump", Accepted for publication by the Journal of Dynamic Systems, Measurement and Control

2) Available at http://www.deh.gov.au/settlements/industry/minerals/booklets/noise/index.html, Website of Department of Environment and Heritage, Government of Australia, Last retrieved on 23rd October, 2005

3) Edge K.A., Darling J., "The Pumping Dynamics of Swash Plate Piston Pumps," *Journal of Dynamic Systems, Measurement, and Control,* Vol. 111 (1989), pp-307-312

4) Harrison A.M., Edge K.A., "Reduction of Axial Piston Pump Pressure Ripple," *Proceedings of the Institution of Mechanical Engineers Part I- Journal of Systems and Control Engineering***,** 214 (1), (2000), pp - 53-63

5) Kojima Eiichi, Yu Jianhong, Ichiyanagi Takayoshi, "Experimental Determining and Theoratical Predicting of Source Flow Ripple Generated by Fluid Power Piston Pumps," *SAE Technical Paper Series*, *Publication by SAE*, Warrendale, PA, USA, 2000-01-2617

6) Ivantysynova Monika, Huange Changchun, Christiansen Sven-Kelana, "Computer Aided Valve Plate Design – An Effective Way to Reduce Noise," *SAE Technical Paper Series, Publication by SAE*, Warrendale, PA, USA, 2004-01-2621

7) Pettersson Maria E., Weddfelt Kenneth G., Palmberg Jan-Ove, “Methods of Reducing Flow Ripple from Fluid Power Piston Pumps – a Theoretical Approach”’ *SAE Technical Paper Series, Publication by SAE*, Warrendale, PA, USA, 911762. pp 1-10

8) Schutten Herman P., Wakefield Danny M., Zimmerer Donald R., Malaney David W., “Noise Reduction at the Second Order Frequency”, *USPTO 5358388* October 25, 1994

9) Achten P.A.J., Van den Brink T.L., Paardenkooper T., Platzer T., Potma H.W., Schellekens M.P.A, Vael G.E.M., “Design and Testing of an Axial Piston Pump Based on the Floating Cup Principle”, *The Eighth Scandinavian International Conference on Fluid Power- Proc. SICFP’03*, Vol. 2 (2004), pp 805-820, Tampere University of Technology

10) Achten P.A.J., “Power Density of the Floating Cup Axial Piston Principle”, *Proceedings of 2004 ASME International Mechanical Engineering Congress and Exposition, November 2004*, pp 11-22

11) Achten P.A.J., Van den Brink T.L., Potma H.W., “Movement of the Cups on the Barrel Plate of a Floating Cup Axial Piston Machine”, *International Journal of Fluid Power*, Vol 5 (2), (2004), pp 25-33

12) Wilkes Roy G., “Reduction of Noise in Hydraulic Systems,” *SAE Technical Paper Series, Publication by SAE*, Warrendale, PA, USA, 952154. pp 105-108

13) Strunk Richard D., “Silencer for Hydraulic Piston Pump Pressure Pulsations,” *SAE Technical Paper Series, Publication by SAE*, Warrendale, PA, USA, 911759.

14) Malaney Dave, Wong Hongbin, Bever Mike, "Experimental and Numerical Study on Vibro-acoustic Performance of Axial Piston Pump", *SAE Technical Paper Series, Publication by SAE*, Warrendale, PA, USA, 2005-01-2320.

15) Landsberger B.J., "Using the Ideal Function Concept for Machine Noise Control". *146th Meeting of the Acoustic Society of America*. (2003) Austin,TX

16) Manring N.D., "Torque on the Cylinder Block of an Axial-piston Swash-plate Type Hydrostatic Pump". Ph.D. Dissertation (1996), Iowa State University.

17) Damtew F.A., "The Design of Piston-Bore Springs for Overwhelming Inertial Effects Within Axial-piston Swash-plate Type Hydrostatic Machines". M.S. Thesis (1998), University of Missouiri-Columbia.

18) Manring N.D., "The Torque on the Input Shaft of an Axial-Piston Swash-Plate Type Hydrostatic Pump," *Journal of Dynamic Systems, Measurement, and Control,* Vol. 120 (1998), pp-57-62

19) Ivantysyn J., Ivantysynova M., Hydrostatic Pumps and Motors: Principles, Design, Performance, Modeling, Analysis, Control and Testing. *Tech Book International, India 2001*.

20) Mehta V.S., Manring N.D., "Torque Ripple Attenuation of an Axial Piston Pump by Continuous Swash Plate Adjustment," Accepted by the 2005 ASME International Mechanical Engineering Congress and Exposition, Orlando, Fl.

21) Manring N.D., "The Discharge Flow Ripple of an Axial-Piston Swash-Plate Type Hydrostatic Pump," *Journal of Dynamic Systems, Measurement, and Control,* Vol. 122 (2000), pp-263-268

APPENDIX

Appendix A :Matlab Model

```
%Mfile to minimize the torque ripple for a piston pump
clc;
clear;
thetamax=360*pi/180;
count = 0;
for N1 = 5:15
   for N2 = 5:15
      delta = 0;
      while delta <= 2*pi/min(N1,N2)
         for Tbar = 1:1
n=1;    theta(1)=0;
while theta(n) < thetamax
   phi1= theta(n);
   if round(N1/2-0.001)==round(N1/2+0.001) %then an even number
      while phi1>2*pi/N1
         phi1=phi1-2*pi/N1;
      end
      T1(n)=(pi/N1)*csc(pi/N1)*cos(pi/N1-phi1);


   else
```

```
        while phi1>pi/N1
            phi1=phi1-pi/N1;
        end
        T1(n)=(pi/(2*N1))*csc(pi/(2*N1))*cos(pi/(2*N1)-phi1);
    end
    phi2=theta(n)+delta;
    if round(N2/2-0.001)==round(N2/2+0.001) %then an even number
        while phi2>2*pi/N2
          phi2=phi2-2*pi/N2;
        end
        T2(n)=Tbar*(pi/N2)*csc(pi/N2)*cos(pi/N2-phi2);
    else

        while phi2>pi/N2
          phi2=phi2-pi/N2;
        end
        T2(n)=Tbar*(pi/(2*N2))*csc(pi/(2*N2))*cos(pi/(2*N2)-phi2);
    end
T(n)=(T1(n)+T2(n));
n=n+1;

theta(n)=theta(n-1)+0.5*pi/180;
```

```
end
T(n) = T(n-1);
T1(n) = T1(n-1);
T2(n) = T2(n-1);
Tmax = max(T);
Tmin = min(T);
if count == 0
    f = Tmax - Tmin;
    countN1 = N1;
    countN2 = N2;
    countdelta = delta*180/pi;
    countTbar = Tbar;
else
    temp = Tmax - Tmin;
    if temp < f
        f = temp;
        countN1 = N1;
        countN2 = N2;
        countdelta = delta*180/pi;
        countTbar = Tbar;

    end
```

```
end

count = count + 1;

delta = delta+0.10*pi/180;
```

VITA

Viral Mehta was born January 1, 1977 in Surat, India. He is currently a Ph.D candidate with the Mechanical and Aerospace Engineering Department at University of Missouri – Columbia. His primary area of interest is hydraulic systems especially noise control of axial piston pumps. Earlier he received his M.S. (Mechanical) from University of Washington, Seattle in 2002 with a special interest in Fuel Cell Engineering. He has worked for Bajaj Auto Ltd., one of the largest automotive companies in India after receiving his Bachelor of Engineering (Mechanical) from S.V. National Institute of Technology, Surat (India) in 1998.